

Review

From molecular metal complex to metal-organic framework: The CO₂ reduction photocatalysts with clear and tunable structureYu-Hui Luo^{a,b}, Long-Zhang Dong^a, Jiang Liu^a, Shun-Li Li^{a,*}, Ya-Qian Lan^{a,*}^a School of Chemistry and Materials Science, Nanjing Normal University, Jiangsu, Nanjing 210023, PR China^b Department of Chemical Engineering, Huaihai Institute of Technology, Jiangsu, Lianyungang 222000, PR China

ARTICLE INFO

Article history:

Received 29 January 2019

Accepted 30 March 2019

Keywords:

Molecular metal complexes (MMCs)

Metal-organic frameworks (MOFs)

Crystal engineering

Photocatalysis

CO₂ reduction reaction (CO₂RR)

ABSTRACT

Photocatalytic reduction of CO₂ to high value-added productions is considered as a green and sustainable approach to reducing excessive CO₂ emissions. Molecular metal complexes (MMCs) and metal-organic frameworks (MOFs) are widely studied as potential photocatalysts for CO₂ reduction reaction (CO₂RR) due to their clear and tunable structures. In this review, we summarize the photochemical CO₂RR based on both homogeneous MMCs and heterogeneous MOFs and discuss molecular engineering approaches and key advances in this field. Discussing the photocatalytic CO₂RR properties of MMCs and MOFs is beneficial to elucidating the structure-activity relationship and reaction mechanism in the photocatalytic process. These discussions will provide scientific and technical guidance for the rational design and development of more creative systems for photocatalytic CO₂RR. In addition, challenges and prospects for future research of photocatalytic CO₂RR based on these coordination compounds are proposed.

© 2019 Elsevier B.V. All rights reserved.

Contents

1. Introduction	87
2. Homogeneous molecular metal complexes	88
2.1. Photocatalysts with noble metal center	88
2.1.1. Re complexes	88
2.1.2. Ru complexes	88
2.1.3. Os complexes	93
2.1.4. Ir complexes	93

Abbreviations: bpy, 2,2'-bipyridine; 4,4'-dcbpy, 2,2'-bipyridine-4,4'-dicarboxylic acid; DMF, *N,N*-dimethylformamide; TEOA, triethanolamine; MeCN, acetonitrile; BNAH, 1-benzyl-1,4-dihydronicotinamide; phen, 1,10-phenanthroline; 6,6'-dmb, 6,6'-dimethyl-bpy; 5,5'-dmb, 5,5'-dimethyl-bpy; 4,4'-dmb, 4,4'-dimethyl-bpy; tpy, 2,2':6',6''-terpyridine; ppy, 2-phenylpyridine; qpy, 2,2':6',2'':6'''-quaterpyridine; dmp, 2,9-dimethyl-1,10-phenanthroline; 1,3-(SiMe₃)₂TIO, 1,3-bis(SiMe₃)-4,5,6,7-tetrahydro-2H-inden-2-one; dF (CF₃)ppy, cyclometalated 2-(2,4-difluorophenyl)-5-trifluoro-methylpyridine; dtbbpy, 4,4'-di-*tert*-butyl-2,2'-bipyridyl; TEA, triethylamine; EDTA, ethylenediaminetetraacetic acid; OMe₂-bpy, 4,4'-(CH₃O)₂-2,2'-bipyridine; MPAC, *N,N*-dimethyl-*N,N*-bis(2-pyridinylmethyl)cyclohexane-1,2-diamine; cyclam, 1,4,8,11-tetra-azacyclotetradecane; N₄H, 2,12-dimethyl-3,7,11,17-tetraazabicyclo-[11.3.1]-heptadeca-1(17),2,11,13,15-pentaene; Me₆-cyclam-diene, 5,7,7,12,14,14-hexamethyl-1,4,8,11-tetra-azacyclotetradeca-4,11-diene; Me₂-cyclam-diene, 5,12-dimethyl-1,4,8,11-tetra-azacyclotetradeca-4,11-diene; Phen2, 3,7-di-[(1,1'-biphenyl)-4-yl]-10-(naphthalen-1-yl)-4a,10a-dihydro-10H-phenoxazine; TPA, tris(2-pyridylmethyl)amine; BQPA, bis(2-quinolylmethyl)-(2-pyridylmethyl)amine; L₁, N[(CH₂)₂NHCH₂(*m*-C₆H₄)CH₂NH(CH₂)₂]₃N; L₂, tris[2-(benzylamino)ethyl]amine; L₃, tris[2-[(9'-anthrylmethyl)amino]ethyl]amine; L₄, tris[2-[(1'-naphthylmethyl)amino]ethyl]amine; L₅, tris[2-(iso-propylamino)ethyl]amine; 12-aneN₄, 1,4,7,10-tetraazacyclododecane; Me₂-cyclam, 5,7-dimethyl-1,4,8,11-tetraazacyclotetradecane; BI(CO₂H)H, 2-(1,3-dimethyl-2,3-dihydro-1H-benzimidazol-2-yl)benzoic acid; BI(OH)H, 1,3-dimethyl-2-(o-hydroxyphenyl)-2,3-dihydro-1H-benzod[imidazole; BIH, 1,3-dimethyl-2-phenyl-2,3-dihydro-1-benzod[imidazole; piq, 1-phenylisoquinoline; pqn, 8-(diphenylphosphanyl)quinoline; CP*, 1,2,3,4,5-pentamethylcyclopentadienyl; bpdc, *para*-biphenyldicarboxylate; 5,5'-dcbpy, 2,2'-bipyridine-5,5'-dicarboxylic acid; cat-bdc, 2,3-dihydroxyterephthalic acid; bdc, 1,4-dicarboxybenzene; HTPP, 2,3,6,7,10,11-hexaaminotriphenylene; H₂DTA, 2,5-diaminoterephthalate; H₂SDCA-NH₂, 2,2'-diamino-4,4'-stilbenedicarboxylic acid; TCPP, 4,4',4'',4'''-(porphyrin-5,10,15,20-tetrayl) tetrabenzoate; THPP, 5,10,15,20-tetrakis(3,4,5-trihydroxyphenyl)porphyrin; THBPP, 5,10,15,20-tetrakis(3,4,5-trihydroxybiphenyl)porphyrin; HAD, adenine; BDA, butanedioic acid; IBA, isobutyric acid; TCA, 4,4',4''-nitritoltribenzoic acid; HCB, hexakis(4'-carboxyl[1,1'-biphenyl]-4-yl)benzene; HCHC, hexakis(4-carboxyphenyl)hexabenzocoronene; H₂bbta, 1H,5H-benzo-(1,2-d:4,5-d')bistriazole; H₂btdd, bis(1H-1,2,3-triazolo-[4,5-b],[4',5'-i]dibenzo[1,4]dioxin; BTC, benzene-1,3,5-tricarboxylate.

* Corresponding authors.

E-mail addresses: slli@njnu.edu.cn (S.-L. Li), yqlan@njnu.edu.cn (Y.-Q. Lan).

2.2.	Photocatalysts with non-noble metal center.	95
2.2.1.	Mn complexes.	95
2.2.2.	Fe complexes	95
2.2.3.	Co complexes	96
2.2.4.	Ni complexes	97
2.2.5.	Cu complexes	98
2.3.	Supramolecular photocatalysts.	99
2.3.1.	Ru unit as the photosensitizer.	99
2.3.2.	Os and Ir unit as the photosensitizer	99
2.3.3.	Porphyrin unit as the photosensitizer.	99
3.	Pure metal-organic frameworks (MOFs).	100
3.1.	Ligands modifications	100
3.1.1.	Metal ions coordination.	100
3.1.2.	Amino groups	106
3.1.3.	Porphyrin and metal porphyrin.	107
3.1.4.	Others	109
3.2.	Functional metal clusters	111
4.	Hybrid systems.	111
4.1.	Hybrid systems based on molecular metal complexes	112
4.1.1.	Composed with inorganic semiconductors	112
4.1.2.	Composed with periodic mesoporous organosilica	117
4.2.	MOFs-composited nanoparticles and MOFs-derived nanoparticles	117
4.2.1.	MOFs-composited nanoparticles	117
4.2.2.	MOFs-derived nanoparticles	120
5.	Conclusions and outlooks	122
	Acknowledgements	122
	References	122

1. Introduction

As the rapid consumption of fossil fuel, excessive emissions of carbon dioxide (CO₂) lead to global warming, sea level rising and in turn impedes the sustainable development of human society [1–3]. Efforts have been devoted to capturing, storing and utilizing the CO₂ to prevent it from being released into the atmosphere [4–8]. In this field, the photochemical reduction of CO₂ to high value-added productions has been considered as a green and sustainable approach [9–15]. However, the reduction potential required for CO₂ reduction is quite negative (vs NHE in neutral aqueous solution) (Table 1) [16], indicating the difficulty and challenge for CO₂ reduction. The photocatalyst is deemed to be a core technology in photochemical CO₂ reduction reaction (CO₂RR). In 1979, Fujishima et al. firstly reported the photocatalytic CO₂RR by using semiconductor photocatalysts [9]. After that, many scientists followed in this field, and significant progress has been achieved in developing new catalysts. Semiconductors, molecular complexes, zeolites and biomaterials have been investigated as photocatalysts for CO₂RR [17–23]. Although strategies focusing on enhancing the surface area and the light-harvesting capability of catalysts have been employed to improve the performance of the catalytic system, the efficiency of photocatalytic CO₂RR is still low. Moreover, the selectivity of the value-added products photocatalytically reduced from CO₂, including CO, CH₄, C₂H₄, CH₃OH, HCOOH, CH₃-

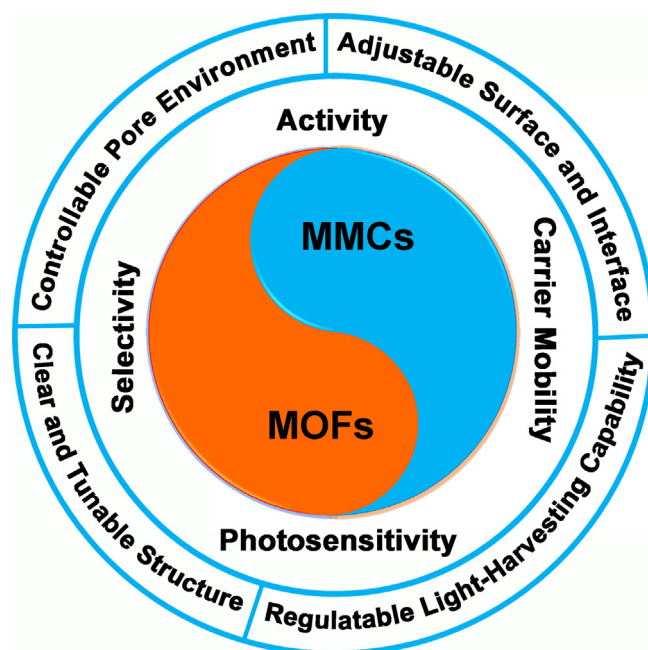
COOH, et al., is uncontrollable by now. Thus, it is still urgent to develop novel photocatalytic systems for CO₂RR.

Molecular metal complexes (MMCs) and metal-organic frameworks (MOFs), both of which are constructed from metal ions/clusters and organic ligands, are attracting increasing attention for their wide applications in sensing, sorption, catalysis and so on [24–32]. Recent studies have shifted towards the design and application of MMCs and MOFs as potential photocatalysts for CO₂RR for their clear and tunable structures (Scheme 1) [33–35]. Molecular Re complexes Re(bpy)(CO)₃X (X = Cl or Br) have been applied as a

Table 1
The reduction potential required for CO₂RR.

Reaction	Redox potential ^a (V)
CO ₂ + 2H ⁺ + 2e ⁻ → HCOOH	-0.61
CO ₂ + 2H ⁺ + 2e ⁻ → CO + H ₂ O	-0.53
CO ₂ + 4H ⁺ + 4e ⁻ → HCHO + H ₂ O	-0.48
CO ₂ + 6H ⁺ + 6e ⁻ → CH ₃ OH + H ₂ O	-0.38
CO ₂ + 4H ⁺ + 4e ⁻ → CH ₄ + 2H ₂ O	-0.24
2H ⁺ + 2e ⁻ → H ₂	-0.41
H ₂ O + 2 h ⁺ → 1/2O ₂ + 2H ⁺	+0.41

^a vs NHE, at pH = 7.



Scheme 1. Advantages of MMCs and MOFs for photocatalytic CO₂RR.

homogeneous photocatalyst to selectively reduce CO_2 to CO since 1983 [36]. Thereafter, many researchers further boosted this field especially in developing molecular catalysts based on earth-abundant transition metals [37]. For MOFs, their catalytic properties can be easily controlled by selecting metal ions/clusters and organic ligands, tuning the environment of channels and the morphology of the crystals, and so on [38–45]. The high CO_2 adsorption capacities of MOFs further inspired their applications as heterogeneous photocatalysts for CO_2RR [46–49]. In fact, enormous attention has been paid to MOFs in this field since 2011 [50–55]. Otherwise, MMCs and MOFs also can composite with inorganic semiconductors, zeolites or polymers to enhance their performances for CO_2RR [56,57]. In 2003, Hirose et al. firstly reported the hybrid system for CO_2 reduction by fixing $[\text{Co}(\text{bpy})_3]^{2+}$ as a catalytic unit and $[\text{Ru}(\text{bpy})_3]^{2+}$ as a photosensitive unit to cation exchange polymer [58]. Later on, Sato et al. reported the covalent combined hybrid photocatalyst with $[\text{Ru}(4,4'\text{-dcbpy})_2(\text{CO})_2]\text{Cl}_2$ as a catalytic unit and N-doped Ta_2O_5 as a photosensitive unit [59].

Although homogeneous MMCs and heterogeneous MOFs are inextricably related, there is no review that comprehensively discusses MMCs and MOFs as a whole in the field of CO_2RR . This review is the first to summarize the entirety of photochemical $\text{CO}_2\text{-RR}$ catalyzed by both MMCs and MOFs and discuss molecular engineering approaches and key advances in this field. Summarizing the photocatalytic CO_2 reduction properties of these well-defined coordination compounds is helpful to elucidating the structure-activity relationship and reaction mechanism in the photocatalytic process. These discussions will provide scientific and technical guidance for the rational design and development of more creative systems for photocatalytic CO_2RR . The review is divided into five sections and starts with an introduction to the background of photocatalytic CO_2RR . The second and third sections summarize the development of pure MMCs and pure MOFs used for photocatalytic CO_2RR , respectively. The use of MMCs and MOFs as co-catalyst or photosensitizer to enhance the photocatalytic performance of the hybrid systems is discussed in the fourth section. In the last section of the review, challenges and recommendations for future research of photocatalytic CO_2RR based on MMCs and MOFs are addressed.

2. Homogeneous molecular metal complexes

MMCs are at the forefront of catalyst research for their tunable structures and multiple redox states [60–72]. In this section, the MMCs with a noble metal center, a non-noble metal center, and di- or multi-metal centers are summarized separately. The roles of MMCs in the photocatalytic CO_2RR system and the reaction mechanism will be discussed. The homogeneous molecular photocatalytic CO_2 reduction systems were summarized in Tables 2 and 3.

2.1. Photocatalysts with noble metal center

2.1.1. Re complexes

Re complexes are noticed for their high CO_2 reduction activity and high product selectivity. In 1983, Lehn and coworkers firstly reported the photocatalytic CO_2 -to-CO reduction by using compound **1a** (Table 2) [36]. The highest turnover numbers (TONs) of 48 was observed within 4 h. Later on, a family of Re complexes with the general structure of $\text{Re}(\text{bpy})(\text{CO})_3\text{Cl}$ are reported as photocatalysts for CO_2RR [73–80]. Their highly stable and tunable structures make an opportunity to in-depth evaluate the mechanism of photocatalytic CO_2RR . In these systems, Re catalysts are excited through irradiation to form a triplet metal-to-ligand charge transfer ($^3\text{MLCT}$) excited states. Thereafter, the excited state of Re complex is quenched by sacrificial reagent to produce $\text{Re}(\text{bpy})^-$

$(\text{CO})_3\text{Cl}$. Lehn et al. proposed that $\text{Re}(\text{bpy})^-(\text{CO})_3\text{Cl}$ released a CO ligand and provided a vacant site for CO_2 activation [73]. Although the CO ligand exchange was confirmed by an isotopic labeling experiment, it was not the main way for CO_2 reduction. Because the exchange process required long reaction time. During the same period, Meyer et al. proposed another acceptable mechanism through the dissociation of Cl^- [81,82]. Actually, $\text{Re}(\text{bpy})^-(\text{CO})_3$ can react with CO_2 even in the dark [83,84].

When the photocatalytic CO_2RR was taken place in the mixed solution of DMF/TEOA, the MeCN ligand of compound **1d** (Table 2) was replaced with DMF and then further replaced by deprotonated TEOA with the O atom coordinates to Re (Fig. 1) [85,86]. The TEOA adducts could capture CO_2 even at atmospheric levels. It provided a new insight that TEOA contributed to the capture of CO_2 and then boosted the catalytic performance of the system.

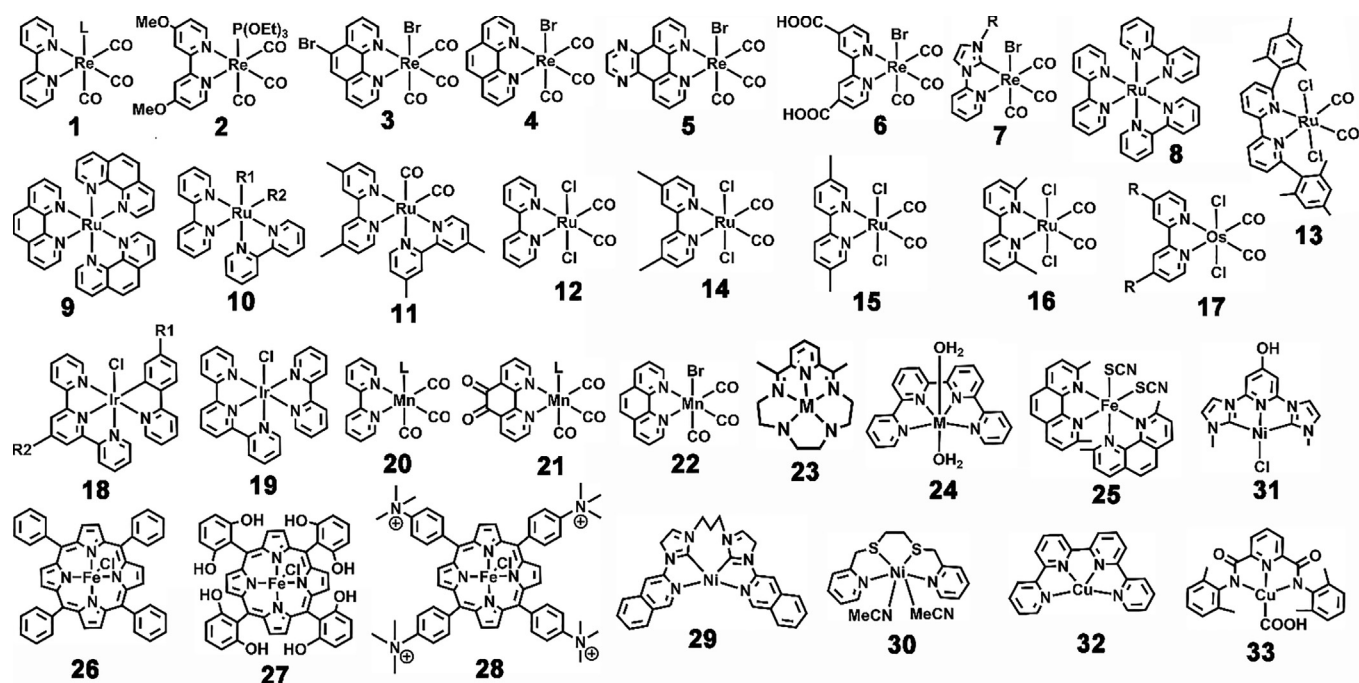
When the bpy ligand of $\text{Re}(\text{bpy})(\text{CO})_3\text{Br}$ was replaced with other aromatic diimine ligands, the catalytic activity of the new $\text{Re}(\text{diimine})(\text{CO})_3\text{Br}$ complex decreased with the decrease of their fluorescence lifetime, indicating that a sufficiently long excited state lifetime is important for photocatalytic CO_2RR [87]. On the other hand, the ligand X of $\text{Re}(\text{bpy})(\text{CO})_3\text{X}$ ($\text{X} = \text{Cl}^-$, Br^- , NCS^- , CN^- ...) will also affect their photocatalytic properties [36,73,83,88–91]. When NCS^- was chosen as a ligand, the active intermediate $\text{Re}(\text{bpy})^-(\text{CO})_3$ was easy to generate because the NCS^- ligand was easy to dissociate [90]. Meanwhile, the photosensitive **1b** could donate the second electron to CO_2 . Thus, compound **1b** showed a higher activity than compound **1a**. Contrarily, compound **1c** showed no photocatalytic activity under similar condition, because the corresponding $\text{Re}(\text{bpy})^-(\text{CO})_3(\text{CN})$ species did not dissociate the CN^- ligand. In addition, the efficiency and durability of Re catalysts would be drastically improved by using a suitable photosensitizer together. For example, when a series of ring-shaped Re complexes were used as the photosensitizers with **1d** as the catalyst, the highest quantum yield (QY, Φ) of 0.82 and TON_{CO} of 526 was obtained in DMF/TEOA solution (Fig. 2) [92]. Other photosensitizers such as $[\text{Ru}(\text{bpy})_3]^{2+}$ could also be used in this system, but with lower QY. The high photosensitive efficiency of the cyclic Re complexes was attributed to two reasons. On the one hand, the Re-rings could be efficient reductive quenched by TEOA under reaction condition. On the other hand, the electrons could fast transfer from the reduced Re-rings to the catalysts. The cyclic Re complexes could also be applied to sensitize other catalysts, giving good product selectivity and excellent QY [93].

With high catalytic performance, the Re complexes will be continuing studied for CO_2RR . However, the reported modifications predominantly involve the tuning of the bpy ligand. Thus, other organic ligands with more coordination sites or different coordination geometries should be considered to develop more efficient systems.

2.1.2. Ru complexes

Unlike Re complexes that exclusively reduce CO_2 to CO, Ru-based photocatalysts can convert CO_2 to both CO and HCOOH [61,94,95]. At the very beginning, $[\text{Ru}(\text{bpy})_3]^{2+}$ was chosen as the photocatalyst for CO_2 reduction [96]. Under the light irradiation, $[\text{Ru}(\text{bpy})_3]^{2+}$ would dissociate one bpy ligand in the DMF/TEOA solution to form $[\text{Ru}(\text{bpy})_2(\text{solvent})_2]^{2+}$ as the actual catalyst for CO_2 -to-HCOOH reduction. The addition of water could assist the bpy ligand dissociation and then enhance the HCOOH production [97]. A contrastive experiment with more stable compound **9** further supported the inference. Later on, compound **10a** and its derivatives were investigated as photocatalysts for CO_2RR [98]. In these systems, the kind of reduction product was greatly depended on the pH of the reaction solution. When TEOA was used as sacrificial reagent, the solution was alkaline and only HCOOH was formed as a reduction product. In contrast, when BNAH was

Table 2
Homogeneous multimolecular photocatalytic CO₂ reduction systems.^a



Compound	PS	Product	TON	QY	Solvent	SD	λ	Ref.
1a ; L = Cl	–	CO	48	–	DMF	TEOA	>400 nm	[36]
1a ; L = Cl	–	CO	–	0.16	DMF	TEOA	<330 nm	[90]
1b ; L = SCN [–]	–	CO	–	0.3	DMF	TEOA	<330 nm	[90]
1c ; L = CN [–]	–	CO	0	0	DMF	TEOA	<330 nm	[90]
1d ; L = MeCN	2	CO	–	0.59	DMF	TEOA	<330 nm	[90]
3	–	CO	9	–	DMF	TEOA	>400 nm	[36]
4	–	CO	11.5	–	DMF	TEOA	>400 nm	[87]
5	–	CO	1.1	–	DMF	TEOA	>400 nm	[87]
6	–	CO	7.7	–	DMF	TEOA	>400 nm	[87]
1d ; L = MeCN	R3pr ³⁺ (Fig. 2)	CO	526	0.82	DMF	TEOA	>400 nm	[92]
7a ; R = Me	[Ir(ppy) ₃] ⁺	CO	14	–	MeCN	BIH	>400 nm	[91]
7b ; R = Ph	[Ir(ppy) ₃] ⁺	CO	26	–	MeCN	BIH	>400 nm	[91]
7c ; R = (4-OC ₆ H ₁₃)Ph	[Ir(ppy) ₃] ⁺	CO	19	–	MeCN	BIH	>400 nm	[91]
7d ; R = (4-CF ₃)Ph	[Ir(ppy) ₃] ⁺	CO	50	–	MeCN	BIH	>400 nm	[91]
8	–	HCOOH	27	–	DMF	TEOA	>400 nm	[96]
8	–	HCOOH	22	–	MeCN	TEOA	>400 nm	[96]
9	–	HCOOH	<1	–	DMF	TEOA	>400 nm	[96]
10a ; R1 = R2 = Cl	[Ru(bpy) ₃] ²⁺	HCOOH	51	–	DMF	TEOA	>400 nm	[97]
10b ; R1 = R2 = MeCN	[Ru(bpy) ₃] ²⁺	HCOOH	91	–	DMF	TEOA	>400 nm	[97]
10c ; R1 = R2 = DMF	[Ru(bpy) ₃] ²⁺	HCOOH	132	–	DMF	TEOA	>400 nm	[97]
10d ; R1 = Cl, R2 = H	[Ru(bpy) ₃] ²⁺	HCOOH	322	–	DMF	TEOA	>400 nm	[97]
10e ; R1 = Cl, R2 = CO	[Ru(bpy) ₃] ²⁺	HCOOH	326	–	DMF	TEOA	>400 nm	[97]
11	[Ru(bpy) ₃] ²⁺	HCOOH	316	–	DMF	BNAH	>400 nm	[99]
12	[Ru(bpy) ₃] ²⁺	HCOOH	255	–	DMF	TEOA	>400 nm	[97]
12	[Ru(bpy) ₃] ²⁺	CO	300	–	DMF-H ₂ O	BNAH	>400 nm	[103]
13	[Ru(bpy) ₃] ²⁺	CO	–	–	DMF-H ₂ O	BNAH	>400 nm	[103]
14	[Ru(bpy) ₃] ²⁺	CO	–	0.12	DMF-H ₂ O	BNAH	>400 nm	[106]
15	[Ru(bpy) ₃] ²⁺	HCOOH	–	0.17	DMF-H ₂ O	BNAH	>400 nm	[106]
16	[Ru(bpy) ₃] ²⁺	CO	–	0.08	DMF-H ₂ O	BNAH	>400 nm	[106]
17a ; R = H	–	CO	11.5	–	DMF	BNAH	>320 nm	[107]
17a ; R = H	–	CO	24	–	DMF	TEOA	>320 nm	[108]
17b ; R = CH ₃	–	HCOOH	8.5	–	DMF	BNAH	>320 nm	[108]
17b ; R = CH ₃	–	CO	19.5	–	DMF	BNAH	>320 nm	[108]
17b ; R = CH ₃	–	CO	45	–	DMF	TEOA	>320 nm	[108]
17c ; R = C(CH ₃) ₃	–	HCOOH	15	–	DMF	BNAH	>320 nm	[108]
17c ; R = C(CH ₃) ₃	–	CO	47	–	DMF	TEOA	>320 nm	[108]
17c ; R = C(CH ₃) ₃	–	HCOOH	8	–	DMF	TEOA	>320 nm	[108]

(continued on next page)

Table 2 (continued)

Compound	PS	Product	TON	QY	Solvent	SD	λ	Ref.
17d ; R = COOCH(CH ₃) ₂	–	CO	7	–	DMF	TEOA	>320 nm	[108]
		HCOOH	2	–				
18a ; R1 = R2 = H	–	CO	38	0.13	MeCN	TEOA	>410 nm	[109]
18b ; R1 = CH ₃ , R2 = H	–	CO	50	0.21	MeCN	TEOA	>410 nm	[109]
18c ; R1 = CF ₃ , R2 = H	–	CO	–	–	MeCN	TEOA	>410 nm	[109]
18d ; R1 = R2 = H	–	CO	178	–	MeCN	TEOA	>400 nm	[110]
18e ; R1 = H, R2 = Ph	–	CO	262	–	MeCN	TEOA	>400 nm	[110]
18f ; R1 = H, R2 = 9-anthryl	–	CO	310	0.1	MeCN	TEOA	>400 nm	[110]
18 g ; R1 = H, R2 = 4-F-Ph	–	CO	248	–	MeCN	TEOA	>400 nm	[110]
19	–	HCOOH	~20	0.021	MeCN	TEOA	>400 nm	[112]
20a ; L = Br	[Ru(dmb) ₃] ²⁺	HCOOH CO	149	–	DMF	BNAH	~480 nm	[113]
			12	–				
20b ; L = MeCN	[Ru(dmb) ₃] ²⁺	HCOOH CO	1.3	–	DMF	BNAH	~470 nm	[117]
			21	–				
21a ; L = Br	[Ru(dmb) ₃] ²⁺	HCOOH	52	–	DMF	BNAH	~480 nm	[118]
		CO	8	–				
21b ; L = MeCN	[Ru(dmb) ₃] ²⁺	HCOOH	58	–	DMF	BNAH	~480 nm	[118]
		CO	15	–				
22	ZnTPP	HCOOH	19	–	MeCN-H ₂ O	TEA	>320 nm	[119]
		CO	119	–				
23a ; M = Co	[Ir(ppy) ₃] ⁺	CO	270	–	MeCN	TEA	>420 nm	[120]
23b ; M = Fe	[Ir(ppy) ₃] ⁺	HCOOH	5	–	MeCN	TEA	>420 nm	[120]
24a ; M = Fe	[Ru(bpy) ₃] ²⁺	CO	3000	–	MeCN	TEOA	~460 nm	[121]
24a ; M = Fe	purpurin	CO	1365	–	MeCN	TEOA	~460 nm	[121]
24b ; M = Co	[Ru(bpy) ₃] ²⁺	CO	2660	–	MeCN	TEOA	~460 nm	[121]
24b ; M = Co	purpurin	CO	790	–	MeCN	TEOA	~460 nm	[121]
25	CuI	CO	273	0.067	MeCN	BIH	~436 nm	[122]
26	–	CO	17	–	MeCN	TEA	>320 nm	[130]
27	–	CO	23	–	MeCN	TEA	>320 nm	[130]
27	[Ir(ppy) ₃] ⁺	CO	140	–	MeCN	TEA	>420 nm	[131]
27	9-anthronitrile	CO	60	–	MeCN	TEA	>400 nm	[131]
28	–	CO	101	–	MeCN	BIH	>420 nm	[132]
28	purpurin	CO	120	–	MeCN-H ₂ O	TEA	>420 nm	[133]
28	[Ir(ppy) ₃] ⁺	CH ₄	159	0.18	MeCN	TEA	>420 nm	[134]
28	[Ir(ppy) ₂ (bpy)] ⁺	CH ₄	3	–	MeCN-H ₂ O	TEA	>420 nm	[135]
		CO	24	–				
28	Phen2	CO	149	–	DMF	TEA	>435 nm	[136]
		CH ₄	29	–				
28	CuInS ₂ QD	CO	450	–	H ₂ O	–	~450 nm	[137]
Co-TPA-Cl	[Ir(ppy) ₃] ⁺	CO	900	–	MeCN	TEA	~460 nm	[159]
Co-TPA-Cl	[Ru(Phen) ₃] ²⁺	CO	790	0.16	MeCN-H ₂ O	TEOA	~450 nm	[162]
Co-TPA-Br	[Ir(ppy) ₃] ⁺	CO	1500	–	MeCN	TEA	~460 nm	[161]
Co-TPA-I	[Ir(ppy) ₃] ⁺	CO	1200	–	MeCN	TEA	~460 nm	[161]
Co-TPA-SCN	[Ir(ppy) ₃] ⁺	CO	1300	–	MeCN	TEA	~460 nm	[161]
Co-BPQA-Cl	[Ru(Phen) ₃] ²⁺	CO	1070	0.22	MeCN-H ₂ O	TEOA	~450 nm	[162]
Co-BQPA-Cl	[Ru(Phen) ₃] ²⁺	CO	1330	0.27	MeCN-H ₂ O	TEOA	~450 nm	[162]
Co-TQA-Cl	[Ru(Phen) ₃] ²⁺	CO	950	0.19	MeCN-H ₂ O	TEOA	~450 nm	[162]
C1	[Ir(ppy) ₃] ⁺	CO	368	–	DMF	TEA	~460 nm	[140]
Co-MPCA-Cl	[Ir(ppy) ₃] ⁺	CO	470	–	DMF	TEA	~460 nm	[141]
Co-MPCA-Br	[Ir(ppy) ₃] ⁺	CO	403	–	DMF	TEA	~460 nm	[141]
Co ₂ -L1	[Ru(Phen) ₃] ²⁺	CO	16,896	–	MeCN-H ₂ O	TEOA	~450 nm	[163]
Co-L2-MeCN	[Ru(Phen) ₃] ²⁺	CO	684	–	MeCN-H ₂ O	TEOA	~450 nm	[163]
CoZn-L1	[Ru(Phen) ₃] ²⁺	CO	65,000	–	MeCN-H ₂ O	TEOA	~450 nm	[165]
Co-L3	[Ru(Phen) ₃] ²⁺	CO	12,680	0.19	MeCN-H ₂ O	TEOA	~450 nm	[167]
Co-L4	[Ru(Phen) ₃] ²⁺	CO	11,280	0.19	MeCN-H ₂ O	TEOA	~450 nm	[167]
Co-L2-OH	[Ru(Phen) ₃] ²⁺	CO	1600	0.19	MeCN-H ₂ O	TEOA	~450 nm	[167]
Co-L5	[Ru(Phen) ₃] ²⁺	CO	11,600	0.19	MeCN-H ₂ O	TEOA	~450 nm	[168]
29	[Ir(ppy) ₃] ⁺	CO	98,000	–	MeCN	TEA	>320 nm	[173]
30	[Ru(bpy) ₃] ²⁺	CO	713	0.014	DMF-H ₂ O	BIH	~450 nm	[174]
31	[Ir(ppy) ₃] ⁺	CO	10.6	–	MeCN	BIH	>320 nm	[175]
32	[Ru(bpy) ₃] ²⁺	CO	12,400	–	MeCN-H ₂ O	BIH	>420 nm	[176]
33	[Ru(Phen) ₃] ²⁺	CO	9900	–	MeCN-H ₂ O	TEOA	~450 nm	[177]

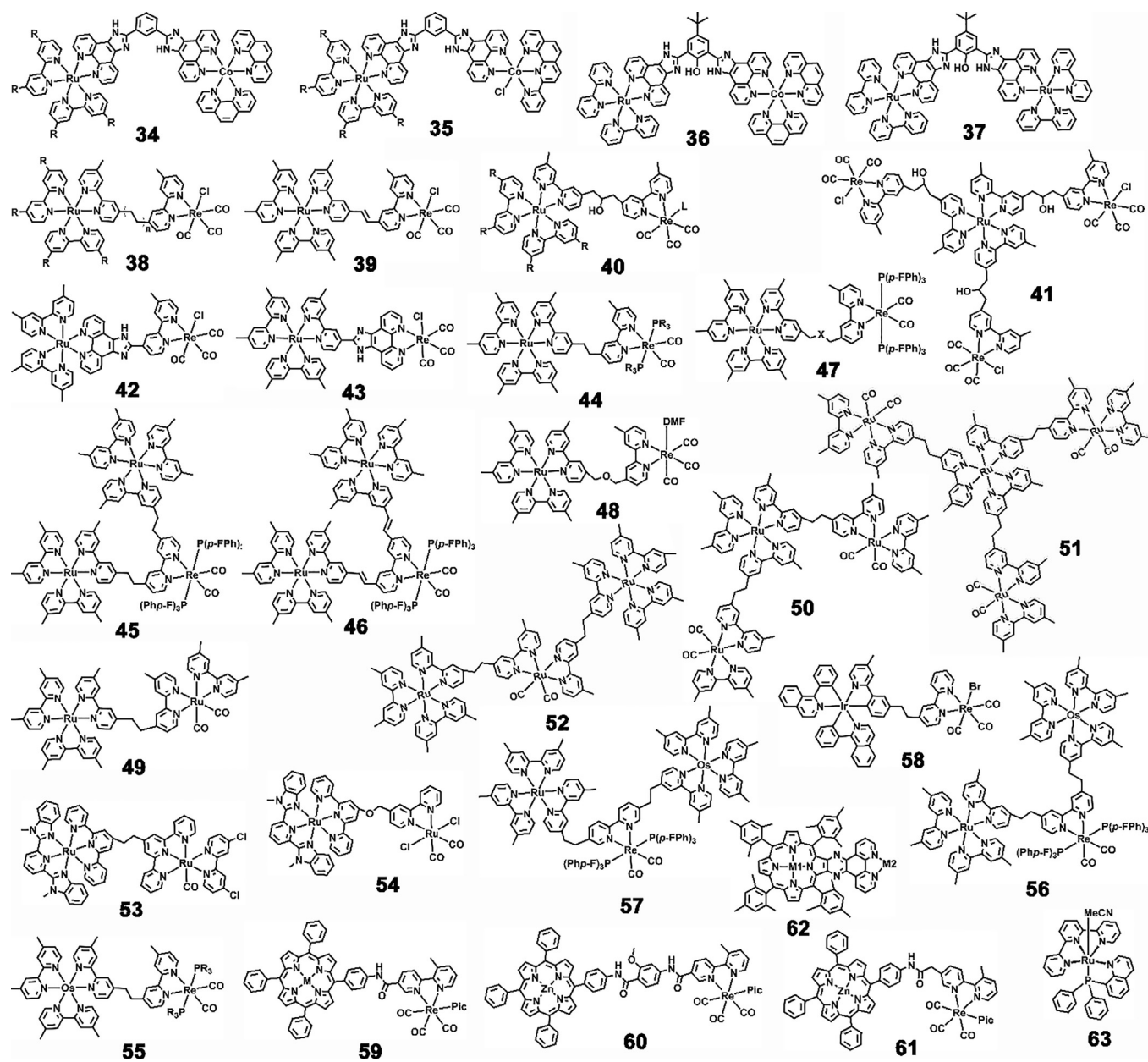
^a TON represents turn over number; QY represents quantum yield; PS represents photosensitizer; SD represents Sacrificial donor; λ represents the wavelength of the irradiation light.

investigated instead of TEOA, a neutral or acidic condition was obtained, both of HCOOH and CO were detected as reduction products. It should be noted that the production of CO and HCOOH in these photocatalytic systems gradually decreased as the formation of a black polymeric Ru precipitate [97–100]. The formation of this Ru polymer could be suppressed by using low concentration Ru catalyst or by adding excessive bpy ligand.

During the photocatalytic process, **10a** released a CO ligand and accepted two photoelectrons from photosensitizers to form the

active intermediate Ru(bpy[−])₂(CO) [101]. Tanaka et al. inferred that Ru(bpy[−])₂(CO) captures one CO₂ molecule through coordination interaction to form Ru(bpy)₂(CO)(CO₂). Thereafter, one H⁺ was added to generate the complex [Ru(bpy)₂(CO)(COOH)]⁺, where HCOOH was released by accepting two electrons. For the CO production cycle, [Ru(bpy)₂(CO)(COOH)]⁺ was also formed as an important intermediate (Fig. 3). However, [Ru(bpy)₂(CO)(COOH)]⁺ was further protonated in the CO cycle and released a water molecule, leading to the formation of **10a**. Thereafter, **10a** got

Table 3
Homogeneous supramolecular photocatalytic CO₂ reduction systems.^a



Compound	Product	TON	QY	Solvent	SD	λ	Ref.
34a; R = H	CO	51	–	MeCN	TEOA	>415 nm	[181]
34b; R = Me	CO	54	–	MeCN	TEOA	>415 nm	[181]
35a; R = H	CO	14	–	MeCN	TEOA	>415 nm	[181]
35b; R = Me	CO	2	–	MeCN	TEOA	>415 nm	[181]
36	CO	70	–	MeCN	TEOA	>415 nm	[181]
37	CO	13	–	MeCN	TEOA	>415 nm	[181]
38a; R = Me, n = 1	CO	180	–	DMF	BNAH	>500 nm	[189]
38b; R = Me, n = 2	CO	120	–	DMF	BNAH	>500 nm	[189]
38c; R = Me, n = 3	CO	120	–	DMF	BNAH	>500 nm	[189]
38d; R = H, n = 1	HCOOH	25	–	H ₂ O	Sodium ascorbate	>500 nm	[195]
38a; R = Me, n = 1	CO	130	0.13	DMF	Bi(CO ₂ H) ₃ H	>500 nm	[196]
39	CO	50	–	DMF	BNAH	>500 nm	[188]
40a; R = H, L = Cl	CO	101	0.062	DMF	BNAH	>500 nm	[183]
40b; R = Me, L = Cl	CO	170	0.12	DMF	BNAH	>500 nm	[183]
40c; R = CF ₃ , L = Cl	CO	50	–	DMF	BNAH	>500 nm	[183]
40d; R = Me, L = P(OEt) ₃	CO	232	0.21	DMF	BNAH	>500 nm	[193]
40e; R = Me, L = Py	CO	97	–	DMF	BNAH	>500 nm	[193]

(continued on next page)

Table 3 (continued)

Compound	Product	TON	QY	Solvent	SD	λ	Ref.
41	CO	240	0.093	DMF	BNAH	>500 nm	[183]
42	CO	14	–	DMF	BNAH	>500 nm	[183]
43	CO	28	–	DMF	BNAH	>500 nm	[183]
44a; R = <i>p</i> -FPh	CO	207	0.15	DMF	BNAH	>500 nm	[190]
44b; R = <i>p</i> -FPh	CO	3029	0.45	DMF	BIH	>500 nm	[190]
44c; R = Ph	CO	144	0.1	DMF	BNAH	>500 nm	[192]
44d; R = OEt	CO	27	0.1	DMF	BNAH	>500 nm	[192]
45	CO	313	–	DMF	BNAH	>500 nm	[187]
	HCOOH	85	–				
46	CO	283	–	DMF	BNAH	>500 nm	[187]
	HCOOH	100	–				
47a; X = S	CO	73	0.09	DMF	BNAH	>500 nm	[194]
47b; X = O	CO	253	0.18	DMF	BNAH	>500 nm	[194]
47c; X = CH ₂	CO	178	0.1	DMF	BNAH	>500 nm	[194]
48	CO	1000	0.4	DMF	BNAH	>500 nm	[191]
49	HCOOH	315	0.038	DMF	BNAH	>500 nm	[99]
50	HCOOH	353	0.03	DMF	BNAH	>500 nm	[99]
51	HCOOH	234	0.017	DMF	BNAH	>500 nm	[99]
52	HCOOH	562	0.041	DMF	BNAH	>500 nm	[99]
52	HCOOH	671	0.061	DMF	MeO-BNAH	>500 nm	[99]
52	HCOOH	641	0.18	DMF	BIH	>500 nm	[197]
52	HCOOH	2766	0.461	DMF	BI(OH)H	>500 nm	[197]
53	HCOOH	11	–	DMA-H ₂ O	BI(OH)H	>500 nm	[198]
	CO	134	0.021				
54	HCOOH	181	–	DMA-H ₂ O	BI(OH)H	>500 nm	[198]
	CO	10	–				
55a; R = FPh	CO	1138	0.12	DMF	BIH	>620 nm	[200]
55b; R = ClPh	CO	762	0.10	DMF	BIH	>620 nm	[200]
56	CO	3552	–	DMF	BIH	>500 nm	[201]
57	CO	4347	0.11	DMF	BIH	>500 nm	[201]
58	CO	130	–	DMF	BNAH	>500 nm	[202]
58	CO	1700	–	DMF	BIH	>500 nm	[202]
59a; M = Pd	CO	2	–	DMF	TEA	>420 nm	[204]
59b; M = Zn	CO	27	–	DMF	TEOA	>520 nm	[205]
60	CO	32	–	DMF	TEOA	>520 nm	[205]
61	CO	332	–	DMF	TEOA	>520 nm	[206]
62a; M1 = FeCl, M2 = Ru	CO	11.4	–	DMF	TEA	>305 nm	[207]
62b; M1 = Zn, M2 = Re	CO	12.8	–	DMF	TEA	>375 nm	[208]
63	CO	58	–	DMA-H ₂ O	BIH	>420 nm	[209]
63	HCOOH	14	–	DMA	TEOA	>420 nm	[209]

^a TON represents turn over number; QY represents quantum yield; PS represents photosensitizer; SD represents Sacrificial donor; λ represents the wavelength of the irradiation light.

photoelectrons from photosensitizers and released a CO molecule. On the other hand, Meyer et al. proposed that the intermediate Ru(bpy)[−](CO) was firstly protonated to form [Ru(bpy)₂(CO)H]⁺, which obtain an electron from photosensitizer to form Ru(bpy)(bpy[−])(CO)H (Fig. 3) [81]. After that, a CO₂ was inserted into the Ru-H bond to produce carboxyl complex Ru(bpy)(bpy[−])(CO)(OCHO). In the next step, Ru(bpy)(bpy[−])(CO)(OCHO) captured a photoelectron and release HCOOH. It should be noted that the unsaturated five-coordinated complex Ru(bpy)[−](CO) in both

Tanaka- and Mayer-mechanisms has not yet been directly detected.

In a biphasic liquid-condensed gas system, CO₂ was photo-reduced to both CO and HCOOH with **10a** as a photocatalyst [102]. When the CO₂ pressure increased from 10 to 150 bar, the

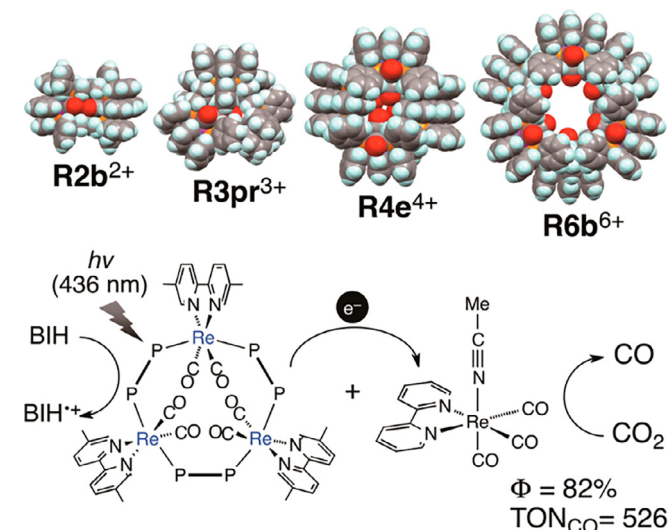


Fig. 1. A schematic diagram of the formation of Re^I(bpy)(CO)₃(R₂NC₂H₄COO) [85]. Copyright 2013 ACS®.

Fig. 2. Photocatalytic CO₂ reduction system composed of ring-shaped Re(I) complexes and compound **1d** [92]. Copyright 2013 ACS®.

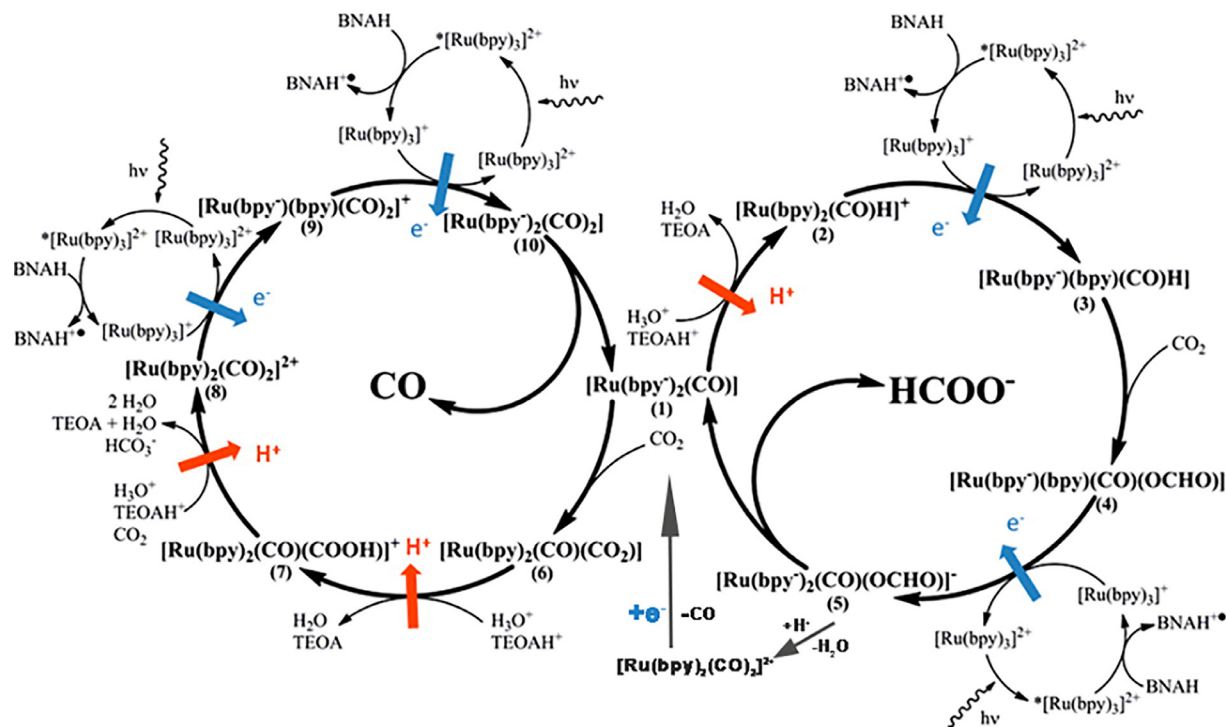


Fig. 3. The CO cycle (Tanaka-mechanism) and the HCOOH cycle (Mayer-mechanism) over $[\text{Ru}(\text{bpy})_2(\text{CO})_2]^{2+}$ [102]. Copyright 2013 ACS©.

CO production increased linearly while HCOOH production on the other hand basically unchanged. These observations mean that the Tanaka-mechanism for CO cycle and Meyer-mechanism for HCOOH cycle occurred under these conditions. Under high pressure, CO₂ molecules were more abundant and forced into the vacant coordination site of the intermediate $\text{Ru}(\text{bpy})_2(\text{CO})$. Although the Meyer-mechanism showed that the HCOOH cycle also undergoes CO₂ insertion, it was not the rate determining step. The rate-limiting step was probably the electron transfer step from $[\text{Ru}(\text{bpy})_2(\text{CO})\text{H}]^+$ to $\text{Ru}(\text{bpy})_2(\text{bpy})(\text{CO})\text{H}$ because the redox potential required to reduce the hydride complex was very negative.

$\text{Ru}(\text{bpy})(\text{CO})_2\text{Cl}_2$ type Ru complexes are also well-studied for CO₂RR [98]. When the photocatalytic CO₂RR was performed in a DMA/water solution with compound **12** as a photocatalyst, both of CO and HCOOH was obtained as the reduction product [103]. Interestingly, the HCOOH to CO ratio increased as the catalyst concentration increase. When the light intensity decreased, the HCOOH to CO ratio would also increase. In this system, a higher catalyst concentration or a lower intensity light promoted the formation of a dimeric Ru(I) complex, which is responsible for the production of HCOOH. To validate the reaction mechanism, the authors prepared a new photocatalyst compound **13**. Ru-Ru bond formation was suppressed due to the steric interaction of the mesityl groups, and then the photoreduction of CO₂ led to CO selectively. Later on, Kubiak et al. noticed a similar phenomenon in electrocatalytic CO₂RR, further confirming the hypothesis [104].

The amide groups on the 5,5'-positions of bpy ligand will affect the reduction potential of **12**, and then affect the reaction rate for photocatalytic CO₂RR (Fig. 4) [105]. Bulky moieties at the amide groups could slightly twist these groups against the bpy plane, causing a negative shift of the first reduction potential of the catalyst. The Turnover frequency (TOFs) for both of CO and HCOOH increased as reduction potential shifted to negative side until approximately -1.5 V. This work provides useful information in designing novel Ru complexes with highly photocatalytic activity towards CO₂ reduction. Later on, methyl groups are introduced

on the 4,4'-, 5,5'- or 6,6'-positions of the bpy ligands to prepare three isomeric Ru catalysts [106]. The catalytic performances of these isomeric catalysts were significantly different. With 6,6'-dmb as a ligand, CO was yielded selectively as the reduction product. However, both CO and HCOOH was produced when used 4,4'-dmb or 5,5'-dmb as ligands.

2.1.3. Os complexes

Os complexes, such as compound **17a** and **17b**, can selectively photocatalytically reduce CO₂ to CO [107,108]. With BNAH as a sacrificial reagent, TONs of 11.5 and 19.5 within 4.5 h were obtained for **17a** and **17b**, respectively. Electron-donating groups on the 4,4'-positions of bpy ligands will increase the TONs of the reduction products since electron-withdrawing groups on the 4,4'-positions will decrease the TONs. In addition, with $[\text{Ru}(\text{bpy})_3]^{2+}$ as a photosensitizer, TONs of CO will be slightly increased.

2.1.4. Ir complexes

In 2013, Sato et al. investigated $[\text{Ir}(\text{tpy})(\text{R-ppy})\text{Cl}]^{n+}$ ($\text{R} = \text{H}, \text{CH}_3$, or CF_3) as photocatalysts for photocatalytic CO₂ reduction in a MeCN/TEOA solution without any other photosensitizer [109]. When $\text{R} = \text{H}$, selectively reduction of CO₂-to-CO was observed with a TON_{CO} of 38. When methyl groups were introduced onto the ppy ligand, the photocatalytic activity of the catalyst was enhanced. A similar enhancement can be obtained by introducing anthryl group on the 4'-position of tpy ligand, with compound **18e** as a photocatalyst, a remarkable TON_{CO} up to 310 was obtained under white light LED irradiation [110]. In contrast, introducing the electron-withdrawing trifluoromethyl group will reduce their activity [109].

A mechanism was proposed with a key intermediate of hydride complex $[\text{Ir}(\text{tpy})(\text{ppy})\text{H}]^+$ (Fig. 5a) [109,111]. Firstly, **18a** was photoexcited and then quenched by sacrificial reductant to give $[\text{Ir}(\text{tpy})(\text{ppy})\text{Cl}]^+$. Another electron was injected to $[\text{Ir}(\text{tpy})(\text{ppy})\text{Cl}]^+$ with the Cl⁻ ligand replaced by H at the same time. After that, the hydride complex $[\text{Ir}(\text{tpy})(\text{ppy})\text{H}]^+$ was photoexcited and quenched by sacrificial reductant to form $[\text{Ir}(\text{tpy})(\text{ppy})\text{H}]$ to react

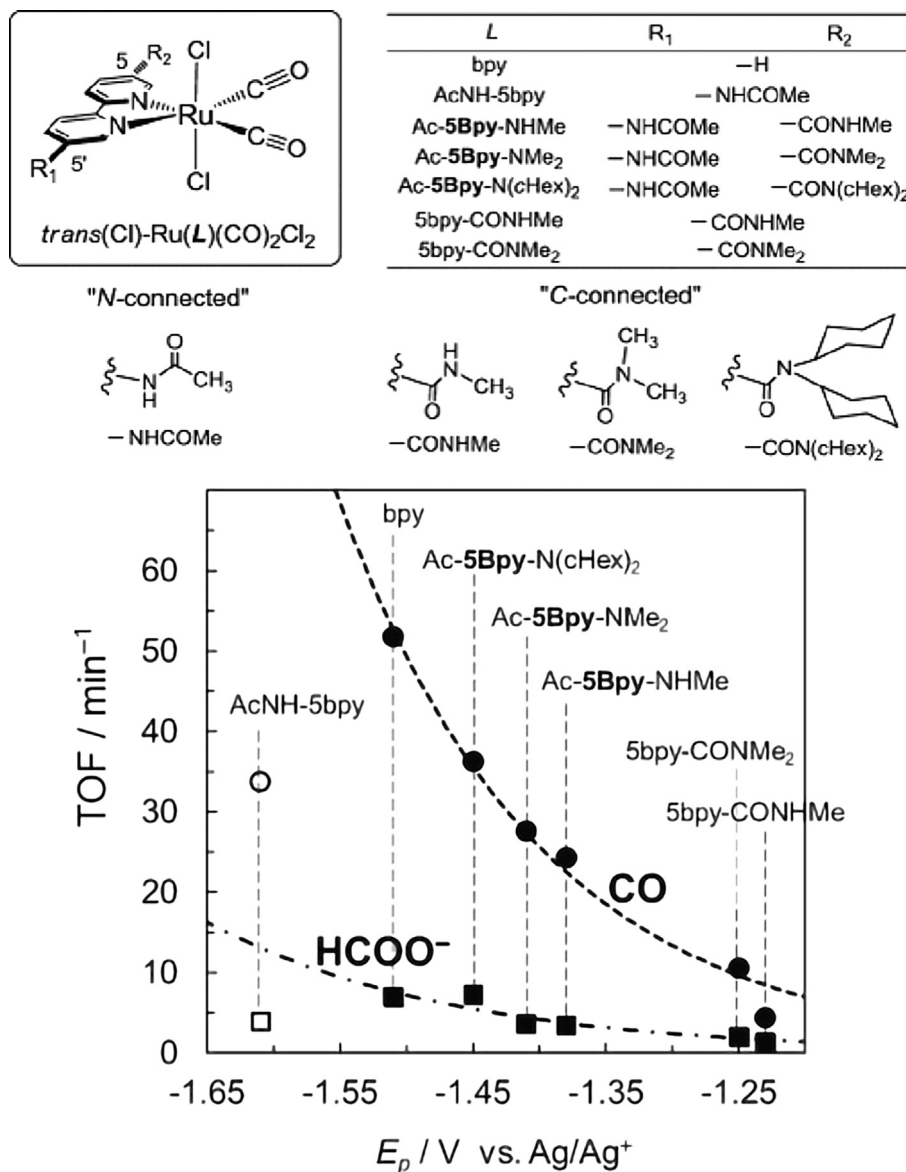


Fig. 4. Bulky amide groups affect the first reduction potential and the activity of the catalysts [105]. Copyright 2015 Wiley-VCH®.

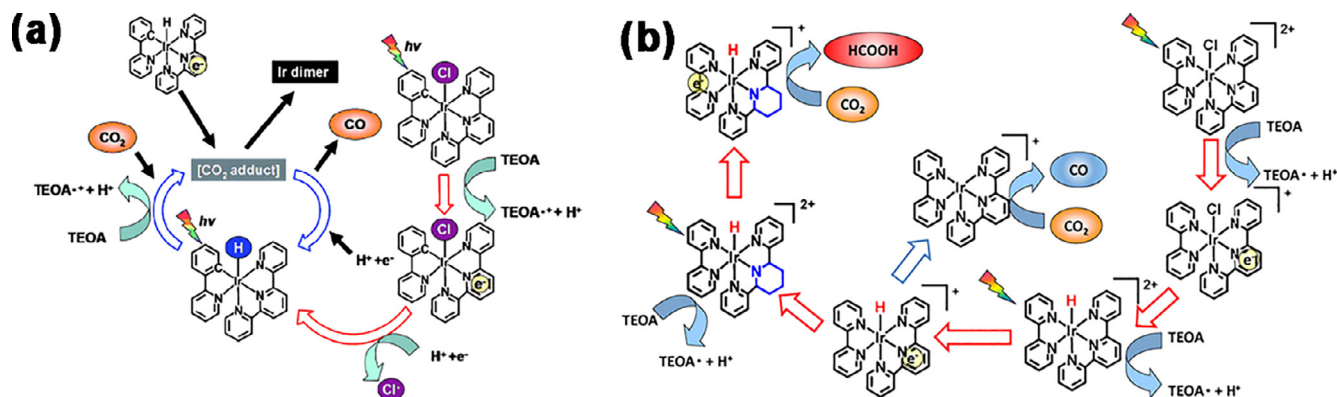


Fig. 5. Reaction mechanism of photocatalytic CO₂RR using **18a** [106] (a) and **19** [112] (b). Copyright 2018 Wiley-VCH®.

with CO₂. In the last step, an electron with a proton was injected into the CO₂ adducts to release CO. It should be noted that this mechanism was contrast to that which is proposed in Ru system.

In the case of Ru system, CO₂ is inserted into the Ru-H bond affording HCOOH. Interestingly, when using compound **19** as a photocatalyst (only change ppy to bpy), CO₂ was selectively reduced to

HCOOH under visible-light irradiation (Fig. 5b) [112]. Such a difference may be attributed to the structural change after introducing bpy ligand to replace ppy. Under the photocatalytic condition, $[\text{Ir}(\text{tpy})(\text{bpy})\text{H}]^{2+}$ was reduced to $[\text{Ir}(\text{piperidine-2,6-di-2-pyridine})(\text{bpy})\text{H}]^{2+}$, which act as the actual photocatalyst for HCOOH production.

2.2. Photocatalysts with non-noble metal center

2.2.1. Mn complexes

Compound **20a** was the first Mn complex applied as the photocatalyst for CO_2RR [113]. During the photocatalytic cycle, **20a** captured a photoelectron from the photosensitizer followed by releasing of the Br^- ligand, leading to the formation of $[\text{Mn}(\text{bpy})(\text{CO})_3]_2$ dimer. Thereafter, the $[\text{Mn}(\text{bpy})(\text{CO})_3]_2$ dimer gave radical species under photoreaction condition for the production of HCOOH [114–116]. The efficiency of the system will be reduced when DMF was instead by DMA or MeCN, and the selectivity of HCOOH production would also be reduced when MeCN was used as the solvent.

Later on, $\text{Mn}(\text{bpy})(\text{CO})_3(\text{CN})$ was applied as the photocatalyst for CO_2RR [117]. Irradiation with 470 nm light yielded both CO and HCOOH. The product distribution was also affected by the solvent. HCOOH was favor produced in DMF/TEOA while CO was favor produced in MeCN/TEOA. No Mn-Mn dimer was formed in this reaction system. During the reaction process, two single-electron-reduced species of $[\text{Mn}(\text{CN})(\text{bpy})(\text{CO})_3]^-$ generated one starting compound $\text{Mn}(\text{CN})(\text{bpy})(\text{CO})_3$ and one active intermediate $[\text{Mn}(\text{bpy})(\text{CO})_3]^-$ for CO_2 reduction. In addition, the selection of π -accepting, redox-active ligand, such as phenanthroline-5,6-dione (phenidone), would lead to other different reaction mechanisms [118].

Although catalysts investigated in the above systems are constructed with abundant manganese, a photosensitizer based on noble-metal Ru is required for CO_2 reduction. It is better to construct a reaction system that avoid using these noble photosensitizers. In this perspective, Bian et al. developed a system with compound **22** as a catalyst and zinc tetraphenylporphyrin (Zn-TPP) as a photosensitizer for photocatalytic CO_2RR [119]. The reaction was performed in a mixed solution of MeCN/ H_2O /TEA giving CO and HCOOH as reduction products. The TONs for both CO and HCOOH increased as the concentration ratio of Mn/Zn increase.

2.2.2. Fe complexes

In this section, Fe based photocatalysts such as Fe-polypyridine, Fe-carbonyl and Fe-porphyrin complexes will be discussed for CO_2RR . Lau and coworkers reported the photocatalytic activity of a Fe complex **23a** bearing pentadentate N_5 ligand [120]. CO_2 was major reduced to HCOOH with a $[\text{Ir}(\text{ppy})_3]^+$ photosensitizer. An isomorphous structure of Co (**23b**) has been investigated as CO_2 reduction photocatalyst, but selectively generate CO. Later on, they developed compounds **24a** and **24b** as photocatalysts for CO_2RR [121]. However, unlike compounds **23a**, CO was obtained as a major product over both Co ($\text{TON}_{\text{CO}} = 2660$) and Fe ($\text{TON}_{\text{CO}} > 3000$) complexes with $[\text{Ru}(\text{bpy})_3]^{2+}$ as a photosensitizer. It is notable that TONs as high as 790 and 1365 are also obtained for the Co and Fe catalyst, respectively, even with purpurin as a photosensitizer.

Ishitani et al. developed a photocatalytic CO_2 reduction system with only abundant metals, wherein compound **25** was used as the catalyst and heteroleptic Cu^{I} complex was used as the photosensitizer (Fig. 6) [122]. CO was obtained as a major product under visible-light irradiation in a MeCN/TEOA solution with BIH as a sacrificial donor. When CuI (as shown in Fig. 6) was used as a photosensitizer, the best efficiency was obtained with TONs = 273 and QY = 6.7%. In this dimeric structure, Cu^{I} center is surrounded by one dmp moiety and two phosphine moieties from two different

tetradentate ligands. Such coordination characters improved the stability of the reduced Cu^{I} complex, and then improved the photocatalytic activity of the system. Later on, they created a much more efficient photocatalytic CO_2RR system by using CuI as photosensitizer and Mn^{I} complex as the catalyst [123]. When $\text{Mn}(\text{OME}_2\text{-bpy})(\text{CO})_3\text{Br}$ was used as photocatalyst, TON_{CO} as high as 1300 with 95% selectivity was obtained. The quantum yield was also increased up to 0.57.

Beller et al. reported the photocatalytic CO_2 -to-CO reduction by using $\text{Fe}_3(\text{CO})_{12}$ as a pre-catalyst, $[\text{Ru}(\text{bpy})_3]^{2+}$ or $[\text{Ir}(\text{ppy})_2(\text{bpy})]^+$ as a photosensitizer, and TEOA as a sacrificial reagent [124]. Interestingly, the addition of excessive bpy would improve the CO yields. Further study with *in situ* FTIR technique showed that the $[\text{Fe}(\text{CO})_3(\text{bpy})]$ was formed as the actual catalyst. Later on, they prepared a series of (cyclopentadienone)iron-tricarbonyl complexes as photocatalysts for CO_2RR [125]. A TON_{CO} of as high as 600 was obtained with $(1,3\text{-(SiMe}_3)_2\text{TIO})\text{Fe}(\text{CO})_3$ as a photocatalyst and $[\text{Ir}(\text{dF}(\text{CF}_3)\text{ppy})_2(\text{dtbbpy})]$ as a photosensitizer. In addition, they further developed a photosensitive homoleptic Cu^{I} complex to replace the Ir complex [126]. The highest performance for CO_2 -to-CO reduction was achieved in 99% selectivity with a TONs of 487 under visible-light irradiation.

Fe porphyrins have also been developed as the photocatalysts for CO_2RR [127]. In the early stages, the efficiency of Fe porphyrin system was low, and the photochemical decomposition of Fe porphyrin molecule indeed occurred. *p*-terphenyl was introduced to compound **26** to overcome these problems [128]. The photoexcited *p*-terphenyl could reduce both of the Fe^{II} species and Fe^{I} species to form the Fe^0 species. Then, the performance of the Fe porphyrin system was increased by 10 times. In addition, the corresponding Co porphyrin system was also investigated for CO_2RR and showed a higher performance than Fe porphyrin system [128,129].

Robert et al. introduced -OH groups on the *o*-positions of the phenyl groups of compound **26** to generate compound **27** [130]. Irradiation of the MeCN/TEA mixed solution containing **27** as a catalyst gave CO with an 85% selectivity. They proposed that the introduced -OH groups can stabilize the CO_2 adducts via hydrogen bonding interactions between the -OH groups and the adducted CO_2 molecule. Later on, they further introduced photosensitizers into the photocatalytic system to prevent the degradation of the porphyrin rings under UV-light irradiation [131]. They paid attention to $[\text{Ir}(\text{ppy})_3]^+$, which is widely used as a photosensitizer in photochemical reactions. When $[\text{Ir}(\text{ppy})_3]^+$ was added into the MeCN/TEA solution of **27**, a TON_{CO} of 140 was obtained with an improved selectivity of 93% under visible-light irradiation. In addition, 9-cyanoanthracene (9-CNA) was also investigated as a photosensitizer in this system. Visible-light irradiation at >400 nm led to CO evolution with a selectivity of 100% and a TONs of 60. During the CO production cycle, 9-CNA was excited and reductively quenched by TEA to generate the anion radical $9\text{-CNA}^{\cdot-}$, which reacted with **27** to produce the active catalytic species.

Under visible-light irradiation, compound **28**, with trimethylamine cation groups on the *p*-positions of the phenyl groups of **26**, could also act as the photocatalyst to reduce CO_2 to CO (100% selectivity) in a MeCN solution of BIH without any other photosensitizer [132]. When purpurin was used as a photosensitizer, the water-soluble **28** could photocatalytically reduce CO_2 to CO in a MeCN/ H_2O solution (1:9 v/v) of TEA giving a TON_{CO} of 120 and a selectivity of 95% [133]. In this system, TEA gave slightly better results than TEOA and EDTA. Thereafter, they tried to develop the efficiency of the photocatalytic system by investigating other photosensitizers. Very interestingly, they found that the **28** in conjunction with $[\text{Ir}(\text{ppy})_3]^+$ and TEA could catalyze the eight-electron reduction of CO_2 to generate CH_4 (Fig. 7) [134]. CH_4 was generated via a two-pot procedure in a selectivity up to 82% and a QY of 0.18%. They proposed that the high reduction property of [Ir

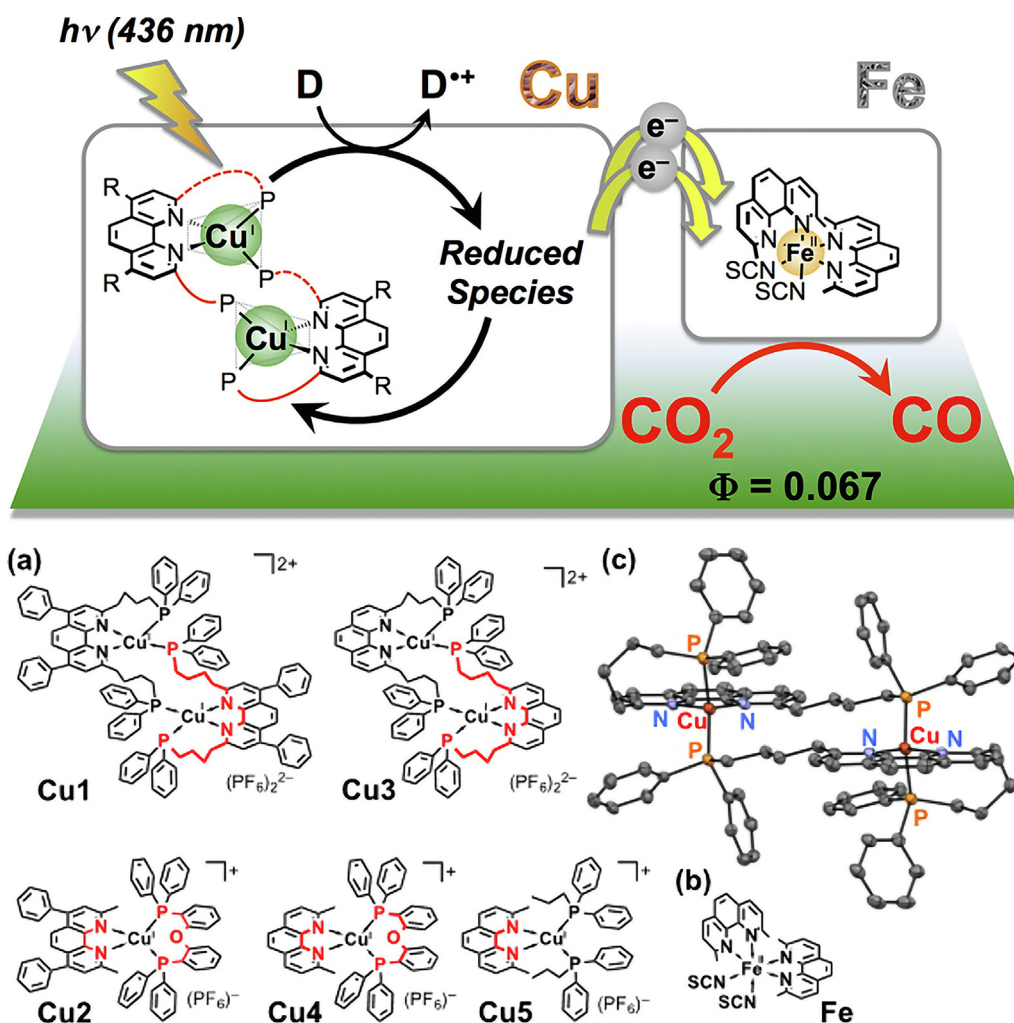


Fig. 6. Photocatalytic CO_2 reduction system with **25** as a catalyst and Cu^I complex as a photosensitizer [122]. Copyright 2016 ACS.

(ppy)₃]⁺ is very important. When [Ir(ppy)₃]⁺ was replaced by [Ru(bpy)₃]²⁺, only CO and H₂ were obtained. This may be attributed to that the less reducing Ru complex was not able to trigger the carbonyl reduction from the Fe^{II}-CO adduct. When [Ir(ppy)₂(bpy)]⁺

was investigated as a photosensitizer, The selectivity of CH₄ reduced to about 10% while the selectivity for CO increased to about 57% under similar condition [135]. When the photocatalytic experiment was performed in a mixed solution of MeCN/H₂O (7:3 V/V), the selectivity for CO further increased to 75% [134]. However, the stability of the catalytic system remains a weakness attributed to the instability of the photosensitizer. Very recently, they use a phenoxazine-based molecule with suitable redox properties as the photosensitizer and **28** as the catalyst, CO_2 was reduced to CO and CH₄ with TONs of 149 and 29, respectively [136]. It is the first example of a molecular system using earth-abundant elements to realize the eight-electron reduction of CO_2 -to-CH₄.

In 2018, Weiss et al. developed modified CuInS₂/ZnS quantum dot (QD) as the photosensitizer for CO_2 -to-CO reduction in water with compound **28** as the photocatalyst [137]. This system achieved a TON_{CO} of 450 and a selectivity of 99%. The high efficiency of this photochemical system was due to the electrostatic interaction between QDs and **28**.

2.2.3. Co complexes

Homogeneous Co complexes, such as Co polypyridyl complexes [120,121,138–142], Co macrocycle complexes [143–158], Co Tripodal complexes [159–168], are promising candidate photocatalysts for CO_2 RR. CoCl₂ was first investigated as the co-catalyst for photochemical CO_2 RR [138]. Both of H₂ and CO was generated as

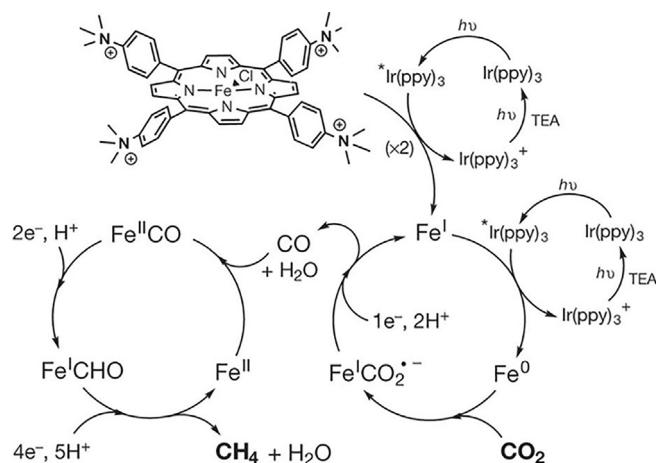


Fig. 7. The proposed mechanism for CO_2 -to-CH₄ reduction using compound **28** as a catalyst and [Ir(ppy)₃]⁺ as a photosensitizer [134]. Copyright 2017 Nature Publisher.

reduction products under visible-light irradiation. When free bpy ligands were added to the reaction system, the production of CO was significantly decreased, but the production of H₂ was increased. In these systems, Co^I species were *in situ* formed as active intermediates for either CO₂ or H₂O reduction [138,139].

Wang and Che et al. reported a Co complex (C1 in Fig. 8a) with chelating N₄ ligand for efficient CO₂-to-CO reduction [140]. In this photocatalyst, the *cis*-geometry and chloride ligands were very important. The remaining adjacent chloride ligand on the *cis*-position could help to stabilize the CO₂ adduct and then facilitated the protonation and the second electron transfer. Later on, another two complexes [Co^{II}(MPCA)Cl₂] and [Co^{II}(MPCA)Br₂] were prepared for photocatalytic CO₂RR (Fig. 8b) [141]. It is found that the rate of CO production over Br coordinated complex was faster, but the stability of Cl coordinated complex was better.

Tetraaza-macrocyclic Co complexes, such as [Co^{II}cyclam]²⁺ and their derivatives, have been widely studied for CO₂RR [143–155]. The reduction products were detected to be CO and HCOOH. Fujita and collaborators made many efforts to propose the mechanism of CO₂ reduction over these macrocyclic Co complexes. [Co^{II}(Me₆-cyclam-diene)]²⁺ and [Co^{II}(Me₂-cyclam-diene)]²⁺ were firstly prepared as catalysts in their studies [150]. In this system, Co²⁺ ion in the catalyst was reduced by excited photosensitizer to Co⁺ and then captured a CO₂ molecule to form 5-coordinate form adduct. After that, charge transfer from the Co center to the coordinated CO₂ was triggered by coordinating MeCN as the sixth ligand. This 6-coordinate form intermediate gave CO as the reduction product. Later on, Frei and coworkers obtained the Co-CO₂ adducts by using [Co^{II}N₄H]²⁺ as the photocatalyst [154,155]. It was the first observation of the two-electron-reduced intermediate of molecule catalyst for CO₂-to-CO reduction.

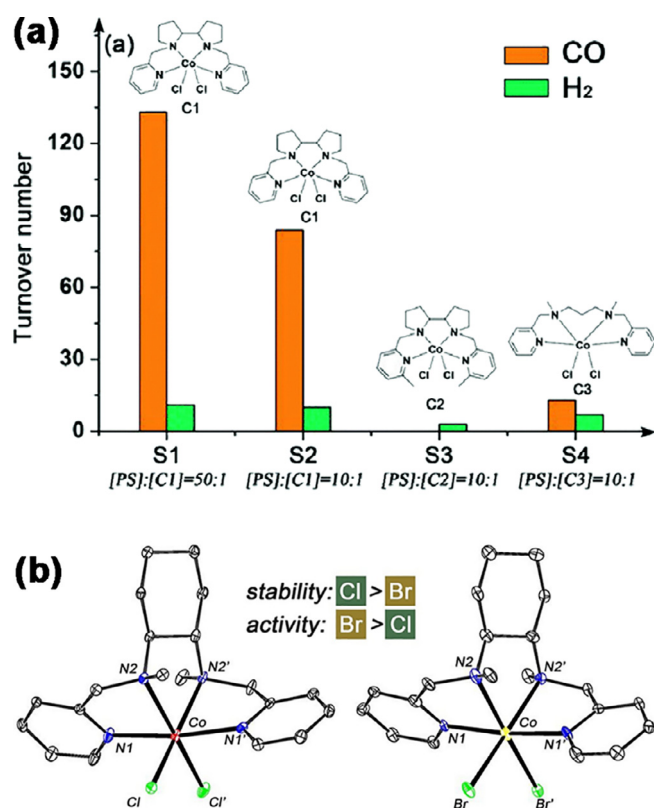


Fig. 8. (a) Photocatalytic reduction of CO₂-to-CO over different Co complexes [140]. Copyright 2016 RSC. (b) CO generation rate over [Co^{II}(MPCA)Br₂] was faster, but the stability of [Co^{II}(MPCA)Cl₂] was better [141]. Copyright 2018 Elsevier.

Chan et al. reported that [Co^{II}(TPA)Cl]⁺ could be performed as a highly efficient catalyst for photocatalytic CO₂ reduction [159]. CO was detected as a major reduction product with a [Ir(ppy)₃]⁺ photosensitizer. When enhanced the fluorescence property and stability of the Ir photosensitizer, [Co^{II}(TPA)Cl]²⁺ would give higher TON_{CO} under a similar reaction condition [160]. In contrast, no CO was produced when using the classic [Ru(bpy)₃]²⁺ photosensitizer. During the photocatalytic cycle, a [Co^I(TPA)]⁺ species was generated by adding one electron and then captured a CO₂ molecule. The coordinated anions of Co-TPA complex also play a discernible effect on their catalytic performance [161]. It was because that coordinated anion could affect the stability of [Co-COOH] intermediate. Later on, Lu and collaborators replaced the pyridyl group of TPA with less basic quinolyl group [162]. It is found that the replacement of the pyridyl groups with quinolyl groups would cause the positive shift of the Co^{III}/reduction waves, indicating Co^{III}/reduction became easier. When two pyridyl groups were replaced with quinolyl groups, [Co(BQPA)Cl] shows the highest catalytic activity for CO₂ reduction, giving a TON_{CO} up to 10,650 (12 h) and almost 100% selectivity to CO.

Later on, Lu et al. reported a dinuclear cobalt cryptate, [Co₂(OH)L₁](ClO₄)₃, for the photocatalytic reduction of CO₂-to-CO (Fig. 9a) [163]. When [Co₂(OH)L₁](ClO₄)₃ was used as the catalyst, CO was produced as a major reduction product (98% selectivity) with a TONs as high as 16896. However, when the corresponding mononuclear Co complex [CoL₂(OH)](ClO₄) was used as the photocatalyst, a much lower TONs of 1600 with a selectivity of only 85% for CO was obtained. The high catalytic activity of dinuclear [Co₂(-OH)L₁]³⁺ was attributed to the short distance of Co...Co (about 5.791(2) Å) in the structure (Fig. 9b). During the catalytic reaction, one Co ion acted as the catalytic site to reduce CO₂, and the other Co ion served as the assistant site to break the C-O bonds to produce CO. Later on, [Co₂(OH)L₁]⁴⁺ was used to assemble with negative water-soluble CdS through electrostatic interactions [164]. The electrostatic assembled hybrids can efficiently catalyze CO₂-to-CO reduction with a selectivity of 95% and a large TON of 1380 in a fully aqueous solution. Very recently, two different metal ions Zn^{II} and Co^{II} were introduced into the cage of L₁ at the same time [165]. It's very interesting that the mixed bimetallic complex shows a TON_{CO} as high as 65000, which is 4- and 19-fold higher than that of [Co₂(OH)L₁](ClO₄)₃ and [Zn₂(OH)L₁](ClO₄)₃, respectively. The enhanced photocatalytic properties were attributed to the dinuclear metal synergistic catalysis effect between Zn^{II} and Co^{II}.

On the other hand, Lu et al. also studied the conjugation effect by using the mononuclear Co complex as a model (Fig. 9c) [167]. When phenyl group in L₂ was replaced by 9'-anthrylmethyl group and 1'-naphthylmethyl group, respectively, the resulting complexes [CoL₃(OH)](ClO₄) and [CoL₄(OH)](ClO₄) showed greatly higher efficiency for CO₂-to-CO reduction. In these systems, the extended conjugation substituent groups would reduce the reduction potential of the Co^{II} catalyst, and then boost the intermolecular electron transfer. However, a higher steric hindrance of substituent groups would hinder CO₂ binding to catalytic center Co^{II} and might reduce the efficiency of the photocatalytic system. In addition, when the phenyl groups in L₂ were replaced by isopropyl groups, the synthesized catalyst [CoL₅(MeCN)](ClO₄)₂ showed a lower reduction potential and displayed 7-times higher activity for CO₂-to-CO reduction than [CoL₂(OH)]ClO₄ (Fig. 9d) [168].

2.2.4. Ni complexes

Spreer et al. firstly reported the photocatalytic activity of [Ni(-cyclam)]²⁺ for CO₂RR [169]. CO (TON = 4.8) was obtained as the major product in a CO₂-saturated aqueous solution with a [Ru(bpy)₃]²⁺ photosensitizer. A Ni-H species was proposed as the pivotal intermediate for CO generation. On the other hand, when [Ni

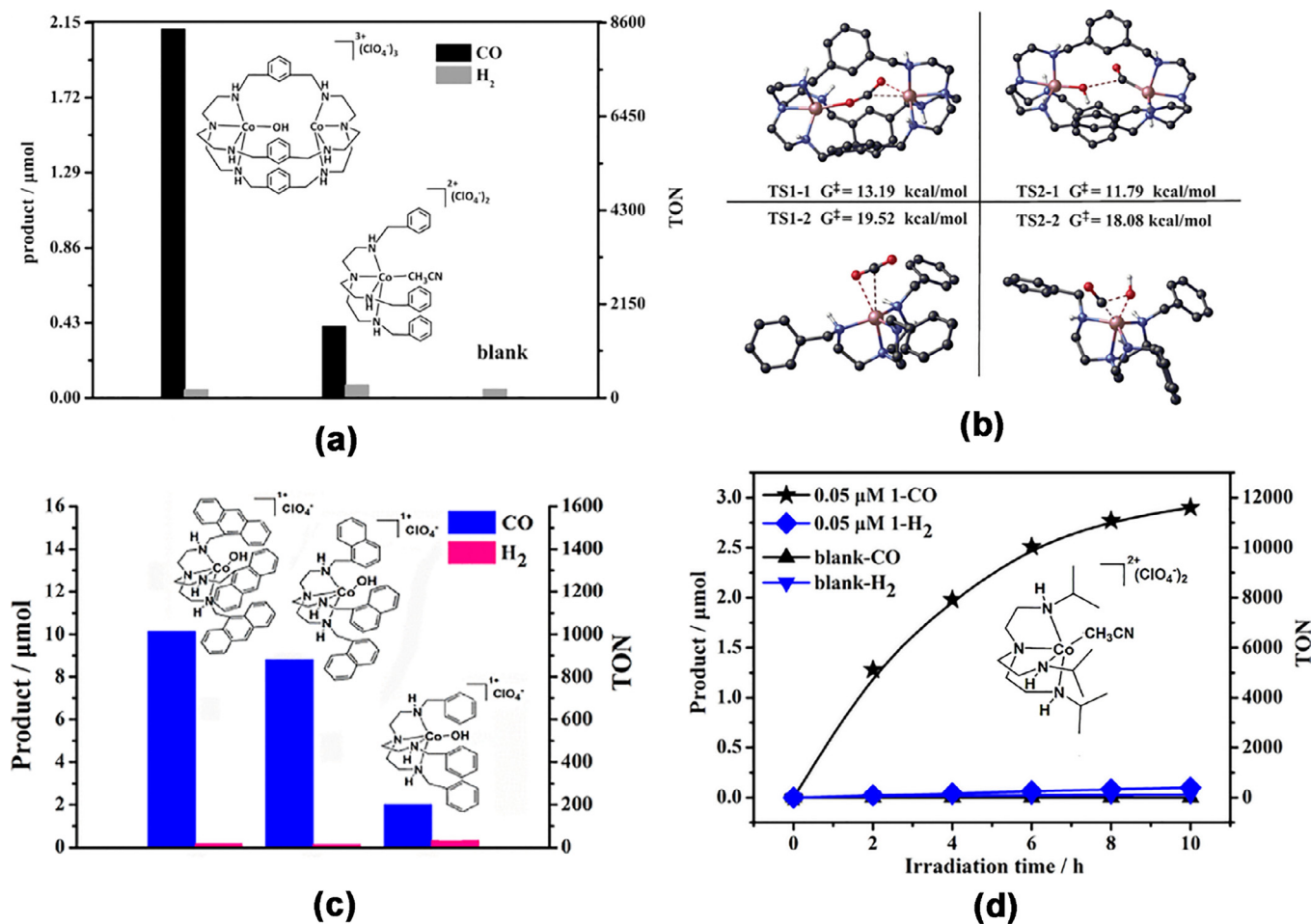


Fig. 9. (a) $[\text{Co}_2(\text{OH})\text{L}_1](\text{ClO}_4)_3$ shows much higher activity than $[\text{CoL}_2(\text{OH})](\text{ClO}_4)_2$ [163]. (b) The energy barriers of the intermediates for $[\text{Co}_2(\text{OH})\text{L}_1](\text{ClO}_4)_3$ and $[\text{CoL}_2(\text{OH})](\text{ClO}_4)_2$ [163]. Copyright 2017 Wiley-VCH. (c) The extended conjugation substituent will enhance the catalytic performance of mononuclear Co complex [167]. Copyright 2018 ACS. (d) photocatalytic CO_2 -to-CO reduction over $[\text{CoL}_5(\text{MeCN})](\text{ClO}_4)_2$ [168]. Copyright 2018 Wiley-VCH.

$(12\text{-aneN}_4)^{2+}$ was used as the photocatalyst, which showed a similar structure with $[\text{Ni}(\text{cyclam})]^{2+}$ (cyclam was also known as 14-ane N_4), CO_2 was reduced to both CO and HCOOH in a CO_2 -saturated aqueous solution [170]. When the photocatalytic CO_2 reduction was performed in a biphasic water-supercritical CO_2 system still with $[\text{Ni}(\text{cyclam})]^{2+}$ as the catalyst [171]. The introduction of the water-supercritical CO_2 interface provided a suitable reaction medium, which intimately linked the adsorption, CO_2 binding, and protonation of intermediates. Thus, this system showed a much higher efficiency towards CO production.

The photocatalytic activities of bi-macrocyclic Ni^{II} complexes for CO_2RR were also studied [172]. For comparison, photocatalytic activities of six different macrocyclic Ni complexes were investigated. When $[\text{Ni}_2(6,6'\text{-Bi}(\text{Me}_2\text{-cyclam}))]^{4+}$ was used as a photocatalyst, the production of CO was 6.8 times higher than that produced by corresponding mono-macrocyclic Ni complex. In this system, both the dimeric structure with saturated macrocycles and the presence of axial methyl groups were important for constructing high performance. $[\text{Ni}_2(6,6'\text{-bicyclam})]^{4+}$, which has the same bi-macrocyclic skeleton as $[\text{Ni}_2(6,6'\text{-bi}(\text{Me}_2\text{-cyclam}))]^{4+}$ but without the methyl groups, generated less amount of CO than the corresponding mono-macrocyclic Ni complex.

Later on, Chang et al. reported a series of Ni^{II} complexes based on distorted square-planar tetradentate ligands [173]. With the lowest overpotential for CO_2 reduction ($E_{\text{onset}} = -1.20\text{ V}$), compound **29** afforded a TON_{CO} as high as 98 000 within 7 h for CO_2 -

to-CO reduction. A trace amount of CH_4 and C_2H_4 was also detected since no H_2 was observed. Later on, a Ni complex **30** based on the S_2N_2 -type tetradentate ligand was reported for CO_2 -to-CO reduction [174]. With $[\text{Ru}(\text{bpy})_3]^{2+}$ as a photosensitizer, a TON_{CO} over 700 with high selectivity of >99% was obtained. Recently, Papish et al. reported a new Ni complex **31** with C-N-C pincer ligands [175]. When introducing the π electron donor group (O^-) on the *para*-position of pyridine, the resulting Ni complex can be protonated or deprotonated reversibly to switch on or off the photocatalytic CO_2 reduction performance. The $-\text{OH}$ substituent appears essential for catalysis. The Ni complex without this $-\text{OH}$ group almost shows no activity toward photochemical CO_2 reduction.

2.2.5. Cu complexes

Although copper is abundant elements in the earth and has been widely used as catalysts, molecular Cu complexes are rarely applied as catalysts for photocatalytic CO_2RR . Until 2017, Leung, Lau and Robert et al. firstly reported CO_2 photoreduction by using Cu^{II} complex **32** as a catalyst [176]. CO was detected as the major reduction product with a trace amount of HCOOH . It is notable that both the yield and formation rate for CO can be greatly enhanced by adding a few amounts of water. An optimum CO yield of 31.2 μmol ($\text{TON}_{\text{CO}} = 12400$) was observed with 3% H_2O . Later on, Lu and coworkers reported another Cu^{II} complex **33** for CO_2RR [177]. A high TON_{CO} of 9900 in 10 h and a high CO selectivity of 98% was obtained in the mixed solvent of MeCN/water.

2.3. Supramolecular photocatalysts

In the supramolecular photocatalytic system, the two functional units (catalytic unit and photosensitive unit) are directly bridged through covalent bonds. Ru complexes are firstly used as photosensitive units in the supramolecular photocatalysts. However, the Ru sensitizers face the shortage of instability under reaction condition and relatively narrow visible-light absorption range (usually < 560 nm). Thus, other photosensitive units, such as $[\text{Ir}(\text{ppy})_3]^+$, $[\text{Os}(\text{bpy})_3]^{2+}$ and porphyrins, were also investigated.

2.3.1. Ru unit as the photosensitizer

Supramolecular photocatalysts with Ru-Ni or Ru-Co bimetal centers have been studied for CO_2 RR since 1992 [62]. In these photocatalysts, a Ru photosensitive unit and a Ni or Co catalytic unit were directly connected to each other with covalent bonds. In the early years, these supramolecular photocatalysts do not exhibit much photocatalytic activity for CO_2 RR [62,178–180]. In 2017, Fontecave et al. reported a series of Ru-Co dinuclear complexes as efficient photocatalysts for CO_2 reduction [181]. The highest TON_{CO} value was obtained as 70 within 16 h. A drawback of these systems is their instability due to, for example, the photodegradation of the Ru-based photosensitive unit.

Ru-Re supramolecular photocatalysts with Ru photosensitive units and Re catalytic units have been investigated to construct a highly efficient photochemical system for CO_2 reduction [182–187]. The first Ru-Re photocatalyst for CO_2 RR was reported by Ishitani et al. in 2005 [183]. They prepared a series of Ru-Re bimetal complexes by bridging different Ru units and $\text{Re}(\text{Me-bpy})(\text{CO})_3\text{Cl}$ unit via a $-\text{CH}_2\text{CH}(\text{OH})\text{CH}_2-$ chain. With $[\text{Ru}(\text{dmb})_3]^{2+}$ as a photosensitive unit, CO was produced with a high TONs of 170, which was much higher than those of the corresponding multimolecular system ($\text{TON}_{\text{CO}} = 101$). When methyl groups on the Ru units were changed to $-\text{CF}_3$ or H, much lower photocatalytic activity was obtained ($\text{TON}_{\text{CO}} = 3$ for $-\text{CF}_3$ and $\text{TON}_{\text{CO}} = 50$ for H). The performance degradation was attributed to the compatibility of reduction potential between the photoexcited Ru unit and Re unit. In the highly efficient supramolecular system, the reduction potential of the photosensitive unit should be equal to and more negative than that of the catalytic unit. In addition, the conjugated linker should be avoided. When the conjugated phenanthroline-imidazolyl was investigated as a bridging ligand instead of $-\text{CH}_2\text{CH}(\text{OH})\text{CH}_2-$, the reducing power of the Re intermediate was lowered, then photocatalytic efficiency became lower. A similar conclusion was also obtained by Fu and coworkers [188]. Including the above-mentioned influence factors, the impacts of the length of the bridging alkyl chain [189], electron donor [190] and the peripheral ligand of the Re unit [191–193] have also been studied. Similar to the case using **1d** as the photocatalyst, Ru-Re complexes also can be converted into TEOA-adducted complexes in the mixed solution of DMF/TEOA [191,194].

It is very important to develop water as the solvent or electron donor in photocatalytic CO_2 RR because it is environmentally friendly and economically viable. Ishitani et al. reported photocatalytic CO_2 -to-HCOOH reduction ($\text{TON}_{\text{HCOOH}} = 25$) in an aqueous solution containing Ru-Re complex as a photocatalyst and ascorbate as an electron donor (Fig. 10a) [195]. It should be noted that the production of this aqueous system is significantly different while the Re based catalysts usually selectively produce CO as previously described. Later on, when $\text{BI}(\text{CO}_2\text{H})\text{H}$ was developed as a sacrificial reagent with $[\text{Ru}(4,4'\text{-dmb})_3]^{2+}$ as a sensitive unit, CO_2 -to-CO reduction ($\text{TON}_{\text{CO}} = 130$) was obtained in an aqueous solution at pH = 9.8 (Fig. 10b) [196].

The Ru-Ru supramolecular photocatalysts with $[\text{Ru}(\text{dmb})_3]^{2+}$ as a photosensitive unit and $\text{Ru}(\text{dmb})_2(\text{CO})_2$ as a catalytic unit were also studied for CO_2 RR [99]. HCOOH was the major product when

DMF/TEOA was used as a solvent and BNAH was used as an electron donor. The system with dinuclear Ru-Ru complex **49** shows much higher performance than the corresponding multimolecular system. Furthermore, a trinuclear Ru-Ru complex **52** with two sensitive units and one catalytic unit showed a higher photocatalytic activity than **49**. In addition, the photocatalytic activity of **52** could be further improved ($\text{TON}_{\text{HCOOH}} = 2766$) by utilizing $\text{BI}(\text{OH})\text{H}$ as sacrificial reagent [197]. In these supramolecular systems, black Ru polymers, which is expected to lower the photocatalytic performance of the reaction system, were not formed [198].

Recently, Ishitani et al. firstly applied the Rh-based supramolecular photocatalysts for CO_2 RR, which consisted of $[\text{Ru}(\text{dmb})_3]^{2+}$ as a photosensitive unit and $[\text{Rh}(\text{dmb})(\text{Cp}^*)\text{Cl}]^+$ as a catalytic unit [199]. CO_2 was reduced to HCOOH with 79% selectivity, which was much higher than that of the corresponding multimolecular system (only 28% selectivity for HCOOH).

2.3.2. Os and Ir unit as the photosensitizer

$[\text{Os}(5,5'\text{-dmb})_3]^{2+}$ was used as a photosensitive unit because its strong singlet-to-triplet absorption band made it absorb long wavelengths of visible-light (up to 730 nm) [200]. Under the visible-light (>620 nm) irradiation, Os-Re complex **55a** selectively reduce CO_2 to CO with a $\text{TON}_{\text{CO}} = 1138$. The corresponding Ru-Re complex could not produce CO at all under the same reaction conditions. In 2018, Ishitani and Yamazaki reported two trinuclear Os-Re-Ru complexes **56** and **57** with one $[\text{Os}(5,5'\text{-dmb})_3]^{2+}$ photosensitive unit, one $[\text{Ru}(4,4'\text{-dmb})_3]^{2+}$ photosensitive unit and one $[\text{Re}(\text{bpy})(\text{CO})_2\{\text{P}(\text{PhF})_3\}_2]^+$ catalytic unit, respectively [201]. Both of **56** and **57** could absorb a wide range of visible-light and selectively catalyze CO_2 -to-CO reduction. The highest TONs of CO formation was observed up to 4347 in the mixed solution of DMA/TEOA with BIH as a sacrificial reagent.

In 2016, an Ir-Re supramolecular photocatalyst **58** was reported with a $[\text{Ir}(\text{piq})_2(\text{dmb})]^+$ sensitive unit and a $\text{Re}(\text{dmb})(\text{CO})_3\text{Br}$ catalytic unit [202]. Compound **58** could reduce CO_2 to CO with a high TON_{CO} of 1700 and a high selectivity of >99%. Although no ligand-substituted was detected at Ir unit, the isoquinoline moieties would be hydrogenated after long-time irradiation.

2.3.3. Porphyrin unit as the photosensitizer

In the early stages, the efficiency of the porphyrin-sensitized supramolecular photocatalyst was low and even gave lower TONs than the corresponding multimolecular system [203–205]. It is because that the subsequent back-electron transfer from the excited catalytic unit to the metalloporphyrin unit lowered their catalytic ability. Thereafter, a methylene group was inserted between the $-\text{NHCO}-$ bridge and the Re unit, and the activity of the modified catalyst was fully improved [206]. In addition, the catalytic activities of the porphyrin-sensitized supramolecular catalysts were easily affected by the wavelength of the irradiated light. When a cutoff filter ($\lambda > 375$ nm) was used, the activities of these catalysts were substantially reduced [207,208].

Based on the above discussion, the efficient supramolecular photocatalysts should contain these characters. (1) The photosensitizer unit should have relatively strong visible-light absorption with high stability. (2) The reduction potential of the excited sensitizers should be negative enough to donate electrons to the catalytic unit. (3) A non-conjugation linker with suitable length should be used. (4) Of course, a high active catalytic unit is also very important.

In both cases of the multimolecular system and the supramolecular system, photoelectrons are required to transfer from the photosensitive unit to the catalytic unit. Therefore, the catalytic performance of the system is usually affected by the efficiency of this electron transfer process. Very recently, a new type Ru molecule **63** was designed with both photosensitive and catalytic

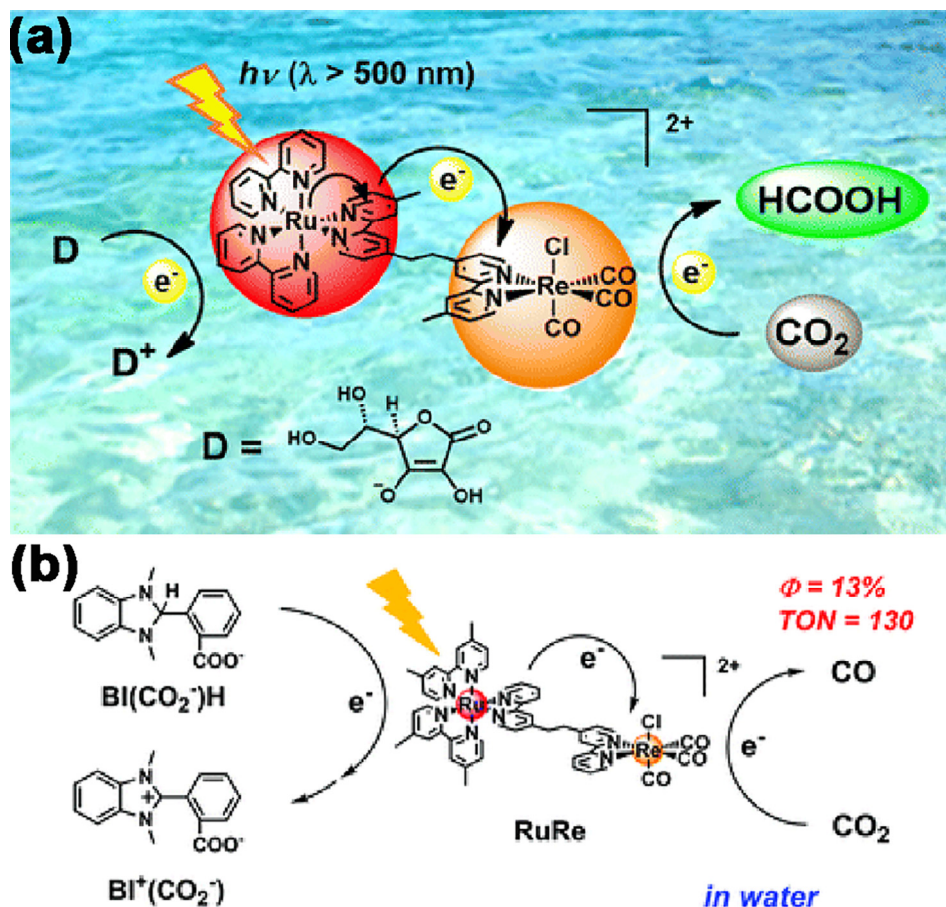


Fig. 10. (a) CO₂ was reduced to HCOOH in water containing ascorbate as an electron donor [195]. Copyright 2015 ACS©. (b) CO₂ was reduced to CO in water containing BI (CO₂H) as an electron donor [196]. Copyright 2016 RSC©.

functions (Fig. 11a) [209]. Under visible-light irradiation, CO₂ was selectively (97%) reduced to CO by **63** in a DMA/H₂O (39:1, v/v) solution with BIH as an electron donor. However, when TEOA was chosen as an electron donor, CO₂ was selectively (99%) reduced to HCOOH in the alkaline solution (DMA/TEOA = 4:1). The different product selectivity in different solution was attributed to the nature of the Ru center. During the photocatalytic process, the function-integrated **63** was firstly excited upon irradiation and then reductively quenched by an electron donor, giving [Ru^{II}(tpy⁻)(pqn)(MeCN)]⁺ (RuP⁻) (Fig. 11b). Thereafter, CO₂ replaced the solvent molecule to produce the CO₂ adduct RuP_{CO₂}⁻. The Ru-C bond of RuP_{CO₂}⁻ was stabilized by phosphine donor via π -back-donation. After that, RuP_{CO₂}⁻ underwent a further one-electron reduction and subsequent protonated to form [Ru^{II}(tpy⁻)(pqn)(CO₂H)]⁺. Under basic conditions, HCOOH was released through a solvent exchange process. In contrast, a dehydration reaction under acidic condition generated [Ru^{II}(tpy)(pqn)(CO)]²⁺, which released CO also via a solvent exchange process.

3. Pure metal-organic frameworks (MOFs)

MOFs represent ideal platforms for studying many functions for their properties can be rationally and systematically modulated [38–49]. Unlike homogeneous metal complexes, MOFs usually act as heterogeneous catalysts for CO₂RR with the following reasons. Firstly, MOFs are constructed from designed building blocks, which allow for the integration of multi-functional modules within the framework. MOFs can be regulated at the atomic level to rivet abundant catalytic sites onto their backbones of the architecture,

which may help to enhance both of the selectivity and activity. Secondly, the pore size and surface areas of MOFs can also be adjusted to improve their capture capacities for small molecules. The highly open framework of MOFs is beneficial to the exposure of active sites and the diffusion of reactants. Otherwise, when MMCs are combined into continuous regular spaces of MOFs for CO₂RR, both of their activity and stability will be improved. Thirdly, the band-gaps and charge carrier mobility of MOF-based photocatalysts can be engineered to enlarge their efficiency. Fourthly, the morphology of MOFs' crystals can be regulated to optimize their photocatalytic performance. Fifthly, MOFs can compose with semiconductor or metal nanoparticles to further improve their photocatalytic performances. These advantages encourage MOFs be applied in the photocatalytic system for CO₂ reduction. Some approaches worked in enhancing the photocatalytic performance of MOFs-based materials are discussed in this part (Scheme 2). The photocatalytic CO₂ reduction systems based on pure MOFs were summarized in Table 4.

3.1. Ligands modifications

3.1.1. Metal ions coordination

Isolating special metal ions onto MOFs' backbones is an approach to functional MOFs with photocatalytic activity for CO₂-RR [210–214]. The metal ions can be combined onto MOFs' backbones through both *in situ* and post-synthetic exchange (PSE) process. The combined metal ions not only can act as photocatalytic active sites to improve the activity of MOFs but also can perform as efficient centers to enhance the light-harvesting ability of

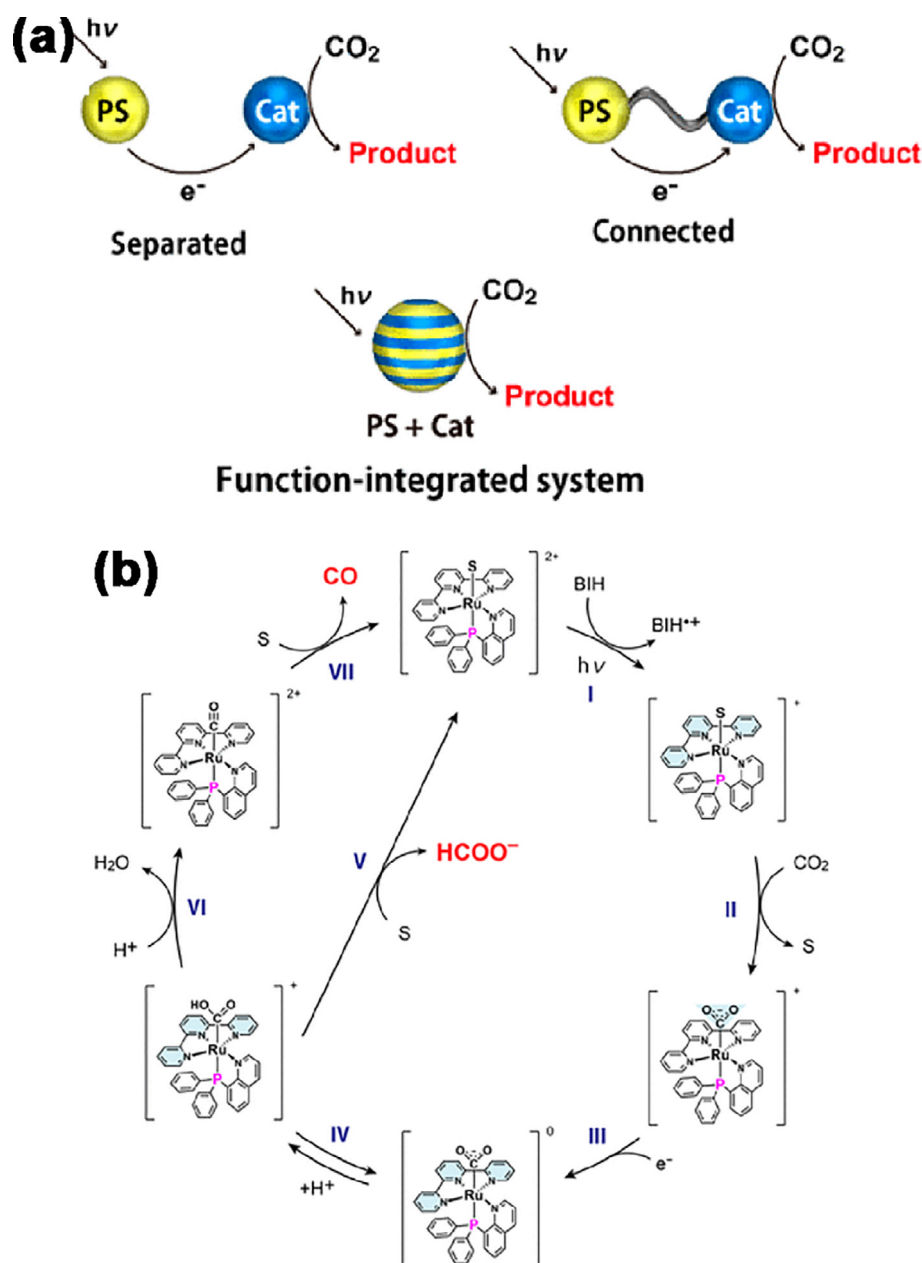
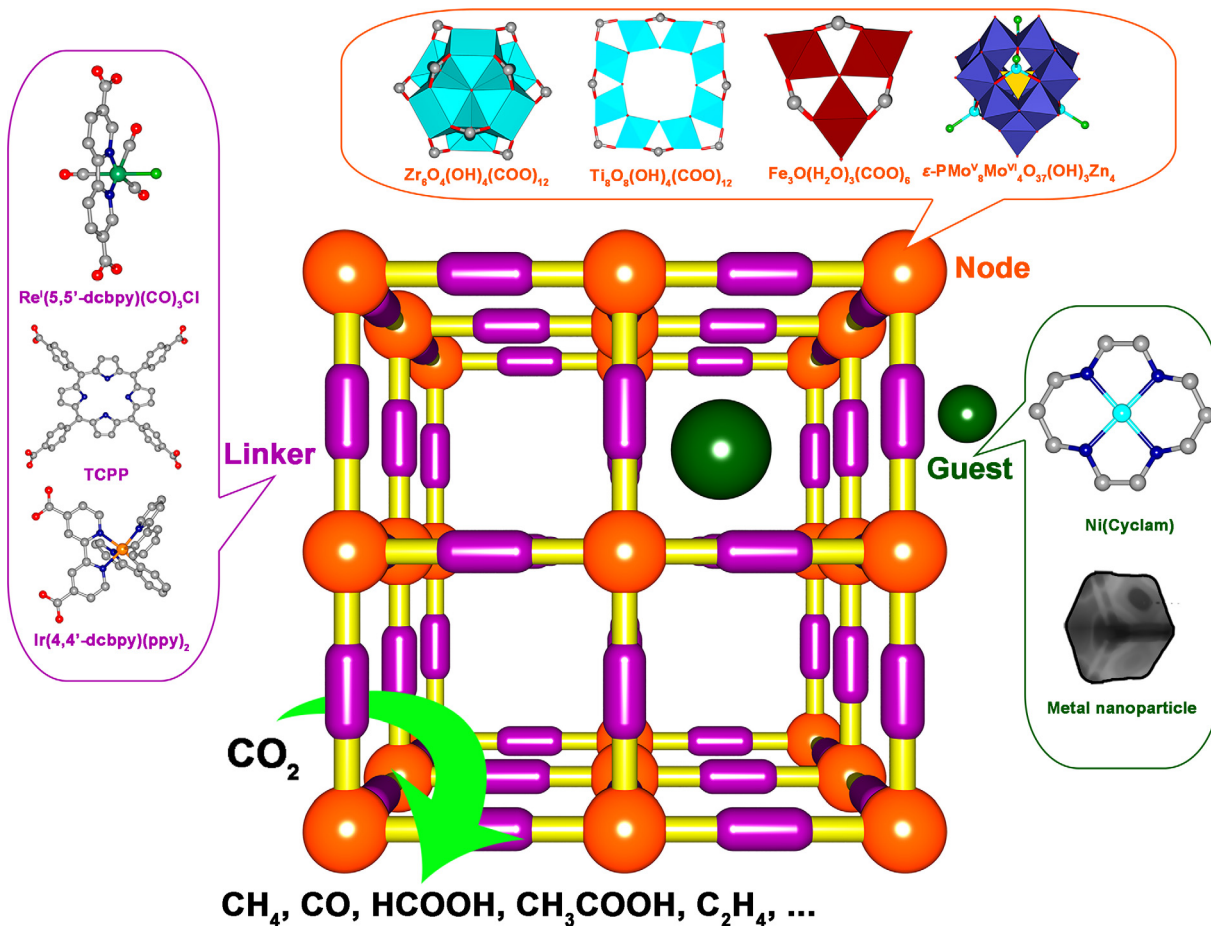


Fig. 11. (a) Scheme of three different photocatalytic systems for CO₂RR. (b) A mechanism for photocatalytic CO₂RR with compound **63** as photocatalyst [209]. Copyright 2018 ACS©.

MOFs. Otherwise, these metal ions can be available spatially isolated in the solid to prevent the accumulation of catalyst. Thus, the stability and recyclability of molecular catalysts can be improved when anchored into MOFs. Lin et al. firstly introduced Re^I into the well-known MOFs UiO-67 for CO₂RR [50]. They treated bpdc and Re^I(5,5'-dcbpy)(CO)₃Cl with ZrCl₄ under the solvothermal condition to produce Re^I doped UiO-67 (Fig. 12a). The BET surface areas of Re doped UiO-67 were demonstrated to be 1092 m²/g with the pore size distribution centering at 6.7 Å. These structural characters make the Re^I centers highly exposed and isolated. Photocatalytic experiments revealed that CO₂ were major reduced to CO by Re^I doped UiO-67 and the TON_{CO} reach 10.9 after 20 h. The recyclability studies showed that the Re^I doped UiO-67 catalyst became inactive after two cycle reactions due to the detachment of Re ions. Even though the performance of Re^I doped UiO-67 was not satisfactory, it still improves both of the activity and stability of the

homogeneous Re^I(dcbpy)(CO)₃Cl. This work provides a modular strategy for designing highly active MOF-based photocatalysts for CO₂RR.

By controlling the density of Re^I(5,5'-dcbpy)(CO)₃Cl in the framework of UiO-67, Yaghi and Yang et al. found that the proximity between photoactive centers was very important [215]. Re^I-UiO-67 (contains 3 Re complexes per unit cell) was found with the highest catalytic activity towards CO₂-to-CO reduction. When the upload Re^I(5,5'-dcbpy)(CO)₃Cl molecules were above 4 per unit cell, the excessive occupation of Re complexes in UiO-67 appears to cause a change in their vibrational state. This change was not favored for CO₂ reduction and would decrease their catalytic activity. On the other hand, the accessible pore volume of Re-UiO-67 reduced as more Re complexes were incorporated in, which would further decrease their activities. When the upload Re^I(5,5'-dcbpy)(CO)₃Cl molecules were below 4 per unit cell, photocatalytic



Scheme 2. MOFs can be regulated at the atomic level to optimize their photocatalytic performance.

activity raised as the number of Re complexes increase. In addition, Ag@Re3-MOF coated by suitable thickness (16 nm) of Re3-MOF provided 7 times enhancement of photocatalytic activity compared to single crystals of Re3-MOF (Fig. 12b). The long-term stability of Ag@Re3-MOF was also improved compared to primary Re3-MOF. Later on, other MOFs are also combined with metal nanoparticles to enhance their photocatalytic activity for CO₂RR. For example, Wang and Sun et al. reported that small Ag nanoparticles could also improve the photocatalytic performance of Co-ZIF-9 for CO₂RR [216]. Xu et al. encapsulated noble metal Pt and Au@Pd nanoparticles within MOF-74-Zn [217]. It was found that Pt nanoparticles were loaded onto the surface while Au@Pd was encapsulated inside of MOF-74-Zn. Interestingly, the Pt/Au@Pd@MOF-74-Zn nanocomposites achieved photocatalytic reduction of CO₂-to-CH₄ at low concentration.

In addition to Re complexes, the Rh complex Cp*Rh(bpy)Cl₂ can also be used to modify MOFs for CO₂RR [218]. By immersing UiO-67 in the solution of Cp*Rh(dcbpy)Cl₂ at room temperature, up to 35% of bpdc of UiO-67 was exchanged. A series of Rh doped UiO-67 were prepared with different number of Rh sites. CO₂ molecules were major reduced to HCOOH over Rh-UiO-67. However, if the Rh loading in Rh-UiO-67 was higher than ~10% molar, the HCOOH product was recomposited into H₂. This work demonstrates that, beyond active catalytic sites combination, site density should also be concerned in order to avoid undesired side-reactions.

Porous heterogeneous catalysts containing special voids with high CO₂ capture capacity are considered to have a positive effect for CO₂ reduction. Kitagawa et al. studied the correlates between

the adsorption property and photocatalytic CO₂RR property of MOFs [219]. A Ru complex [Ru^{II}(5,5'-dcbpy)(tpy)(CO)](PF₆)₂ was incorporated into UiO-67 by the PSE method. It is interesting that Ru-UiO-67 can uptake more CO₂ than unmodified UiO-67. This result can be attributed to the decrease in the pore size and the increase in the affinity sites for adsorbates by the loading of Ru complexes. When the photocatalytic CO₂RR was carried out under saturated CO₂, Ru-UiO-67 represented a high TON_{CO} value of 156 within 6 h. When photoreduction of CO₂ was carried out under low CO₂ concentrations (diluted with Ar), the catalytic activity of Ru-UiO-67 almost unchanged even under 5% CO₂. The CO to HCOOH ratio for Ru-UiO-67 was also higher than that for molecular Ru complex under all examined conditions. Such heterogeneous catalysts may be prioritized for practical application because the partial pressure of CO₂ in industrial waste gas is usually low.

The redox property of the anchored metal ions is also important. Kang and Cohen et al. prepared Ga^{III}/Cr^{III}-doped UiO-66-CAT through two steps of PSE method (Fig. 13) [220]. They firstly introduced pristine UiO-66 into H₂O/DMF solution of catbdc²⁻ and kept the temperature at 85 °C for 48 h to obtain UiO-66-CAT that contains ~34% catbdc²⁻ and ~66% bdc²⁻ ligand. Thereafter, the Ga^{III}/Cr^{III} ions were anchored by using respective metal salts aqueous. Both of Ga^{III}-UiO-66-CAT and Cr^{III}-UiO-66-CAT show photocatalytic activity for CO₂RR. After 6 h irradiation, TONs were calculated as ~11 for Cr^{III}-UiO-66-CAT and ~6 for Ga^{III}-UiO-66-CAT, respectively. During the photocatalytic reaction, the catbdc linkers absorbed lights and transferred electrons to metals. The higher photocatalytic efficiency of Cr^{III}-UiO-66-CAT than Ga^{III}-UiO-66-

Table 4
Heterogeneous photocatalytic CO₂ reduction systems based on pure MOFs.^a

Compound	Product	TON	Yield	PS	SD	Solvent	λ	Ref.
Co ₃ (HL) ₂ ·4DMF·4H ₂ O	CO HCOOH	–	50 nmol 1.9 μ mol	[Ru(bpy) ₃] ²⁺	BNAH	DMA	>420 nm	[211]
RuCl@UiO-67	CO HCOOH	9.7 70.7	–	[Ru(bpy) ₃] ²⁺	TEOA	MeCN	~420 nm	[212]
RuOH ₂ @UiO-67	CO HCOOH	8.6 69.1	–	[Ru(bpy) ₃] ²⁺	TEOA	MeCN	~420 nm	[212]
RhCl@UiO-67	CO HCOOH	2.7 38.9	–	[Ru(bpy) ₃] ²⁺	TEOA	MeCN	~420 nm	[212]
RhOH ₂ @UiO-67	CO HCOOH	4.6 61.1	–	[Ru(bpy) ₃] ²⁺	TEOA	MeCN	~420 nm	[212]
UiO-67-Re(CO) ₃ Cl	CO	10.9	–	–	TEA	MeCN	>300 nm	[50]
UiO-67-Re(CO) ₃ Cl	CO	0.4	–	–	TEA	MeCN	>400 nm	[215]
Ag@UiO-67-Re(CO) ₃ Cl	CO	2.8	–	–	TEA	MeCN	>400 nm	[215]
Ag@Co-ZIF-9	CO	–	28.4 μ mol	[Ru(bpy) ₃] ²⁺	TEOA	MeCN-H ₂ O	>420 nm	[216]
Cp*Rh@UiO-67	HCOOH	47	–	[Ru(bpy) ₃] ²⁺	TEOA	MeCN	>415 nm	[218]
UiO-67-Ru(terpy)CO	CO HCOOH	17.5 99.9	–	[Ru(bpy) ₃] ²⁺	TEOA	DMA	>385 nm	[219]
UiO-66-CrCAT	HCOOH	11.22	–	–	BNAH	DMA	>420 nm	[220]
UiO-66-GaCAT	HCOOH	6.14	–	–	BNAH	DMA	>420 nm	[220]
UiO-67-Mn(dcbpy)(CO) ₃ Br	HCOOH	110	–	[Ru(dmbpy) ₃] ²⁺	BNAH	DMF	~470 nm	[221]
Y[Ir(ppy) ₂ (dcbpy)] ₂ [OH]	HCOOH	–	38 μ mol	–	TEOA	MeCN	>420 nm	[222]
Cd ₃ [Ru-L ₁] ₂ ·2(Me ₂ NH ₂)	HCOOH	–	16.1 μ mol	–	TEOA	MeCN	>420 nm	[223]
Cd[Ru-L ₂] ₃ ·3(H ₂ O)	HCOOH	–	17.1 μ mol	–	TEOA	MeCN	>420 nm	[223]
Eu-Ru(phen) ₃ -MOF	HCOOH	–	47 μ mol	–	TEOA	MeCN	>420 nm	[224]
MOF-253(Al)-Ru(CO) ₂ Cl ₂	HCOOH CO	2.9 7.1	0.67 μ mol 1.86 μ mol	–	TEOA	MeCN	>420 nm	[225]
Ru-MOF-253(Al)-Ru	HCOOH CO	35.8 7.3	8.23 μ mol 1.91 μ mol	–	TEOA	MeCN	>420 nm	[225]
Ru-MOF-253(Al)-Re	HCOOH CO	23.4 5.4	9.50 μ mol 2.23 μ mol	–	TEOA	DMF-H ₂ O	>400 nm	[226]
Cd ₂ [Ru(dcbpy) ₃] ₂ ·12H ₂ O (flower)	HCOOH	–	24.7 μ mol	–	TEOA	MeCN	>420 nm	[227]
Cd ₂ [Ru(dcbpy) ₃] ₂ ·12H ₂ O (microcrystals)	HCOOH	–	17.7 μ mol	–	TEOA	MeCN	>420 nm	[227]
Cd ₂ [Ru(dcbpy) ₃] ₂ ·12H ₂ O (bulkcrystals)	HCOOH	–	9.7 μ mol	–	TEOA	MeCN	>420 nm	[227]
Hf ₁₂ -Ru-Re	CO	3849	–	–	BIH	MeCN	>400 nm	[230]
Hf ₁₂ -Ru-Mn	CO	2092	–	–	BNAH	–	–	–
	CO	1367	–	–	BIH	MeCN	>400 nm	[230]
	CO	240	–	–	BNAH	–	–	–
Ni MOFs	CO	–	12.5 μ mol/h	[Ru(bpy) ₃] ²⁺	TEOA	MeCN-H ₂ O	>400 nm	[231]
Ni ₃ (HITP) ₂ nanosheets	CO	–	274 μ mol	[Ru(bpy) ₃] ²⁺	TEOA	MeCN-H ₂ O	~420 nm	[232]
NH ₂ -MIL-125	HCOOH	–	8.14 μ mol	–	TEOA	MeCN	>420 nm	[234]
MIL-125-NH ₂	HCOOH	0.77	–	–	TEOA	MeCN	~466 nm	[235]
MIL-125-NHMe	HCOOH	0.284	–	–	TEOA	MeCN	~466 nm	[235]
MIL-125-NHET	HCOOH	0.51	–	–	TEOA	MeCN	~466 nm	[235]
MIL-125-NHiPr	HCOOH	0.71	–	–	TEOA	MeCN	~466 nm	[235]
MIL-125-NHBu	HCOOH	0.825	–	–	TEOA	MeCN	~466 nm	[235]
MIL-125-NHCyp	HCOOH	0.725	–	–	TEOA	MeCN	~466 nm	[235]
MIL-125-NHCy	HCOOH	8.83	–	–	TEOA	MeCN	~466 nm	[235]
MIL-125-NHhep	HCOOH	1.151	–	–	TEOA	MeCN	~466 nm	[235]
NH ₂ -UiO-66(Zr)	HCOOH	–	13.2 μ mol	–	TEOA	MeCN	>420 nm	[237]
[Zr ₆ O ₄ (OH) ₄ (SDCA-NH ₂) ₆] ₈ DMF	HCOOH	–	19.6 μ mol	–	TEOA	MeCN	>420 nm	[238]
PCN-222	HCOOH	–	30 μ mol	–	TEOA	MeCN	>420 nm	[240]
MOF-525-Co	CO CH ₄	– –	2.42 μ mol 0.42 μ mol	–	TEOA	MeCN	>400 nm	[242]
Zr-THPP-Co	CO	–	0.28 μ mol h ^{–1}	–	TEOA	MeCN	>420 nm	[243]
MOF-545-Rh	HCOOH	–	6.1 mol mol _{cat} ^{–1}	–	TEOA	MeCN	>400 nm	[244]
Co-ZIF-9	CO	–	41.8 μ mol	[Ru(bpy) ₃] ²⁺	TEOA	MeCN-H ₂ O	>420 nm	[245]
Co-ZIF-67 nanosheets	CO	–	15.57 μ mol	[Ru(bpy) ₃] ²⁺	TEOA	MeCN-H ₂ O	>420 nm	[247]
AD-MOF-1	HCOOH	–	7.16 μ mol	–	TIPA	MeCN-H ₂ O	>420 nm	[248]
AD-MOF-2	HCOOH	–	22.16 μ mol	–	TIPA	MeCN-H ₂ O	>420 nm	[248]
Ni(Cyclam)@Gd-TCA	HCOOH	–	22.7 μ mol	–	TEOA	MeCN-H ₂ O	>365 nm	[249]
Co-TCA	HCOOH	13.5	39.36 μ mol	[Ru(bpy) ₃] ²⁺	TEOA	MeCN-H ₂ O	>420 nm	[250]
Ni ₃ (TCA) ₂ (dpe) ₃ (H ₂ O) ₃	CO	–	22.3 μ mol	[Ru(bpy) ₃] ²⁺	TIPA	MeCN-H ₂ O	>420 nm	[251]
Co ₃ (TCA) ₂ (dpe) ₃ (H ₂ O) ₃	CO	–	22.8 μ mol	[Ru(bpy) ₃] ²⁺	TIPA	MeCN-H ₂ O	>420 nm	[251]
Cu ₃ (TCA) ₂ (dpe) ₃ (H ₂ O) ₃	CO	–	1.7 μ mol	[Ru(bpy) ₃] ²⁺	TIPA	MeCN-H ₂ O	>420 nm	[251]
NNU-28	HCOOH	–	26.4 μ mol	–	TEOA	MeCN	>420 nm	[252]
PCN-136	HCOOH	–	10.52 μ mol	–	TIPA	MeCN-H ₂ O	>420 nm	[253]
Pbz-MOF-1	HCOOH	–	3.53 μ mol	–	TIPA	MeCN-H ₂ O	>420 nm	[253]
NENU-605	CH ₄	–	170 nmol	[Ru(bpy) ₃] ²⁺	TEOA	H ₂ O	>420 nm	[254]
NENU-606	CH ₄	–	402 nmol	[Ru(bpy) ₃] ²⁺	TEOA	H ₂ O	>420 nm	[254]
MIL-53	HCOOH	–	29.7 μ mol	–	TEOA	MeCN	>420 nm	[257]
NH ₂ -MIL-53	HCOOH	–	46.5 μ mol	–	TEOA	MeCN	>420 nm	[257]
MIL-101	HCOOH	–	59 μ mol	–	TEOA	MeCN	>420 nm	[257]
NH ₂ -MIL-101	HCOOH	–	178 μ mol	–	TEOA	MeCN	>420 nm	[257]

(continued on next page)

Table 4 (continued)

Compound	Product	TON	Yield	PS	SD	Solvent	λ	Ref.
MIL-88	HCOOH	–	9 μmol	–	TEOA	MeCN	>420 nm	[257]
NH ₂ -MIL-88	HCOOH	–	30 μmol	–	TEOA	MeCN	>420 nm	[257]
MAF-X27-OH	CO	–	17.2 μmol	[Ru(bpy) ₃] ²⁺	TEOA	H ₂ O	= 420 nm	[258]
NH ₂ -UiO-66(Zr/Ti)	HCOOH	6	–	–	BNAH	MeCN	>420 nm	[260]
Ni(TPA/TEG)	CO	11.5	136.9 μmol	[Ru(bpy) ₃] ²⁺	TEOA	MeCN-H ₂ O	>420 nm	[262]

^aTON represents turn over number; PS represents photosensitizer; SD represents Sacrificial donor; λ represents the wavelength of the irradiation light.

CAT was due to the increased electron transfer ability. The difference in charge transferability of these trivalent ions may be due to differences in their outer shell electronic configurations (Cr^{III} [Ar]3d³ versus Ga^{III} [Ar]3d¹⁰). Cr-species were easier to accept electrons than Ga-species because the redox potential of Cr^{III}/Cr^{II} was lower than Ga^{III}/Ga^{II}.

The abundant elements Mn(bpy)(CO)₃Br have also been combined onto the backbone of UiO-67 [221]. PSE method was used to prepare the Mn-doped UiO-67 because the thermal stability of Mn(CO)₃ moiety under solvothermal process was poor. As Mn-complexes are fixed on the framework of MOFs as isolated active sites, both of the photocatalytic activities and the long-term stabilities of them are improved. It shows a TON_{HCOOH} of about 110 within 18 h and can recycle used over three catalytic runs.

Noble metals, such as Ru and Ir are widely used to enhance MOFs' visible-light absorption. Luo and coworkers synthesized an

Ir-based coordination polymer (Ir-CP) with [Ir(ppy)₂(4,4'-dcbpy)]⁺ units [222]. The photocatalytic CO₂ reduction over the Ir-CP giving 38.0 μmol HCOOH within 6 h. The high performance of Ir-CP was attributed to the highly light-harvesting capability of Ir unit, which showed a very broad light-harvesting range (~650 nm) and a long PL lifetime of 29.05 μs . Later on, they reported another two MOFs modified by Ru-polypyridine complex (Fig. 14a) [223]. Both of Ru-MOFs could efficiently catalyze CO₂-to-HCOOH reduction. By treating the pre-prepared [Ru(5,5'-dcbpy)₃]⁴⁺ with Cd(ClO₄)₂, Ru-MOF-1 was obtained with non-interpenetrated networks. Ru-MOF-2 with 2-fold interpenetrated network was synthesized by using [Ru(4,4'-dcbpy)₂bpy)]²⁺ as building blocks. Under visible-light irradiation for 6 h, Ru-MOF-1 and Ru-MOF-2 gave similar HCOOH productions of 16.1 and 17.2 μmol , respectively. However, when the photocatalytic reactions were performed over 6 h, Ru-MOF-2 showed a higher photostability than Ru-MOF-1. The differ-

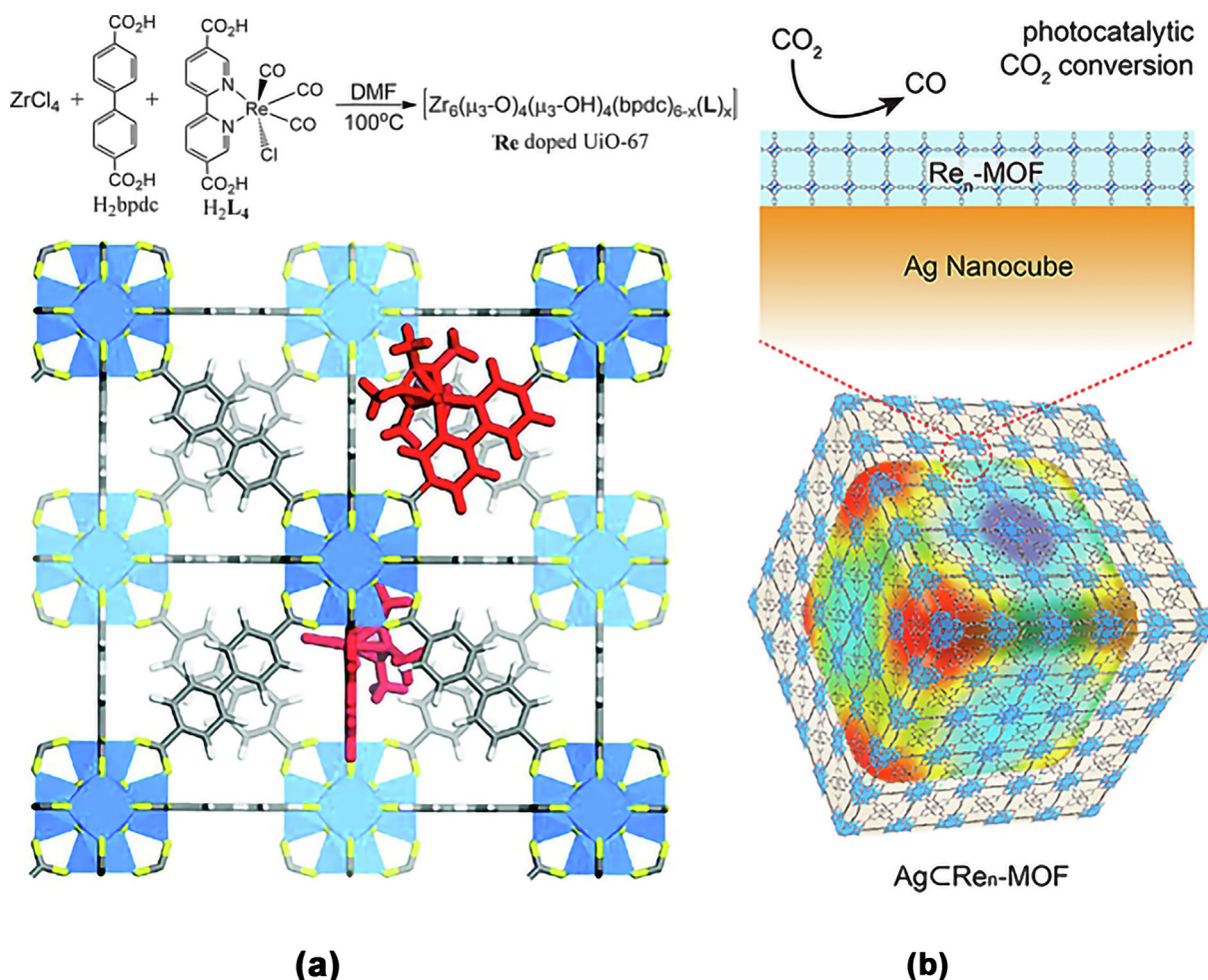


Fig. 12. (a) Synthesis of Re-UiO-67 and its structure [50]. Copyright 2011 ACS. (b) Ag ⊂ Re₃-UiO-67 for plasmon-enhanced photocatalytic CO₂ reduction [215]. Copyright 2017 ACS.

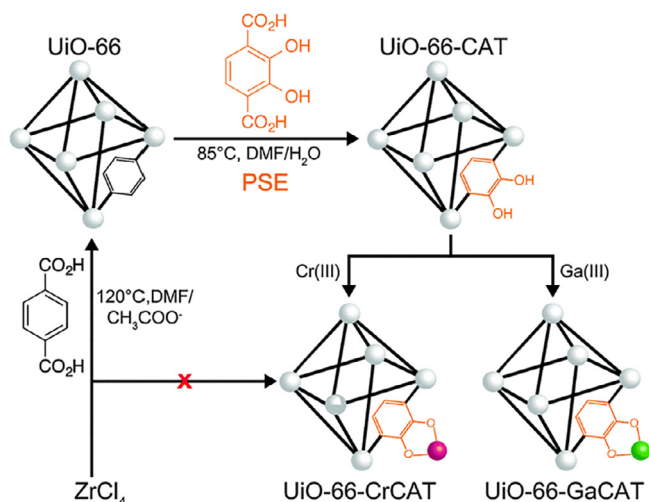


Fig. 13. Preparation of Cr-UiO-66 and Ga-UiO-66 via PSE method [220]. Copyright 2015 RSC.

ent stabilities of these Ru-MOFs were attributed to their different entanglement of networks. The 2-fold interpenetrated framework of Ru-MOF-2 was stabilized by π - π stacking interactions between the dcbpy²⁻ from the neighboring nets.

Kong and co-workers reported a 2-fold interpenetrated Ru-MOF-Eu containing [Ru(phen)₃]²⁺ as a light harvesting unit and dinuclear [Eu]₂ cluster as a catalytic unit (Fig. 14b) [224]. Under visible-light illumination, photoinduced electrons transfer from [Ru(phen)₃]²⁺ units to [Eu^{III}]₂ clusters to generate Eu^{II} active sites. CO₂ was selectively reduced to HCOOH with a yield of 47 μ mol and a formation rate of 321.9 μ mol h⁻¹ mmol_{MOF}⁻¹.

Several functional moieties can be introduced into one MOF platform at the same time to produce more active photocatalyst. Here, MOF-253 was chosen as a model [225]. At the beginning, only Ru carbonyl complexes Ru(dcbpy)(CO)₂Cl₂ were introduced into the framework of MOF-253. After 8 h irradiation, only 0.67 μ mol of HCOOH, 1.86 μ mol of CO and 0.09 μ mol of H₂ were produced over MOF-253-Ru. Although the photocatalytic activities of MOF-253-Ru were higher than that of pure MOF-253, its performance was not satisfactory. Thereafter, Ru(bpy)₂Cl₂ was further introduced into MOF-253 for its light-harvesting capability. The photocatalytic performance of the sensitized Ru-MOF-253-Ru was significantly improved. In addition, the performance of Ru-MOF-253-Ru was found to closely relate to the mole ratio of the anchored Ru(bpy)₂Cl₂ and Ru(CO)₂Cl₂. When the mol ratio of Ru(bpy)₂Cl₂/Ru(CO)₂Cl₂ was 1:1, up to 8.23 mmol HCOO⁻, 2.73 mmol CO and 1.91 mmol H₂ was produced after 8 h irradiation. Later on, Ru(bpy)₂Cl₂ and Re(bpy)(CO)₃Cl have also been introduced into the framework of MOF-253 [226]. The enhanced photocatalytic

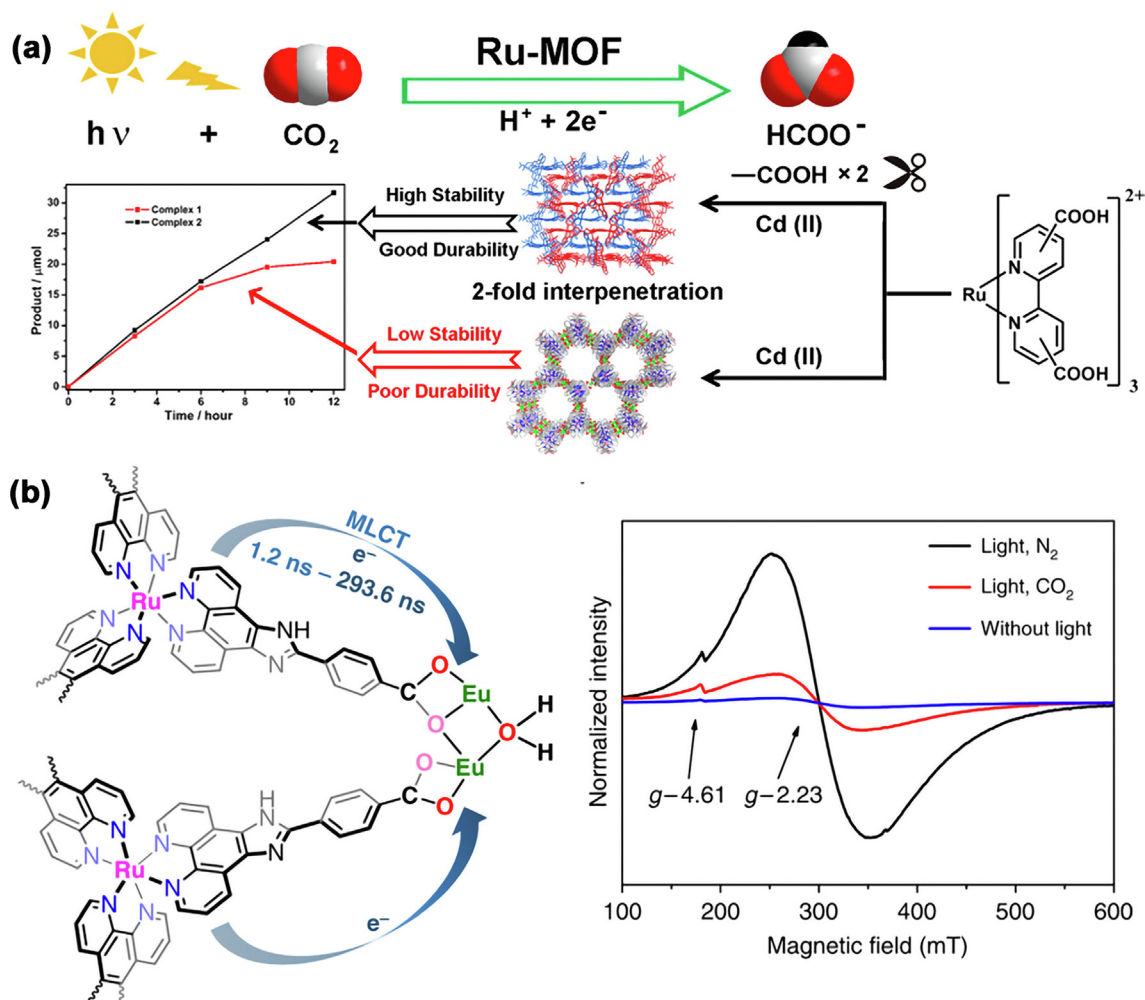


Fig. 14. (a) Scheme of photocatalytic CO₂ reduction over 2-fold interpenetration and non-interpenetration Ru-MOFs [223]. Copyright 2015 ACS. (b) The pathways of photoelectrons transfer from Ru(phen)₃ to [Eu]₂ cluster and the EPR spectra of Ru-MOF-Eu under different conditions [224]. Copyright 2018 Nature publisher.

activity of Ru-MOF-253-Re was ascribed to the improved visible-light absorption and the existence of an efficient photoinduced charge transfer from Ru sensitizer to Re catalytic center.

The hierarchical nano-architectures of MOFs are engineered for enhancing their photocatalytic activity towards CO₂RR. Luo et al. reported a fascinating 3D hierarchical flower-like nanostructure of a functional Ru-MOF, namely, [Cd₂Ru(4,4'-dcbpy)₃]-12H₂O [227]. The nanoflowers were constructed from dozens of 2D nanosheets with a size of about several hundred nanometers in width and 50–70 nm in thickness. The monodisperse nanoflower showed a typical diameter in the range of 10–20 μm. The amount of produced HCOOH reached 24.7 μmol and the product formation rate was calculated as 77.2 μmol g⁻¹ h⁻¹. Such formation rate was much higher than that of micro flakes (52.7 μmol g⁻¹ h⁻¹) and bulk crystals (30.6 μmol g⁻¹ h⁻¹). The high photocatalytic activities of Ru-MOF nanoflowers were attributed to their large surface area as well as their high energy transfer efficiency.

The ultrathin two-dimensional (2D) MOF nanosheets are attracting increasing attention in recent years for their unique properties [228,229]. Lin et al. reported a new photosensitive MOF nanosheet based on Hf₁₂ clusters and [Ru(bpy)₃]²⁺ derived dicarboxylate ligands (Fig. 15a) [230]. After anchoring M(bpy)(CO)₃X (M = Re and X = Cl or M = Mn and X = Br) derived capping molecules on the Hf₁₂ clusters through carboxylate exchange reactions, the resultant Ru-Hf₁₂-M showed high activity for photocatalytic CO₂ reduction. The high photoactive of Ru-Hf₁₂-M may be attributed to the proximity of the MOF skeleton to the capping ligands (1–2 nm), which facilitated electron transfer from the [Ru(bpy)₃]²⁺ photosensitive unit to M^I(bpy)(CO)₃X catalytic unit. Later on, another monolayer MOF (Ni-MOLs) with abundant coordinatively unsaturated Ni sites was prepared by ultrasonication method (Fig. 15b) [231]. Photocatalytic experiments showed that the Ni-MOLs showed excellent catalytic activity for CO₂-to-CO reduction. For example, Ni-MOLs exhibited a high QY of 1.96% with

a 96.8% selectivity even in diluted CO₂ (10%). However, isostructural Co-MOLs showed almost no activity in diluted CO₂. Such results revealed that the metal nodes were also very important. The strong CO₂ binding affinity of Ni-MOLs could stabilize the Ni-CO₂ adducts and facilitates CO₂-to-CO reduction.

Conductivity MOF nanosheets are also good candidates for photocatalytic CO₂RR (Fig. 15c) [232]. These nanosheets show advantages of high conductivity for charge transportation. By using Ni₃(HITP)₂ as a catalyst and [Ru(bpy)₃]²⁺ as a photosensitizer, CO₂-to-CO reduction with 97% selectivity and 34500 μmol g⁻¹ h⁻¹ yield rate was achieved.

3.1.2. Amino groups

The bandgap of MOFs can be engineered by tailoring the organic components [233]. Actually, a modification of organic ligand is required in many cases in order to maximize photonic efficiency. In the field of CO₂RR, amino substituted terephthalic acid (H₂ATA) is one of most widely used organic ligand in terms to enhance MOF's visible-light harvesting ability. NH₂-MIL-125(Ti) was the first reported amino modified MOFs for CO₂-to-HCOOH reduction (Fig. 16a) [234]. Compare to the parent MIL-125, NH₂-MIL-125 not only showed a broader light absorption range in the visible region but also showed an enhanced CO₂ adsorption capacity. The only detected product over NH₂-MIL-125 was HCOOH with a yield of about 8.14 μmol within 10 h. ESR results, as well as the color changes under test condition, revealed that the photo-generated Ti³⁺ moieties were responsible for the formation of HCOOH (Fig. 16b). This work represents that the substituted ligands of MOFs can act as a photosensitizer to sensitize metal nodes in CO₂RR.

Later on, the photocatalytic performances of MIL-125 based catalyst were further promoted through structural modification or reaction interface construction. A series of isorecticular framework of NH₂-MIL-125 were prepared through decorating the amino

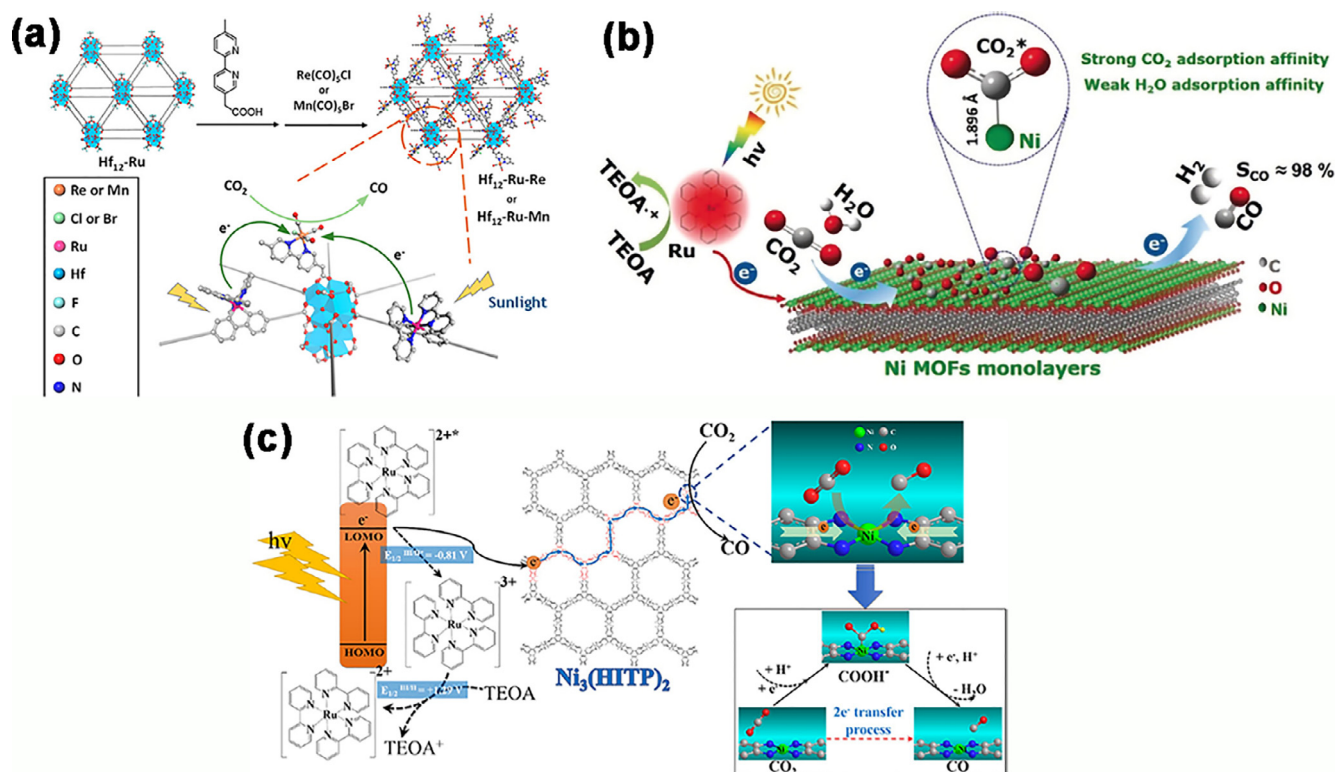


Fig. 15. (a) Synthesis of Ru-Hf₁₂-M (M = Re or Mn) and its photocatalytic activity towards CO₂ reduction [230]. Copyright 2018 ACS®. (b) Photocatalytic CO₂ reduction over Ni-MOLs [231]. Copyright 2018 Wiley-VCH®. (c) Photocatalytic CO₂ reduction over Ni₃(HITP)₂ [232]. Copyright 2018 Elsevier®.

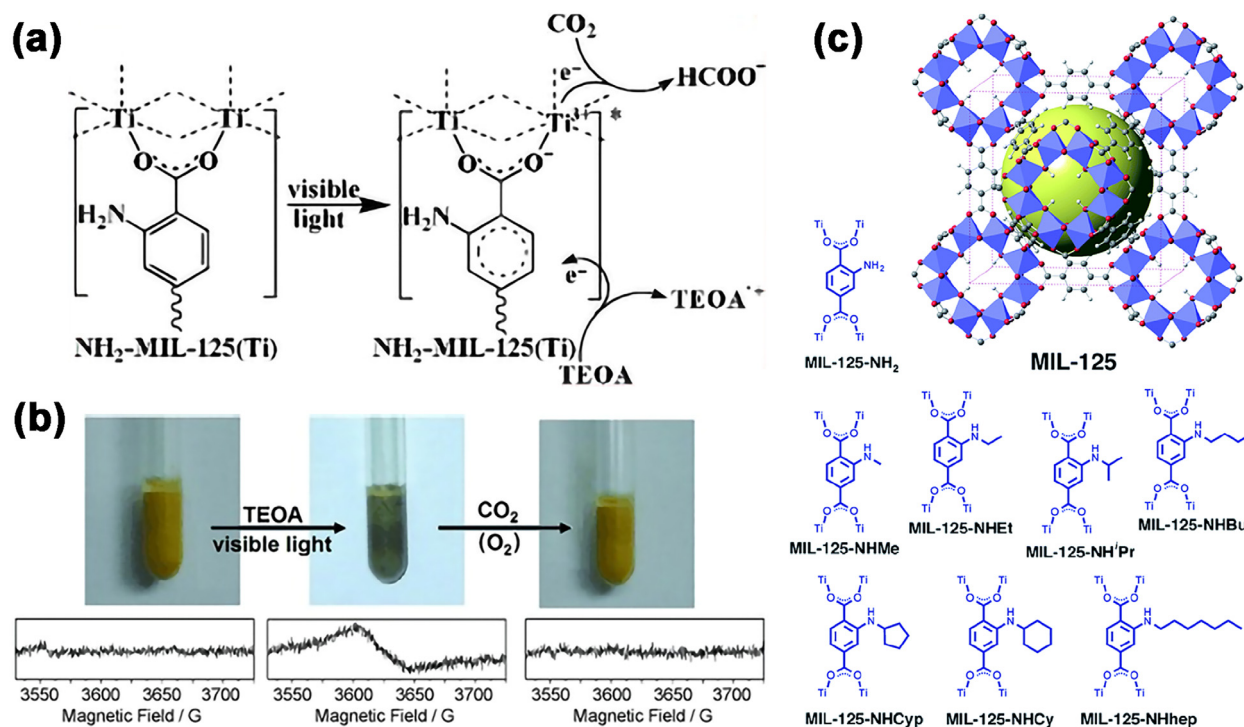


Fig. 16. (a) Photocatalytic CO₂RR over NH₂-MIL-125 [234]. (b) Photos and corresponding ESR spectra of NH₂-MIL-125 under different conditions [234]. Copyright 2012 Wiley-VCH. (c) Structures of isorecticular frameworks of NH₂-MIL-125 [235]. Copyright 2017 RSC.

groups with alkyl chains (Fig. 16c) [235]. The decorated NH₂-MIL-125 solids exhibited reduced optical bandgaps, which were directly related to the inductive donor ability of the alkyl substituents. Although the secondary N-alkyl functionalized MOFs showed a lower CO₂ absorption than that of the parent NH₂-MIL-125, they showed higher catalytic efficiency due to their smaller bandgap and longer excited-state lifetime. The most efficient catalyst was NHCyp-MIL-125 ($E_g = 2.30$ eV, $\tau = 68.8$ ns), revealing a much higher QY (1.80%) than NH₂-MIL-125 ($\Phi = 0.31\%$, $E_g = 2.56$ eV, $\tau = 12.8$ ns). Zhang et al. reported a CO₂/water interfacial strategy for enhancing the efficiency of photocatalytic CO₂RR [236]. This novel route was preferred for its advantages, such as environment-friendly, large interfacial area and enhanced and easily tuned catalytic efficiency. NH₂-MIL-125 was investigated as the photocatalyst in this strategy. The TOF of HCOOH over NH₂-MIL-125 can reach $58.1 \mu\text{mol g}^{-1} \text{h}^{-1}$ at 11.02 MPa, which is twice times higher than that over NH₂-MIL-125 in MeCN solution. Interestingly, the TOFs over other MOFs such as MIL-125, UiO-66 and NH₂-UiO-66 are all enhanced by using this strategy.

The amino functional strategy has also applied to modify the platform of UiO-66 type Zr-MOFs to develop their photocatalytic CO₂RR properties. NH₂-UiO-66(Zr) shows photocatalytic activity for CO₂-to-HCOOH reduction under visible-light irradiation [237]. During the reaction process, the photoelectron transfer from ATA to the Zr₆ clusters to generate Zr^{III}. Furthermore, when introducing H₂DTA onto the framework of NH₂-UiO-66(Zr) (mole ratio of ATA/DTA is 4:1), the obtained mixed NH₂-UiO-66(Zr) showed improved performance for CO₂RR. Later on, Chen et al. prepared a UiO-type Zr-MOFs (Zr-SDCA-NH₂) by employing conjugated amine-functionalized dicarboxylic ligand [238]. The combination of conjugated groups and amino groups in H₂SDCA may largely elevate the ligand light absorption capacity. Zr-SDCA-NH₂ showed a broad visible-light absorption with an absorption edge at about 600 nm. Thus, Zr-SDCA-NH₂ exhibited photocatalytic activity for CO₂-to-HCOOH reduction with a formation rate of $96.2 \mu\text{mol h}^{-1} \text{mmol}^{-1}_{\text{cat}}$.

3.1.3. Porphyrin and metal porphyrin

Porphyrin or metalporphyrin with high catalytic activity are important functional ligands for constructing MOFs with variety applications [239]. These conjugated ligands with visible-light harvesting ability may avoid the use of rare noble-metal based photosensitizers. In 2015, Jiang et al. reported the photocatalytic CO₂RR properties of PCN-222, a stable mesoporous Zr-MOF constructed from Zr₆ cluster and TCPP (Fig. 17a) [240]. The amount of the only reduced product HCOOH reached up to $30 \mu\text{mol}$ in 10 h. During the photocatalytic process, the photoelectrons transfer to Zr₆ clusters generating Zr^{III} ions (Fig. 17b). They further point out that the emergence of an extremely long-lived electron trap state in PCN-222 suppresses the electron-hole recombination. Therefore, PCN-222 shows a higher photocatalytic activity for CO₂RR than original porphyrin ligand TCPP. This work makes significant contributions in both mechanisms clarify and highly efficient visible-light-responsive catalyst design.

The porphyrin macrocycle in the MOFs can be metallized with metal ions and then improves the photocatalytic performance of MOFs. Transition metal ions modulated into porphyrin macrocycle generally contain exposure open metal sites and do not aggregation during the reaction. Cu²⁺ ions were firstly utilized to modify porphyrin MOF catalyst for photocatalytic CO₂RR [241]. Compared to the primary porphyrin MOF, Cu modified MOF showed enhanced CO₂ capture capacity and much higher photocatalytic activity for CO₂-to-MeOH reduction. These improvements were attributed to the chemically adsorption and activation of CO₂ molecules on the exposure Cu sites. Later on, Ye et al. reported two new composites via incorporating coordinatively unsaturated Co or Zn ions into the porphyrin units of MOF-525 (Zr₆O₄(OH)₄(-TCPP-H₂)₃) (Fig. 17c) [242]. MOF-525-Co showed the highest activity for CO₂ reduction while parent MOF-525 showed the lowest activity. Some reasons have been proposed to explain these phenomena. Firstly, the unsaturated metal sites could adsorb and activate the CO₂ molecules (Fig. 17d). Secondly, the Co/Zn ions in the

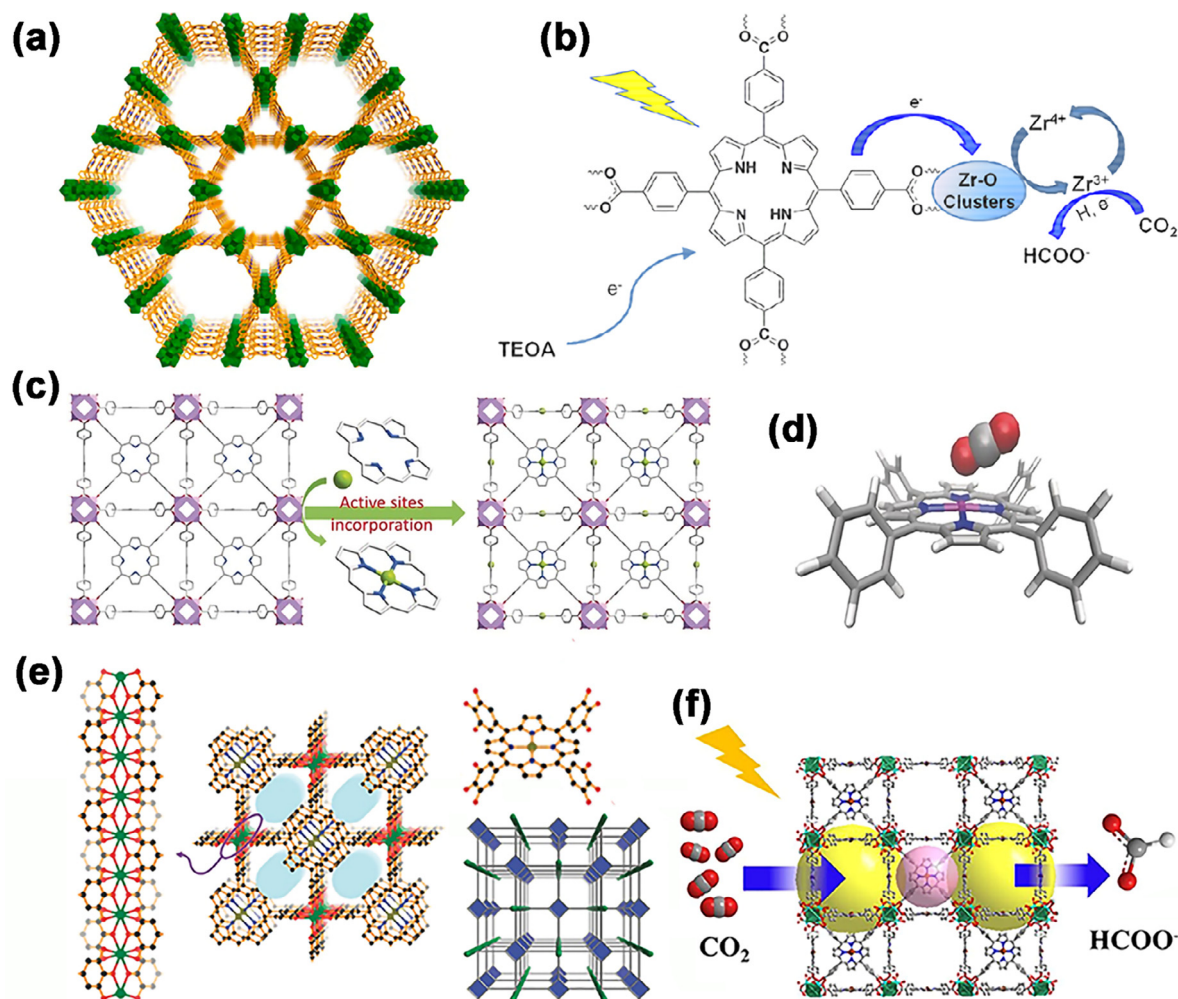


Fig. 17. (a) Structure of PCN-222. (b) Mechanism for CO_2 reduction over PCN-222. [240] Copyright 2015 ACS®. (c) Construction of MOF-525-Co. (d) Optimized structure for CO_2 adsorption on a Co-TCPP. [242] Copyright 2016 Wiley-VCH®. (e) Structures of ZrPP-1 [243]. Copyright 2017 Wiley-VCH®. (f) Representation of photocatalytic CO_2RR over Rh-PMOF-1 [244]. Copyright 2018 Elsevier®.

porphyrin center can greatly boost the electron-hole separation. The introduced metal centers gain the photoelectrons from porphyrin directly for CO_2 reduction. The reduction products over MOF-525-Co were detected to be CO and CH_4 with evolution rates of $200.6 \text{ mmol g}^{-1} \text{ h}^{-1}$ and $36.67 \text{ mmol g}^{-1} \text{ h}^{-1}$, respectively.

Lin and co-workers reported two isostructural Zr-pyrogallol porphyrin MOFs constructing from porphyrinic phenolates and Zr-oxide rods, ZrPP- n ($n = 1$ for THPP, $n = 2$ for THBPP) (Fig. 17e) [243]. ZrPP-1 can remain intact in both acid and base solution over one week. As the pore space of ZrPP-1 was separated into numerous traps, it showed a high CO_2 adsorption capacity. In addition, various transition metal ions, including Zn, Cu, Fe and Co, were also inserted into the porphyrin centers to study their effects on the catalytic properties. ZrPP-1-Co showed the highest CO generation rate of $14 \text{ } \mu\text{mol g}^{-1} \text{ h}^{-1}$ with 96.4% selectivity. Further inspect into the structure revealed that the neighboring metalloporphyrins at a distance of $7.4 \text{ } \text{\AA}$ were suitable to bind the CO_2 molecules, giving a more stable CO_2 adduct and promoting the CO_2 -to-CO reduction.

In 2018, Zhang and Su et al. reported an Rh(III)-porphyrin based Zr-MOF (Rh-PMOF-1) with a BET surface area of $3015 \text{ m}^2 \text{ g}^{-1}$ (Fig. 17f) [244]. Rh-PMOF-1 shows a highly CO_2 uptake of $42 \text{ cm}^3 \text{ g}^{-1}$ at 308 K . Under the visible-light irradiation, photo-induced electrons transfer from Rh-porphyrin units to Zr^{IV} clusters to generate Zr^{III} for CO_2 reduction. Photocatalytic CO_2 -to- HCOOH reduction with 99% selectivity was achieved over Rh-PMOF-1. In addition,

Rh-PMOF-1 can be recycled for three catalytic runs as a truly heterogeneous catalyst.

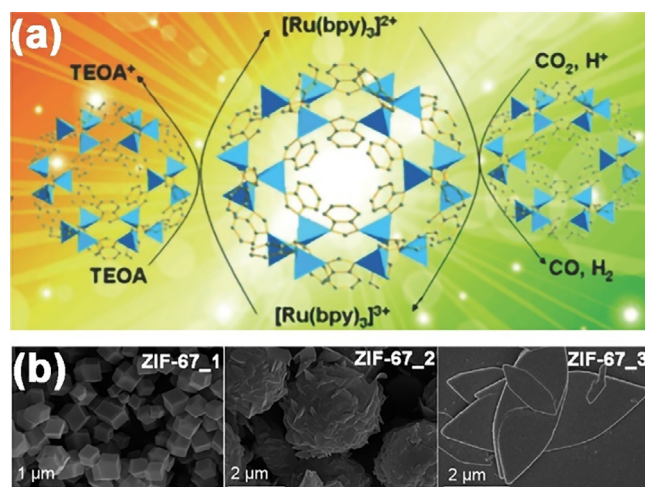


Fig. 18. (a) Representation of photocatalytic CO_2 reduction over Co-ZIF-9 [245]. Copyright 2014 Wiley-VCH®. (b) SEM images of ZIF-67 with different morphologies [247]. Copyright 2018 RSC®.

3.1.4. Others

Other ligands with special characteristics, such as large π -conjugated group and high visible-light harvesting abilities, have also been applied for constructing MOFs with photocatalytic CO₂RR properties. In 2014, Wang et al. reported the photocatalytic CO₂RR property of Co-ZIF-9, a porous framework composed of Co²⁺ ions and benzimidazole (blm) ligands (Fig. 18a) [245]. Upon visible-light illumination, CO₂ was reduced to CO along with the evolution of H₂. When Co-MOF-74 (with 2,5-dihydroxyterephthalic acid as the ligand) was used instead of Co-ZIF-9 as the catalyst, the catalytic efficiency was greatly decreased. This may be attributed to the high CO₂ capture capacity of Co-ZIF-9 (the blm ligands show high chemical affinity to CO₂). Such finding suggests that assembling various functional organic ligands into porous MOF materials will open up new opportunities in artificial photosynthesis. Later on, they developed ZIF-67 nanocrystals, a porous framework composed of Co²⁺ ions and 2-methylimidazole (2-Melm) ligands, as the catalyst to reduce CO₂ [246]. It was found that CO₂ was reduced

to CO with an evolution rate of 37.4 $\mu\text{mol}/30\text{ min}$. However, with ZIF-8 (with the same framework with ZIF-67 but with Zn²⁺ center) as the catalyst, a much lower CO evolution rate was obtained. Thus, the highly efficient performance of ZIF-67 was attributed to both of the high CO₂ uptakes and the investigation of Co²⁺. In 2018, Liu and Sun et al. reported that the morphology of ZIF-67 can also affect their photocatalytic activity towards CO₂RR (Fig. 18b) [247]. They prepared three different types of ZIF-67 with different morphologies. As the 2D leaf-like ZIF-67 showed the highest CO₂ capture capability, it exhibited higher catalytic activity than both rhombic dodecahedral and pitaya-like morphology.

Very recently, Lan et al. reported a “Two-in-One” strategy for efficient CO₂RR [248]. Two eco-friendly biomimetic MOFs were prepared for their study ([Co₂(AD)₄H₂(BDA)]·DMF·2H₂O (AD-MOF-1) and [Co₂(AD)₄H₂(IBA)₂]·DMF (AD-MOF-2)) (Fig. 19a and b). Firstly, the -NH₂ of HAD ligands acted as auxochromic groups to make MOFs responsive to visible light. Secondly, the uncoordinated aromatic nitrogen of HAD (on the *o*-position of -NH₂) acted

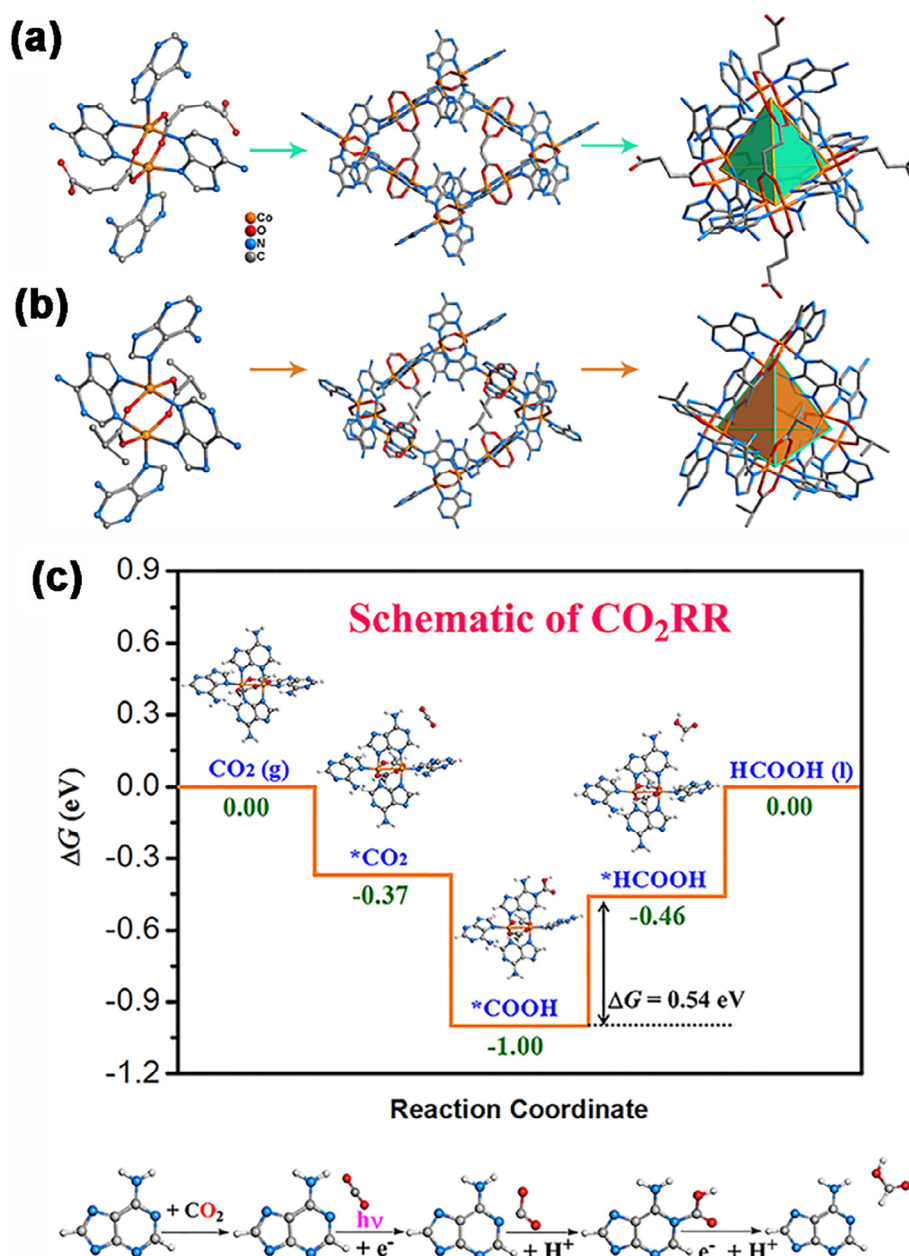


Fig. 19. (a) and (b) Structures of AD-MOF-1 and AD-MOF-2. (c) Reaction path of CO₂-to-HCOOH reduction under visible-light irradiation. [248] Copyright 2019 Wiley-VCH®.

as an active position for CO₂RR (Fig. 19c). Photocatalytic CO₂RR was carried out in pure aqueous solution without any other photosensitizer. Under the visible-light irradiation for 5 h, HCOOH production over AD-MOF-2 was detected to be as high as 22.16 μmol ($443.2 \text{ mol g}^{-1} \text{ h}^{-1}$). These results indicated that the “Two-in-One” strategy efficient improved the photocatalytic CO₂RR performance of the MOFs.

He et al. prepared a 3D Gd-MOF based on TCA³⁻ ligands and Gd-oxygen chains for CO₂RR [249]. Solid-state electrochemistry showed a redox potential of the Gd-TCA⁺/Gd-TCA couple at 0.82 V (vs SCE), indicating that the redox potential of the excited state Gd-TCA⁺/Gd-TCA* couple was -2.30 V . The excited state potential of Gd-TCA was negative enough to reduce Ni(Cyclam)Cl₂, which is well-known for its catalytic property for CO₂ reduction. Fluorescence technique also confirmed that the photo-induced electron could transfer from Gd-TCA to Ni(Cyclam)Cl₂. Thus, an artificial system for CO₂RR was created with Gd-TCA and Ni(Cyclam)Cl₂. Upon visible-light irradiation for 12 h, the system produced about 22.7 μmol HCOOH.

Later on, Sun et al. reported a novel pillared-layer MOF [Co₃(-OH)₃(TCA)(4,4'-bpy)_{1.5}] (Co₆-MOF) with highly CO₂ adsorption capacity of $38.17 \text{ cm}^3 \text{ g}^{-1}$ at 298 K [250]. The high CO₂ capacity of Co₆-MOF advised it to act as the photocatalyst for CO₂RR. However, when only Co₆-MOF was added as a photocatalyst, no reduction product was detected. Thereafter, a [Ru(bpy)₃]²⁺ photosensitizer was added, and then yields of 39.36 μmol CO and 28.13 μmol H₂ were obtained. During the reduction process, the excited electrons were transferred from the [Ru(bpy)₃]²⁺ to the LUMO of the Co-MOF. Thereafter, the charged Co₆-MOF facilitated the reduction of CO₂.

Very recently, Li and Lan et al. reported three isostructural monometallic MOFs (MOF-Ni, MOF-Co and MOF-Cu) for CO₂RR

(Fig. 20a) [251]. CO and H₂ were detected as the reduction product in a CO₂-saturated MeCN/H₂O (13:1) solution with triisopropanolamine as an electron donor. The amount of CO produced over MOF-Ni, MOF-Co and MOF-Cu were detected to be 22.3 μmol , 22.8 μmol and 1.7 μmol , respectively. Although MOF-Ni and MOF-Co gave similar CO yields, MOF-Ni exhibited a much higher CO selectivity (97.7%) than MOF-Co (47.4%). Photocurrent characterizations showed that the different catalytic activity of these MOFs was attributed to their different charge separation efficiency. Otherwise, the higher selectivity for MOF-Ni was attributed to its strong coupling effect between Ni and CO₂ (Fig. 20b) and high free energy for proton reduction (Fig. 20d).

The ligands with large π -conjugated fragments can enhance both of the photophysical and electrochemical properties of MOFs. When 4,40-(anthracene-9,10-diylbis(ethyne-2,1-diyl))dibenzoic acid was applied to assemble with Zr⁴⁺ under solvothermal condition, NNU-28 was prepared with broad-band visible-light absorption up to 650 nm [252]. In addition, NNU-28 also showed high CO₂ uptake of $33.42 \text{ cm}^3 \text{ g}^{-1}$ at 298 K. Thus, NNU-28 is investigated as the photocatalyst for CO₂RR. NNU-28 showed high activity for CO₂RR without any other photosensitizer, giving an HCOOH formation rate of $183.3 \text{ mmol h}^{-1} \text{ mmol}_{\text{cat}}^{-1}$. The high catalytic activity of NNU-28 was achieved by both sensitizing Zr-oxo cluster through the LMCT process and generating radicals of the anthracene-based ligands (Fig. 21a). Very recently, Zhou and Lan et al. reported another two isomorphous Zr-MOFs with HCBB (pbz-MOF-1) and HCHC (PCN-136) ligand, respectively (Fig. 21b) [253]. When HCBB was replaced by HCHC via a single-crystal-to-single-crystal process, the formation of large π -conjugated fragments dramatically enhanced the photocatalytic activity of PCN-136. HCOOH evolution rate over PCN-136 was about 3 times higher than that over pbz-MOF-1.

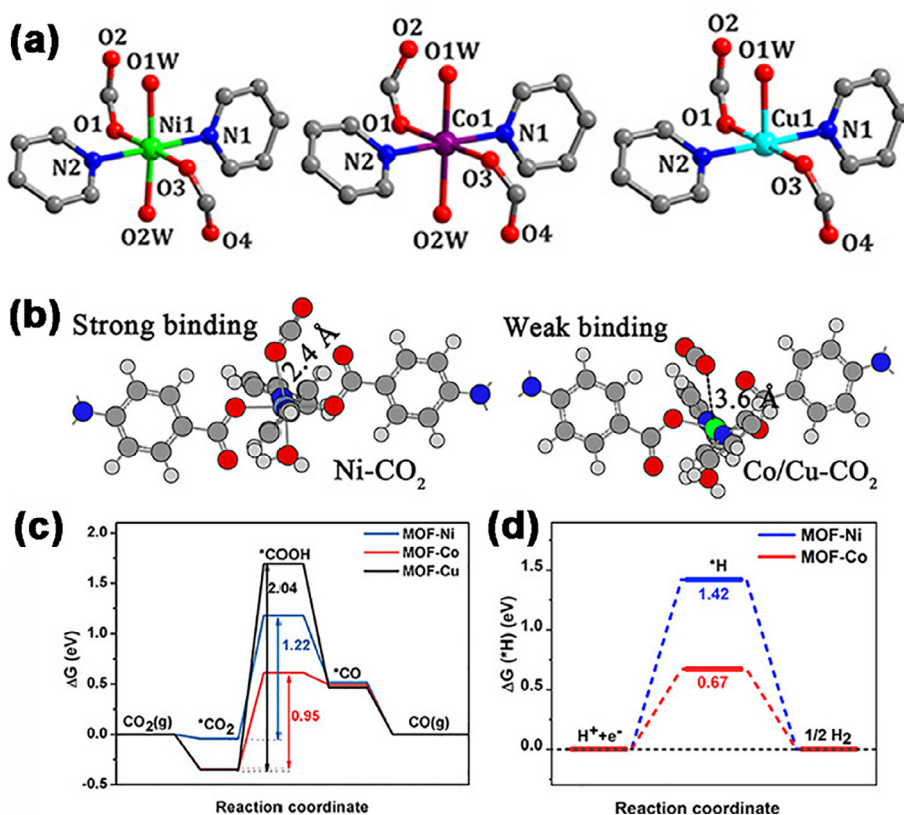


Fig. 20. (a) Coordination environments of Ni, Co and Cu ions in MOFs. (b) Simulated distances between CO₂ and metal ions. (c) The free energy diagram of CO₂RR. (d) The free energy diagram of H₂ evolution reaction. [251] Copyright 2019 ACS.

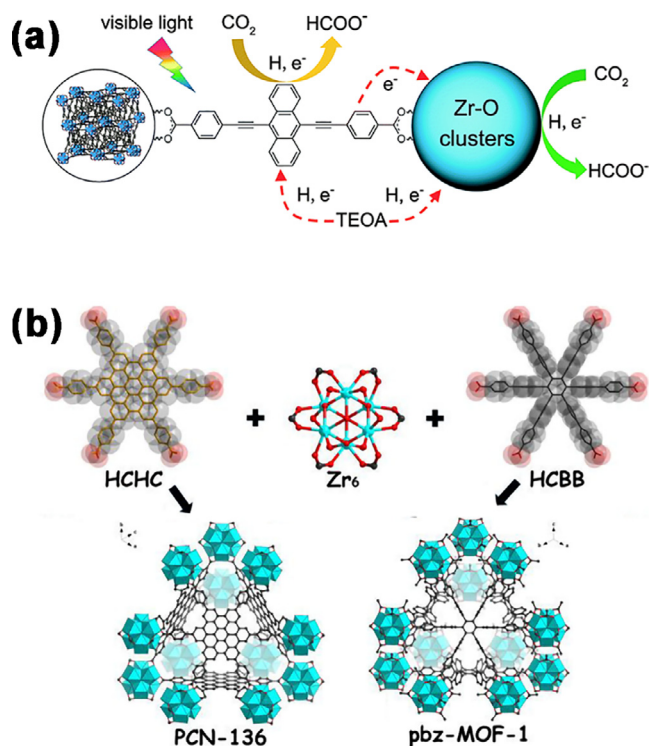


Fig. 21. (a) Dual photocatalytic routes for CO₂ reduction over NNU-28 [252]. Copyright 2016 RSC. (b) Structures of PCN-136 and pbz-MOF-1 [253]. Copyright 2019 ACS.

Recently, Su and Lan et al. reported two inorganic frameworks based on strong reductive [P₄Mo₆^V] units [254]. In this structure, the [P₄Mo₆^V] cluster was served as a multi-electron donor, and the transition metal ions were treated as active sites for CO₂ reduction (Fig. 22). CH₄ was detected as the major reduction product. This work inspires that combining strong reductive component into the framework is a feasible strategy to construct catalysts for reducing CO₂ to hydrocarbons.

3.2. Functional metal clusters

Some of MOFs containing inherent coordinatively unsaturated metal sites can activate the CO₂ molecules through coordination effect. Otherwise, CO₂ adsorption heats of MOFs with open metal sites are relatively high, leading to substantial selective CO₂ uptake [255,256]. With these advantages in hands, MOFs with open metal sites suggest a significant research direction. Three Fe-MOFs (MIL-101(Fe), MIL-53(Fe) and MIL-88B(Fe)) with same BDC ligand have been chosen as photocatalysts for CO₂RR [257]. All of three Fe-MOFs could reduce CO₂ to HCOOH. Such results confirm that the photo-induced electrons transfer from O²⁻ to Fe³⁺ is responsible for CO₂RR. When modified these MOFs with the NH₂-BDC, photocatalytic activity for CO₂ reduction was obviously improved due to the synergetic effect of dual excitation pathways (Fig. 23a).

The synergistic effect of neighboring sites of open metal centers can also promote the catalytic performance of MOFs-based photocatalyst in CO₂RR. The cooperation effect between the open metal sites and their neighboring μ -OH⁻ groups has been confirmed by comparing the photocatalytic activities of a series of Co-MOFs [258]. Two isostructural honeycomb-like Co-MOFs, namely, [Co₂(μ -Cl)₂(bbta)] (MAF-X27-Cl) and [Co₂(μ -OH)₂(bbta)] (MAF-X27-OH), were chosen for study. TOFs of CO evolution over MAF-X27-OH was 4.4 times higher than that of MAF-X27-Cl. Otherwise,

the CO selectivity of MAF-X27-OH (97.2%) was also much higher than that of MAF-X27-Cl (63.6%). The only difference between the two structure was the μ -Cl/ μ -OH groups at the neighboring sites of Co, indicating the usefulness of the μ -OH⁻ groups (Fig. 23b). In addition, another isorecticular MOF [Co₂(μ -OH)₂(btdd)] (MAF-X27I-OH) with expanded pore size was prepared. MAF-X27I-OH showed higher CO selectivity (98.2%) and TOFs (0.059 s⁻¹) than MAF-X27-OH, because its larger pore size allows quicker diffusion of the reactants/products.

By substituting Zr ions of NH₂-UiO-66 with Ti ions, the resulting mixed metal NH₂-UiO-66(Zr/Ti) showed enhanced activity for photocatalytic CO₂RR (Fig. 23c) [259]. It was because that the substituted Ti ions in the framework helps to improve the interfacial charge transfer from excited NH₂-bdc to Zr^{IV}. Then, Zr^{III} was formed as the active species for photocatalytic CO₂-to-HCOOH reduction. Later on, Kang and Cohen et al. reported a similar approach. They indicated that the Ti-doped NH₂-UiO-66 can supply an added light absorption route, slow down the recombination rate of photogenerated electron-hole pairs and improve the charge separation [260]. In addition, they introduced diamine-substituted ligands into the framework to prepare the mix modified MOFs (mixed-metal and mixed-ligand) (Fig. 23d). The mix modified MOFs achieved an average TON_{HCOOH} of 6 in 6 h, indicating that each Ti site transferred about 13 electrons to CO₂ over the course of each catalytic run. These works showed a controllable way to construction MOF-based photocatalysts with the desired performance. As more and more MOFs with mixed metal clusters are reported, this strategy will become more efficiency for constructing high active photocatalysts for CO₂RR [261].

Defects in the solid heterogeneous photocatalyst can also provide active sites for CO₂RR. Xu and Zheng et al. prepared a spongy nickel-organic photocatalyst through laser-induced solution reactions [262]. In the synthesis process, soft triethylene glycol (TEG) was used to replace part of rigid BDC. When TEG was weaved into the Ni-TPA framework, a highly disordered and defective metal-organic hybrid (Ni(TPA/TEG)) was prepared due to the lack of essential carboxylic groups (Fig. 24a and b). The defects of as-synthesized crystalline Ni(TPA/TEG) can be performed as the catalytic active sites for CO₂ reduction. After a 2 h reaction, about 95.2 μ mol of CO was yielded over Ni(TPA/TEG), giving an evolution rate of 15,866 μ mol h⁻¹ g⁻¹. Remarkably, the selectivity of gas production (CO) was nearly 100%. The spongy Ni(TPA/TEG) catalyst could keep its activity and selectivity after five recycle photocatalytic reaction. In addition, the produced CO could be used as a reactant for the production of liquid fuels (HCOOH and CH₃COOH) after decorating the spongy catalysts with Rh or Ag nanocrystals (Fig. 24c–f).

4. Hybrid systems

Although pure MMCs and MOFs possess many advantages for CO₂RR, their low charge transfer capability severely hinder the improvement of their performance. Otherwise, as homogeneous catalysts, MMCs are difficult to be separated from the homogeneous systems. In recent years, a variety of hybrid photocatalysts have been fabricated by combining MMCs or MOFs with solid materials to overcome the above shortages. This strategy shows the following two advantages. Firstly, a heterojunction formed in the nanocomposites can increase charge separation and then increase photocatalytic CO₂RR activity. The long-term stabilities of MMCs or MOFs are also improved after compositing. Secondly, homogeneous MMCs will turn to heterogeneous catalysts after composite, and they can easier be separated from the reaction system. Therefore, this strategy is deemed to be a new aspect for developing CO₂ reduction photocatalysts with practical

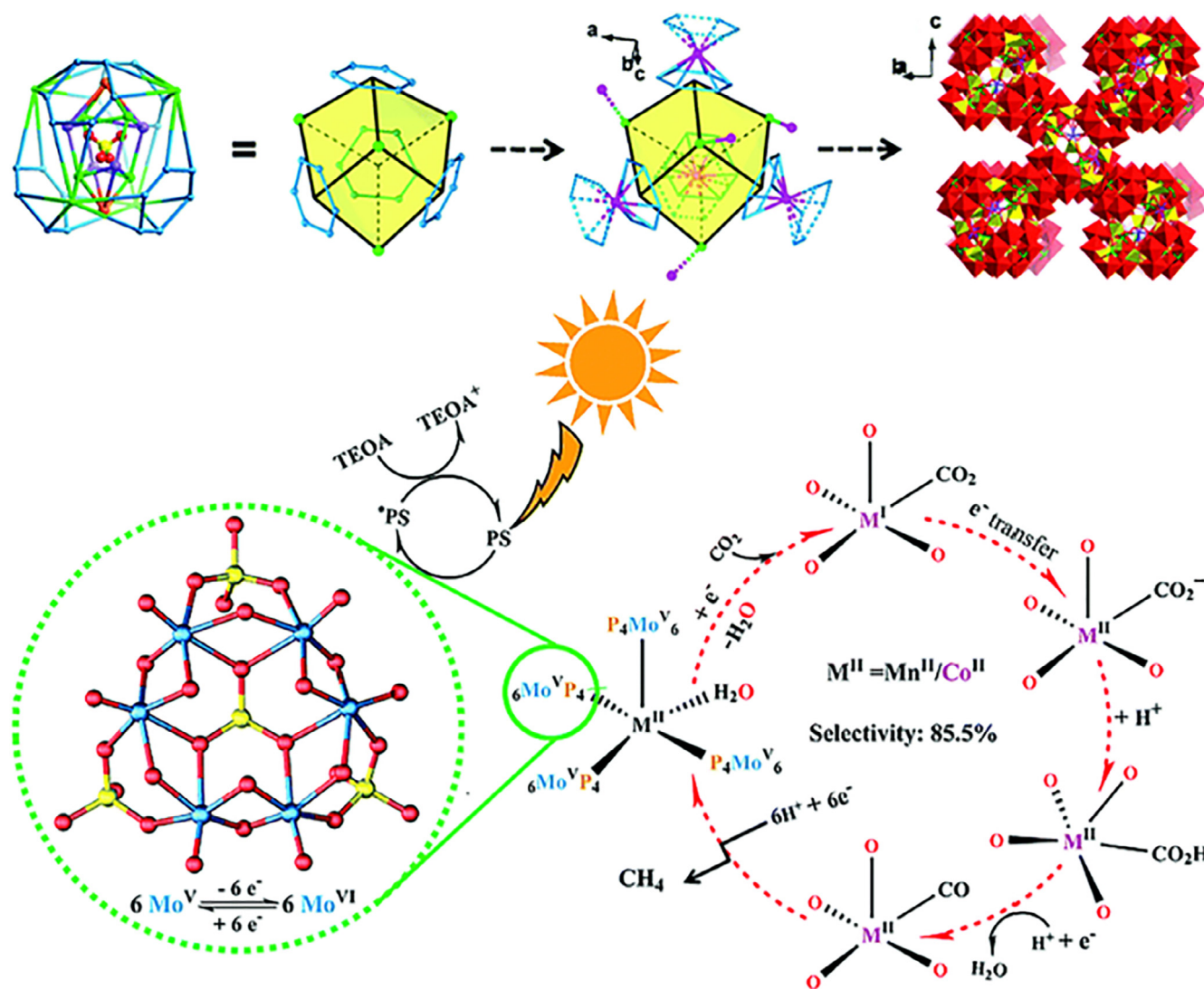


Fig. 22. Representation of catalytic CO₂ reduction over NENU-605 [254]. Copyright 2019 RSC©.

application. The photocatalytic CO₂ reduction systems contain MMCs-based hybrids and MOFs based hybrids were summarized in Tables 5 and 6, respectively.

4.1. Hybrid systems based on molecular metal complexes

Some approaches have been investigated to combine MMCs with inorganic semiconductors [59,263–289], organosilicas [290–294] and other solids [58,295–305]. In this section, methods for combining MMCs with inorganic semiconductors and organosilicas will be discussed in detail.

4.1.1. Composed with inorganic semiconductors

Inorganic semiconductors, which are generally composed of earth-abundant elements, normally act as photosensitizers in the hybrid CO₂RR systems. Three different types of hybrid systems will be discussed (Scheme 3).

In the first type hybrid system, photoelectrons are transferred from the conduction band (CB) of semiconductors to MMCs. Thereafter, CO₂ was reduced by the activated metal complexes. In this type hybrids, the potential of the CB minimum of the semiconductor should be more negative than the CO₂ reduction potential. Sato et al. firstly reported a hybrid CO₂ reduction catalyst by connecting

compound **64** with *p*-type semiconductor (N-doped Ta₂O₅) through the carboxylic group [59]. Photocatalytic CO₂ reduction yielded HCOOH, CO and H₂ with a selectivity of 75% for HCOOH (TON_{HCOOH} = 89). Later on, they noticed that when the anchor group was changed from –COOH to –PO₃H, the HCOOH evolution rate grew about 5 times [263]. In contrary, when no anchor groups on the Ru complex, the system shows the lowest photocatalytic performance.

Maeda and co-workers reported a hybrid photocatalyst for CO₂-RR through combining graphitic carbon nitride (g-C₃N₄) with compound **67** [264]. In this system, g-C₃N₄ worked as a photosensitive unit while Ru complex worked as a catalytic unit. Under the visible-light irradiation, the hybrid could reduce CO₂ to HCOOH with a selectivity of >80% and a TONs of up to 200. Later on, they found that both surface area and crystallinity of g-C₃N₄ would affect the photoactivity of the hybrid catalyst [265]. When the mesoporous were introduced into g-C₃N₄ materials, the loading amount of Ru catalyst was increased and the length of electron-hole migration was reduced. Then, the activity of the hybrid catalyst was enhanced. However, too much introduction of mesoporous will increase the density of defects, leading to an activity drop. Thereafter, they further adjusted the electrons injection and electronic interactions between the g-C₃N₄ and Ru complex

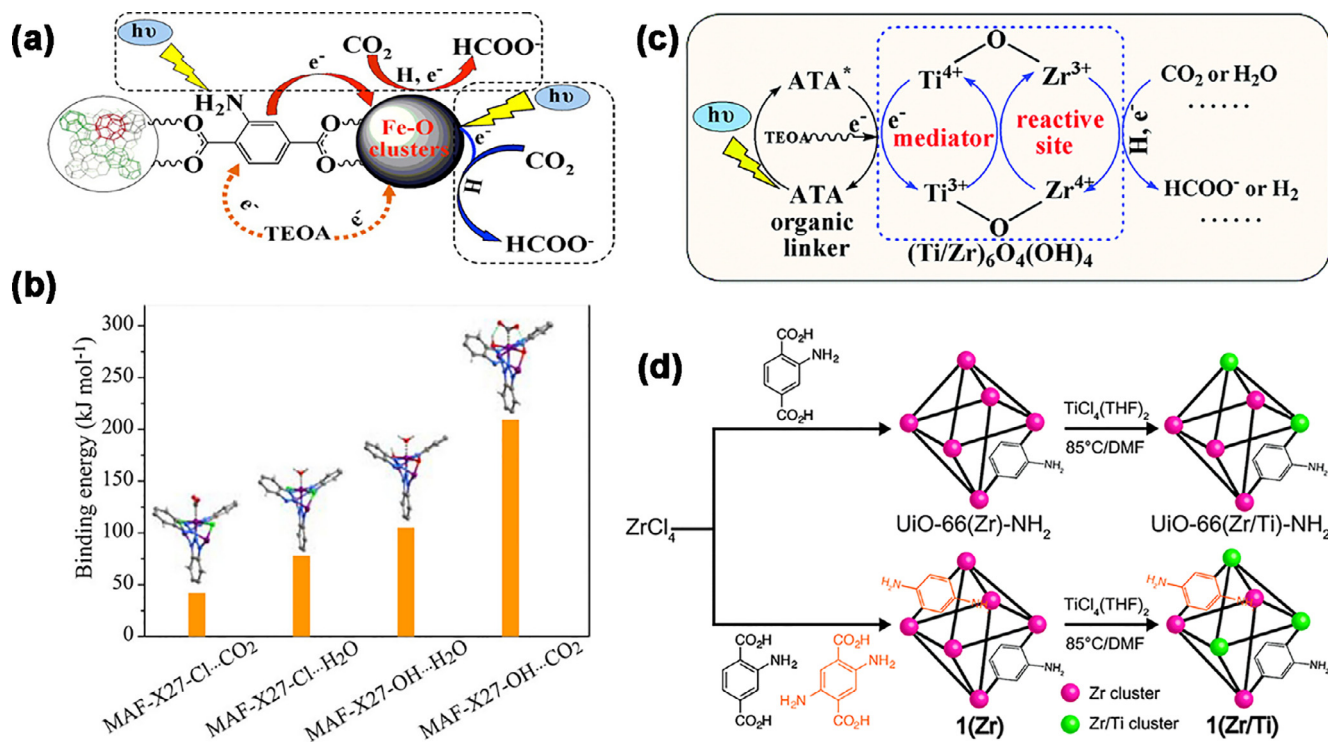


Fig. 23. (a) Representation of dual excitation pathways in NH₂-MIL-101 [257]. (b) CO₂ and H₂O binding energies of MAF-X27-Cl and MAF-X27-OH [258]. Copyright 2018 ACS. (c) A mechanism for the catalytic activity enhancement of NH₂-Uio-66(Zr/Ti) [259]. (d) Synthesis of mix modified NH₂-Uio-66(Zr/Ti) [260]. Copyright 2015 RSC.

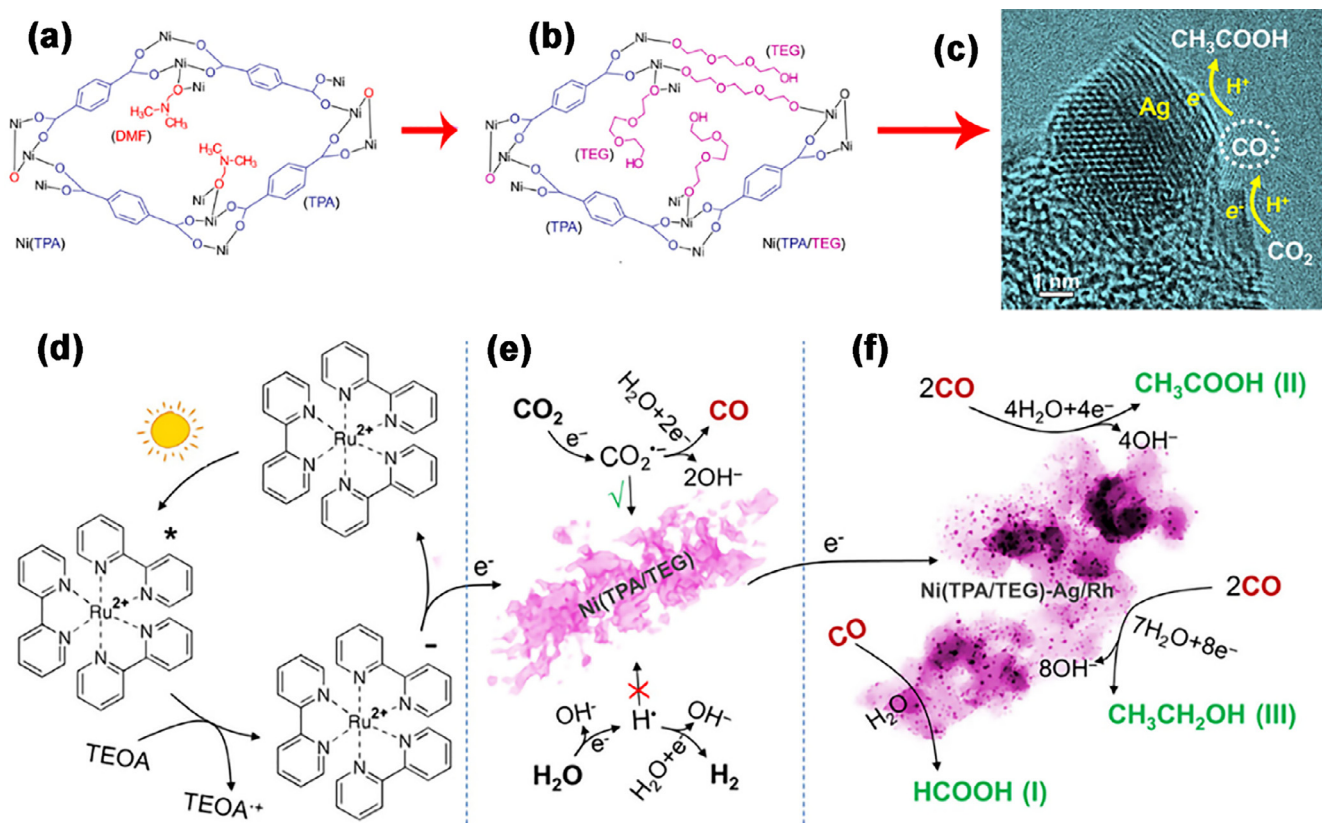
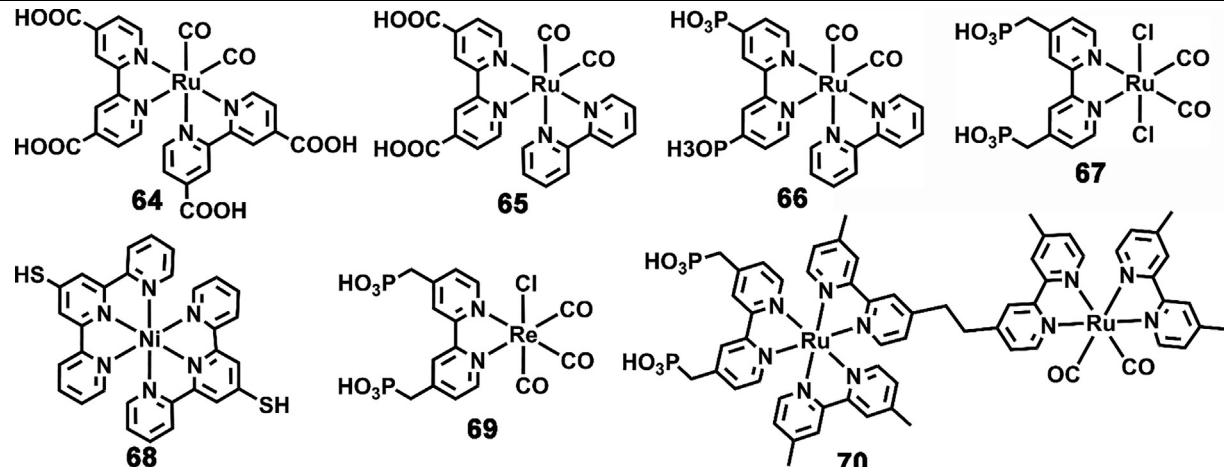


Fig. 24. Structures of Ni-TPA (a) and Ni(TPA/TEG) (b). (c) STEM image of Ag@Ni(TPA/TEG). (d) Electrons transfer from [Ru(bpy)₃]²⁺ to Ni(TPA/TEG). (e) CO₂ was reduced to CO over Ni(TPA/TEG). (f) HCOOH, CH₃COOH, and CH₃CH₂OH were produced over Ag/Rh@Ni(TPA/TEG) [262]. Copyright 2017 Science Journals.

Table 5
Photocatalytic CO₂ reduction with MMCs-based hybrids.^a

							
Compound	Product	TON	Yield	Solvent	SD	λ	Ref.
64 /N-doped Ta ₂ O ₅	HCOOH	89	–	MeCN	TEOA	>410 nm	[59]
65 /N-doped Ta ₂ O ₅	HCOOH	24	–	MeCN	TEOA	>410 nm	[263]
66 /N-doped Ta ₂ O ₅	CO	17	–	MeCN	TEOA	>410 nm	[263]
	HCOOH	118	–				
67 /mpg-g-C ₃ N ₄	CO	67	–	MeCN	TEOA	>400 nm	[264]
	HCOOH	200	–				
67 /g-C ₃ N ₄	HCOOH	20	1.2 μmol	MeCN	TEOA	>400 nm	[266]
66 /g-C ₃ N ₄	HCOOH	55	3.4 μmol	MeCN	TEOA	>400 nm	[266]
66 /g-C ₃ N ₄	HCOOH	141	8.8 μmol	DMA	TEOA	>400 nm	[266]
Fe-TCPP/g-C ₃ N ₄	CO	5.7	6.52 mmol g ^{−1}	MeCN-H ₂ O	TEOA	>420 nm	[268]
24a /mpg-g-C ₃ N ₄	CO	155	12.4 μmol	MeCN	TEOA	>400 nm	[270]
68 /CdS QD	CO	20	4.02 μmol	DMF	TEOA	>400 nm	[271]
Fe-TCPP/ZnCdS	CO	–	1.28 μmol	MeCN-H ₂ O	TEOA	>420 nm	[272]
69 /Dye (Fig. 25a)/TiO ₂	CO	435	–	DMF	BIH	>420 nm	[273]
69 /Ir-PS (Fig. 25b)/TiO ₂	CO	300	–	DMF-H ₂ O	BIH	>420 nm	[276]
69 /Dye (Fig. 25c)/TiO ₂	CO	1028	103 μmol	DMF-H ₂ O	BIH	>550 nm	[277]
66 /TiO ₂ /InP	HCOOH	–	–	H ₂ O	–	>400 nm	[279]
66 /SrTiO ₃ /InP	HCOOH	–	1.45 μmol	H ₂ O	–	>400 nm	[280]
Fe-TCPP/CdS/Bi ₂ S ₃	CO	–	38.6 μmol	MeCN-H ₂ O	TEOA	>420 nm	[281]
70 /Ag/TaON	HCOOH	41	996 nmol	MeOH	MeOH	<400 nm	[282]
	CO	2.8	68 nmol	DMA	TEOA	>400 nm	[284]
70 /Ag/CaTaO ₂ N	HCOOH	114	–				
70 /Ag/C ₃ N ₄	HCOOH	–	5.0 μmol	H ₂ O	EDTA·2Na	>400 nm	[285]
66 /Ag/C ₃ N ₄	HCOOH	–	10.4 μmol	DMA	TEOA	<400 nm	[286]

^a TON represents turn over number; SD represents sacrificial donor; λ represents the wavelength of the irradiation light.

through modifying the anchor groups [266]. When g-C₃N₄ and Ru center were connected by -PO₃H group directly, the hybrid catalyst showed the highest photoactivity.

Other MMCs have also been composite with g-C₃N₄ to prepare high efficient photocatalyst for CO₂ reduction [267–270]. When composed molecular catalyst Fe-TCPP with g-C₃N₄, the resulting hybrid can photocatalytically reduce CO₂ to CO with a selectivity of 98% [268]. The carboxyl groups could enhance electron interactions between g-C₃N₄ and Fe-TCPP and then enhanced their photocatalytic activity. Robert and collaborators reported a hybrid photocatalyst consisting of a mesoporous g-C₃N₄ and an iron complex [Fe(qpy)(H₂O)₂]²⁺ for photocatalytic CO₂RR [270]. Upon irradiation under the visible-light (λ ≥ 400 nm), the hybrid system gave a TON_{CO} of 155 with a selectivity of 97% and an apparent QY of about 4.2%.

Some of the photosensitive metal sulfides have been combined with MMCs for photocatalytic CO₂RR. Reisner et al. connected nickel bis(terpyridine) complexes with CdS QDs through anchor groups, such as -COOH, PO₃H and -SH [271]. In this hybrid, CdS QDs worked as a photosensitizer and nickel bis(terpyridine) complex worked as a catalytic center. Under visible-light illumination in water, photocatalytic CO₂-to-CO reduction with a >90% selectivity

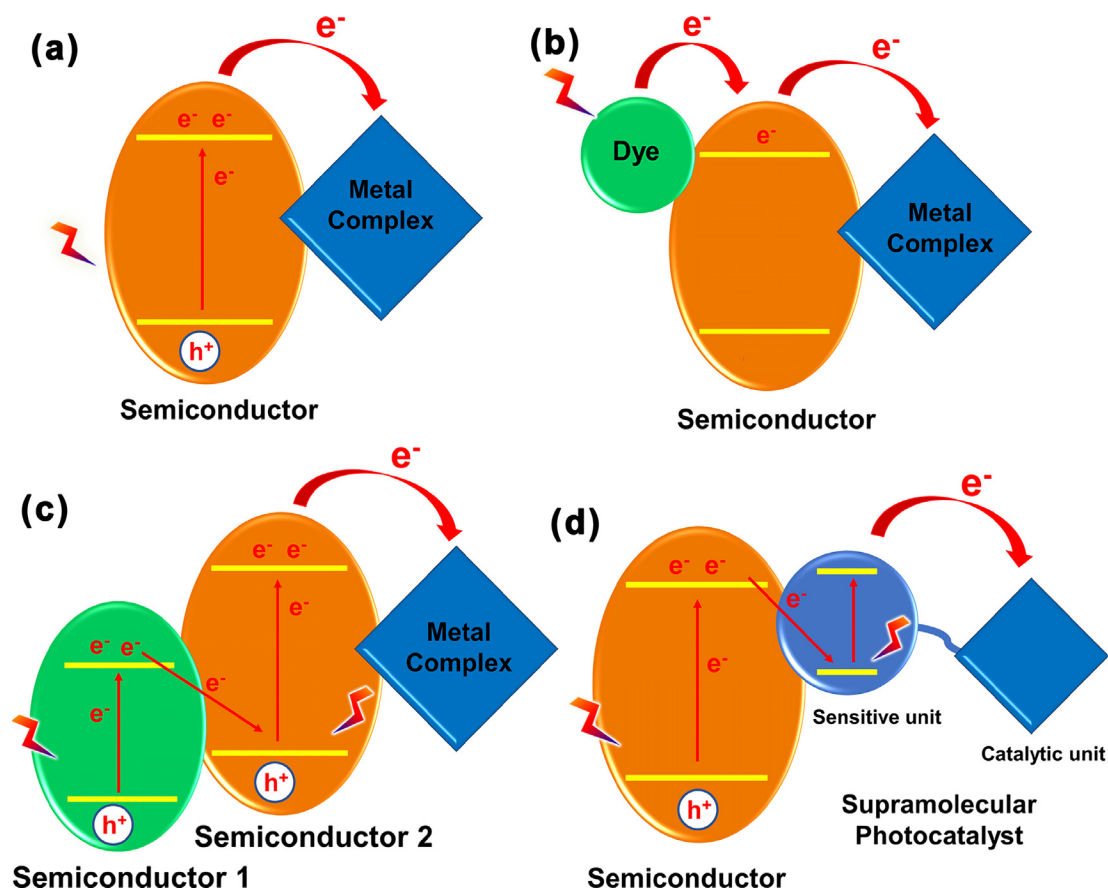
was achieved when -SH was chosen as anchor group. Later on, He and collaborators reported that introduction of Zn into CdS could enhance the activity, selectivity and stability of the obtained photocatalysts [272]. The presence of Zn could build efficient electron transfer channels between sulfide complex and Fe-TCPP, and then greatly facilitated the interfacial charge transfer.

Sometimes, three components hybrid systems were constructed for CO₂RR because some of the inorganic semiconductors are insensitive to visible light. These systems include a dye photosensitizer for “electron pool”, an inorganic semiconductor for “conductor” and a molecular metal complex for “catalysis”. Kang and collaborators reported a series of hybrid photocatalysts based on this strategy [273,274,276,277]. The first example was reported with a dye-sensitized TiO₂ (Fig. 25a) and a molecular Re complex **69** [273]. During the photocatalytic process, the dye photosensitive units on the surface of TiO₂ were excited by light, and then the photoelectrons were injected into the CB of TiO₂ and transferred to the catalytic units immobilized on the TiO₂. Then, CO₂ was reduced at Re unit to generate CO (TON_{CO} > 435). The hybrid system with only TiO₂ and **69** can also photocatalytically reduce CO₂ to CO but with a much lower TON [275]. Later on, they reported a high efficient dye-sensitized ternary system by using Zn-

Table 6
Photocatalytic CO₂ reduction with MOFs-based hybrids.^a

Compound	Product	Yield	Solvent	SD	λ	Ref.
ZIF-8/Zn ₂ GeO ₄	CH ₃ OH	0.86 μmol	H ₂ O	Na ₂ SO ₃	>320 nm	[306]
ZIF-8/Cu-TiO ₂	CH ₃ OH	2238 ppm	DMA	TEOA	>320 nm	[307]
	CO	2170 ppm				
Co-ZIF-9/g-C ₃ N ₄	CO	20.8 μmol	MeCN-H ₂ O	TEOA	>420 nm	[308]
Co-ZIF-9/CdS	CO	50.4 μmol	MeCN-H ₂ O	TEOA	>420 nm	[309]
Co-ZIF-9/TiO ₂	CO	8.79 μmol	H ₂ O	–	>200 nm	[310]
	CH ₄	0.99 μmol				
HKUST-1/TiO ₂	CH ₄	3.2 μmol	H ₂ O	–	< 400 nm	[311]
HKUST-1/Cu ₂ O/TiO ₂	CH ₄	155 $\mu\text{mol g}^{-1} \text{h}^{-1}$	H ₂ O	–	>320 nm	[312]
	CO	85 $\mu\text{mol g}^{-1} \text{h}^{-1}$				
CPO-27-Mg/TiO ₂	CH ₄	23.5 $\mu\text{mol g}^{-1}$	H ₂ O	–	~365 nm	[313]
	CO	40.9 $\mu\text{mol g}^{-1}$				
MOF-74-Mg/Zn ₂ GeO ₄	CO	12.94 $\mu\text{mol g}^{-1}$	MeCN-H ₂ O	–	>200 nm	[314]
NH ₂ -UiO-66/CsPbBr ₃	CH ₄	3.08 $\mu\text{mol g}^{-1}$	EtOAc-H ₂ O	–	>420 nm	[315]
	CO	98.574 $\mu\text{mol g}^{-1}$				
ZIF-67/CsPbBr ₃	CH ₄	4.736 $\mu\text{mol g}^{-1}$	H ₂ O	–	>420 nm	[316]
	CO	1.516 $\mu\text{mol g}^{-1}$				
BIF-20/g-C ₃ N ₄	CH ₄	1.86 $\mu\text{mol g}^{-1}$	MeCN	TEOA	>420 nm	[317]
	CO	6.46 $\mu\text{mol g}^{-1}$				
UiO-67-Co/CdS	CO	235 $\mu\text{mol g}^{-1} \text{h}^{-1}$	MeCN	TEOA	>420 nm	[318]
GNP-TiO ₂	CH ₄	62 ppm	H ₂ O	–	>200 nm	[327]
(derived from Au@MIL-125)						
Fe@C (derived from MIL-101)	CO	2196.17 μmol	–	H ₂	>420 nm	[328]
Co ₃ O ₄ -NS (derived from ZIF-67)	CO	4.52 $\mu\text{mol h}^{-1}$	MeCN-H ₂ O	TEOA	>400 nm	[329]
		([Ru(bpy) ₃] ²⁺)				
In ₂ S ₃ -CdIn ₂ S ₄ (derived from MIL-68)	CO	825 $\mu\text{mol h}^{-1} \text{g}^{-1}$	MeCN-H ₂ O	TEOA	>400 nm	[330]
In ₂ S ₃ -CuIn ₂ S ₄ (derived from MIL-68)	CO	19.00 $\mu\text{mol g}^{-1} \text{h}^{-1}$	MeCN-H ₂ O	TEOA	>400 nm	[331]
In ₂ O ₃ -ZnIn ₂ S ₄ (derived from MIL-68)	CO	3075 $\mu\text{mol h}^{-1} \text{g}^{-1}$	MeCN-H ₂ O	TEOA	>400 nm	[332]
CdS (derived from ZIF-8)	CO	3758 $\mu\text{mol h}^{-1} \text{g}^{-1}$	MeCN-H ₂ O	TEOA	>400 nm	[333]

^a SD represents sacrificial donor; λ represents the wavelength of the irradiation light.



Scheme 3. Three different types of hybrid systems based on MMCs and semiconductors. (a) MMC directly connect with a semiconductor. (b) Three components hybrid system based on dye, semiconductor and MMC. (c) and (d) represent two different types of artificial Z-scheme.

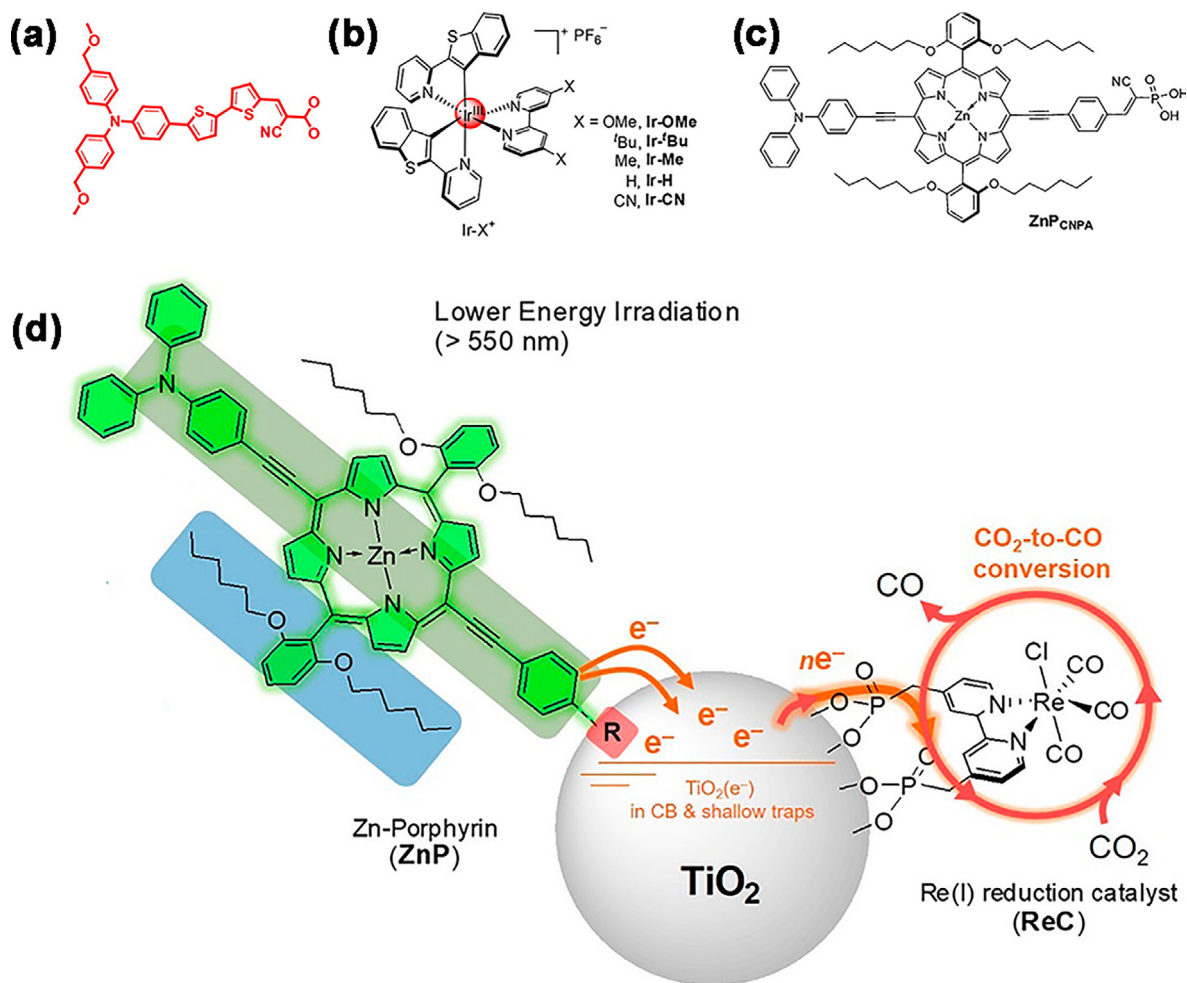


Fig. 25. (a), (b) and (c) Some classic molecular dyes used in the dye-sensitized ternary system. (d) Strategies used for enhancing the performance of Zn-porphyrin-[TiO₂]-Cat system [277]. Copyright 2018 ACS.

porphyrin complex as the dye (Fig. 25c) [277]. Three synthetic modifications were performed on the Zn-porphyrin dye to improve the performance of the Zn-porphyrin-[TiO₂]-Cat system (Fig. 25d). Firstly, extending the π -conjugation to achieve facile lower energy sensitization. Secondly, incorporating linear hexyl groups to avoid dye aggregation. Thirdly, the cyanophosphonic acid was chosen as an anchor group to increase the long-term stability. With these advance strategies executed, the hybrid Zn-porphyrin-[TiO₂]-Cat hybrid showed a TON_{CO} of 800 for CO evolution over an extended time period of 90 h under the irradiation of red light (>550 nm, light intensity of 207 mW/cm²).

In the third type hybrid system (so-called “Z-scheme”), two-step excitation process using two-photons have been achieved with two strategies [278]. The first was constructed by two kinds of semiconductor and one MMCs. The second was constructed by combining a semiconductor and a supramolecular photocatalyst. At the very beginning, TiO₂, *p*-type InP and Ru polymer based on compound **66** were combined to constructed a Z-scheme photocatalyst (Fig. 26a) [279]. The ternary hybrid can act as photocathode in the photoelectrochemical cell to catalyze CO₂-to-HCOOH reduction. In this photoelectrochemical cell, TiO₂ and InP/[RuCP] was separated by proton exchange membrane and connected with a wire. Later on, TiO₂ was replaced by SrTiO₃ (STO), and the QY was improved from 0.03% to 0.14% [280]. In fact, STO/InP/[RuCP] could perform photo-induced CO₂ reduction in a one-

compartment reactor with no wire connector and no proton exchange membrane.

He and collaborators reported a hybrid photocatalyst constructed by Fe-TCPP as a catalyst and CdS/Bi₂S₃ heterostructure as a photosensitizer (Fig. 26b) [281]. In this hybrid, the formation of CdS/Bi₂S₃ heterostructure (Z-scheme) could increase the charge separation and utilization. With these advantages, CdS/Bi₂S₃-0.5 h/FeTCPP yielded 8.2 times of CO and 1.7 times of H₂ higher than CdS/FeTCPP.

Ishitani and collaborators constructed the second artificial Z-scheme by combining Ag-loaded TaON and supramolecular photocatalyst (Fig. 26c) [282]. In the hybrid system, the Ru(Me-bpy)CO₂Cl₂ unit worked as a reducing center while Ag/TaON worked as an oxidizing center. During the photocatalytic process, two-step excitations of Ag/TaON and the [Ru(dmb)₃]²⁺ unit occurred. In this type hybrid, the selected semiconductor must be optically excited under visible-light irradiation, and its conductive band should be more negative to allow the photoelectrons transfer to the [Ru(dmb)₃]²⁺ unit (Fig. 26d) [283]. In addition, Ag-CaTaO₂N and Ag-g-C₃N₄ nanosheets could also be investigated as the semiconductor component, photocatalytic reduction of CO₂-to-HCOOH was obtained over these hybrids [284,285]. The roles of the loaded Ag particles in the hybrids were not clear by now, but they were indispensable for photocatalytic reaction. When Ag particles were replaced with Pt particles, no HCOOH was obtained [282,286].

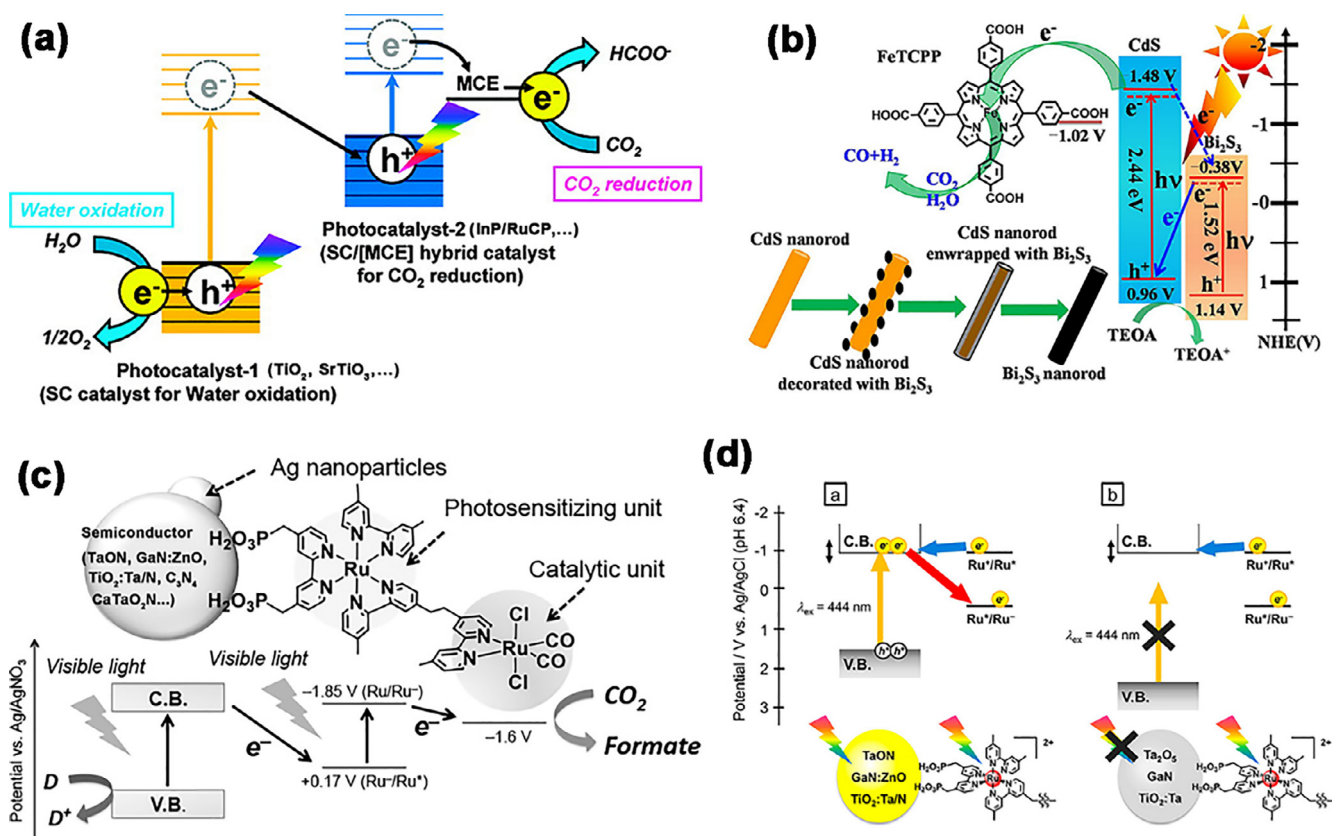


Fig. 26. (a) The first type of artificial Z-scheme based on two kinds of semiconductor and one MMC [279]. Copyright 2011 ACS. (b) Scheme of CO₂ photoreduction over CdS/Bi₂S₃-0.5 h/FeTCPP [281]. Copyright 2018 Elsevier. (c) The second artificial Z-scheme based on a semiconductor and a supramolecular photocatalyst [282]. Copyright 2013 ACS. (d) In the second type artificial Z-scheme, the semiconductor compound must be optically excited under visible-light irradiation [283]. Copyright 2018 ACS.

4.1.2. Composed with periodic mesoporous organosilica

Periodic mesoporous organosilica (PMO) with open framework structure and light harvesting capability has been used as a platform for loading MMCs for photocatalytic CO₂RR. Inagaki and Ishitani et al. reported a hybrid photocatalyst constructed with PMO and molecule Re(I) complex. Under the UV-light irradiation, the photoelectrons transfer from PMO to the Re center, generating 4.4 times more CO than direct excitation of the Re complex [290]. Later on, they introduced acridone or methylacridone groups onto the wall of PMO for visible-light harvesting [291]. Light energy absorbed by acridone groups was funneled to Re center for selectively CO₂-to-CO reduction.

Ishida et al. combined catalytic unit Ru(bpy)₃(CO)₂Cl₂ and photosensitive unit [Ru(bpy)₃]²⁺ on the framework of bpy-PMO (Ru(PS) *x*-Ru(Cat)*y*-bpy-PMO) for CO₂RR (Fig. 27a–c) [292]. When *x* = 0.11 and *y* = 0.0055, the highest total TOF of CO and HCOOH was obtained as 162 h⁻¹. In this system, the product selectivity for CO became higher when the ratio of [Ru(PS)]_{*x*} to [Ru(Cat)]_{*y*} was increased. Similarly, the Ru/Re co-doped bpy-PMO also showed high activity for CO₂RR [293]. However, when only Re (bpy)₃(CO)₂Cl complex was combined with bpy-PMO, the hybrid showed very low activity under visible-light irradiation. Thereafter, [Ru(bpy)₃]²⁺ was further introduced as a photosensitive unit. The catalytic activity of Ru-Re-bpy-PMO was highly enhanced due to the efficient electron transfer from the Ru sensitive unit to the Re center (Fig. 27d and 27e). Recently, Fontecave et al. introduced earth abundant Mn complex [Mn(CO)₅Br] onto the framework of bpy-PMO to construct a well-defined photocatalyst for CO₂RR (Fig. 27f) [294]. The resulting hybrid [Mn(bpyPMO)(CO)₅Br] could photocatalytically reduce CO₂ to both CO and HCOOH with [Ru(bpy)₃]₂Cl₂ as a photosensitizer.

4.2. MOFs-composited nanoparticles and MOFs-derived nanoparticles

4.2.1. MOFs-composited nanoparticles

MOFs were used to assemble with semiconductors to prepare efficient photocatalysts for CO₂RR, the different roles of MOFs in the hybrids are represented in Scheme 4.

ZIF-8 nanoparticles with high CO₂ adsorption capacity were firstly applied to promote the photocatalytic activity of Zn₂GeO₄ for CO₂RR [306]. The dissolved CO₂ adsorption capacity of Zn₂GeO₄/ZIF-8 (171.4 mg g⁻¹) was much higher than that of Zn₂GeO₄ (45.2 mg g⁻¹). As a result, compared to Zn₂GeO₄, Zn₂GeO₄/ZIF-8 showed an enhancement of 62% for CH₃OH evolution. Later on, Maina et al. controlled encapsulate TiO₂ and Cu-TiO₂ nanoparticles within ZIF-8 membrane through rapid thermal deposition method to prepare efficient CO₂ reduction photocatalysts [307]. The photocatalytic CO₂ reduction over this hybrid membrane in DMA solution gave MeOH and CO as major products. Compared to bare ZIF-8 membrane, Cu-TiO₂ co-doped ZIF-8 membrane exhibited 233% and 70% enhancement for CO and MeOH evolution, respectively. The excellent photocatalytic performance of the hybrid membrane was due to the synergistic effect between the semiconductor components and ZIF-8.

Wang et al. developed ZIF-9 as an efficient photocatalyst for CO₂RR with a [Ru(bpy)₃]₂Cl₂ photosensitizer [245]. However, there are still some shortages with this photochemical system [308,309]. For example, the low photostability of [Ru(bpy)₃]²⁺ would lead to a decrease of catalytic activity. Thus, they designed a Co-ZIF-9/g-C₃N₄ composite by mixing Co-ZIF-9 with metal-free and photochemically stable semiconductor g-C₃N₄ [308]. Under visible-light irradiation, photo-induced electrons transfer from g-C₃N₄ to Co-ZIF-9 cocatalyst to reduce CO₂ molecules. Co-ZIF-9 in the

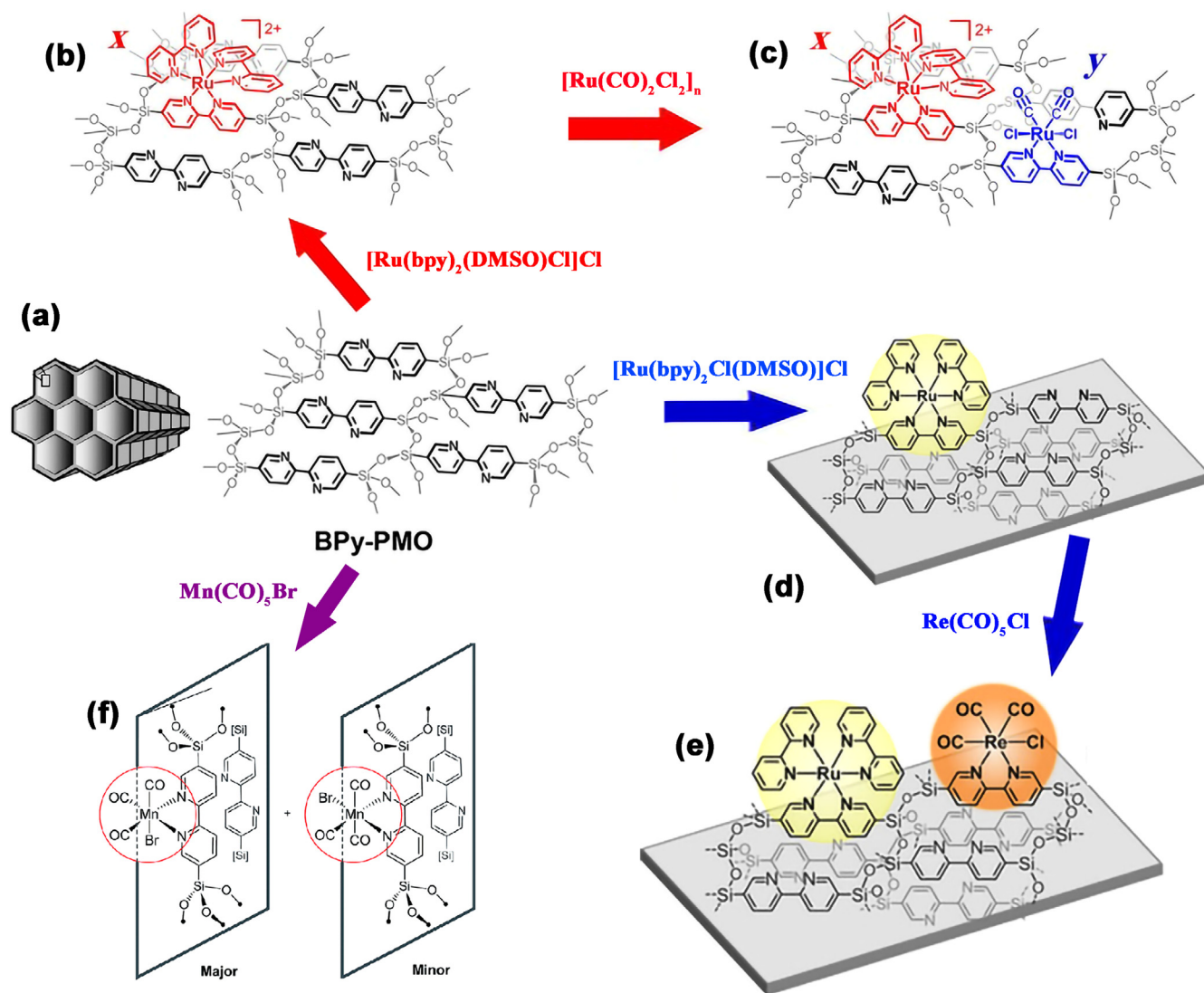


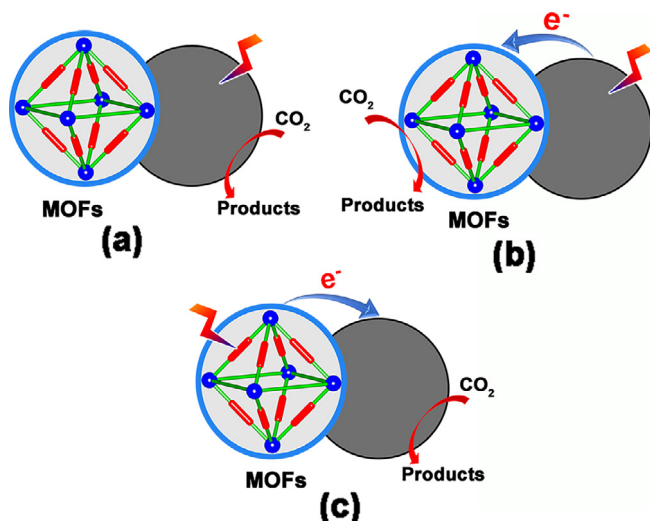
Fig. 27. (a) Structure of bpy-PMO. (b) and (c) Synthesis of Ru(PS)_x-Ru(Cat)_y-bpy-PMO [292]. Copyright 2017 Wiley-VCH. (d) and (e) Construction of Ru-Re-bpy-PMO [293]. Copyright 2018 Wiley-VCH. (f) Structure of Mn(bpyPMO)(CO)₃Br [294]. Copyright 2017 RSC.

composite could facilitate the CO₂ adsorption and the light-induced charge separation, and then enhance the photocatalytic activity. After that, they designed another composite of Co-ZIF-9/CdS by mixing Co-ZIF-9 with photosensitive semiconductor CdS (Fig. 28) [309]. Similar to the Co-ZIF-9/g-C₃N₄ composite, synergistic effect between Co-ZIF-9 and CdS can also promote the photocatalytic efficiency. Under visible-light irradiation, CO₂ was reduced to CO (82% selectivity) with a formation rate of 50.4 μmol/h in a mixed solution of MeCN/H₂O/TEOA. Later on, Ye et al. prepared Co-ZIF-9/TiO₂ composite though *in situ* synthetic method [310], in which Co-ZIF-9 and TiO₂ are closely bonded with each other. Thus, the charge transfer from TiO₂ to Co-ZIF-9 become more efficiency. Both CO and CH₄ were determined as the reduction product. One drawback of this work was the lack of isotopic trace experiment to ascertain the carbon source of the reduction product.

The key to boosting the photocatalytic efficiency of MOFs/semiconductor composites is to enhance the photoelectrons transfer from semiconductor to MOFs. Xiong and coworkers reported a Cu₃(BTC)₂@TiO₂ core-shell structure by coating nanocrystalline TiO₂ onto the Cu₃(BTC)₂ core (Fig. 29a and b) [311]. The Cu₃(BTC)₂@TiO₂ can selectively reduce CO₂ to CH₄. CO₂-sorption mea-

surements showed that the developed core-shell Cu₃(BTC)₂@TiO₂ retain the ability of Cu₃(BTC)₂ to capture CO₂. In addition, the fast electrons transfer from the excited TiO₂ to the Cu₃(BTC)₂ suppressed the electron-hole recombination in the TiO₂ and provided long lifetime electrons for CO₂ reduction. As a result, the Cu₃(BTC)₂@TiO₂ yielded 5 times more CH₄ than bare TiO₂. Later on, wang et al. developed a ternary nanocomposite based on Cu₃(BTC)₂ for photo-reducing CO₂ to CO and CH₄ (Fig. 29c) [312]. The decoration of TiO₂ with Cu₂O and Cu₃(BTC)₂ could significantly increase the charge carrier density of the catalyst due to the promoted light absorption and electron/hole separation. In addition, TiO₂/Cu₂O/Cu₃(BTC)₂ composite possessed plenty of coordinatively unsaturated sites, where CO₂ molecules were efficient activated.

CPO-27-Mg with abundant open alkaline metal sites and high CO₂ absorption capacity has been selected to composite with inorganic semiconductors to prepare efficient photocatalyst for CO₂RR [313]. Recombination CPO-27-Mg and TiO₂ under hydrothermal condition giving CPO-27-Mg/TiO₂ nanocomposite with promoted photocatalytic activity for CO₂ reduction to CO and CH₄. On the other hand, CPO-27-Mg can also composite with Zn₂GeO₄ to form CPO-27-Mg/Zn₂GeO₄ nanocomposite [314]. The CO₂ adsorption



Scheme 4. Three different types of hybrid photocatalysts based on MOFs and semiconductors. (a) MOF acts as the host of photocatalyst. (b) MOF acts as the cocatalyst. (c) MOF acts as the photosensitizer. The gray ball represents semiconductor.

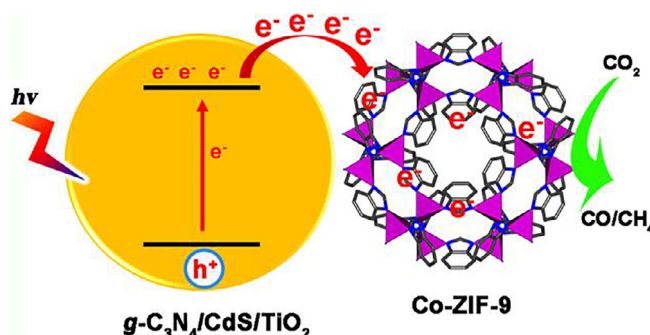


Fig. 28. Mechanism for photocatalytic CO₂RR in Co-ZIF-9 based hybrid system.

isotherms illustrated that the CO₂ absorption capability of CPO-27-Mg/Zn₂GeO₄ was much higher than that of Zn₂GeO₄ nanorods. In addition, the hybrid catalyst exhibited superior charge-transfer properties. Thus, Zn₂GeO₄/CPO-27-Mg exhibited a high performance for CO₂-to-CO reduction with only H₂O as the reducing agent and the hydrogen source.

The nanocomposite of perovskite-type CsPbBr₃ and NH₂-UiO-66 exhibited highly photocatalytic activity for CO₂RR, due to the improved electron extraction and transfer, large surface area and enhanced visible-light absorption capacity [315]. When the loaded CsPbBr₃ QDs content was 15 wt%, the highest amount of CO was obtained as 98.57 μmol g⁻¹. Later on, a core@shell CsPbBr₃@ZIF-67 was prepared for photocatalytic CO₂RR [316]. The CsPbBr₃@ZIF-67 nanocomposite yielded 2.66 times more CH₄ than naked CsPbBr₃.

Ye et al. combined BIF-20, a zeolite-like porous boron imidazolate framework, with g-C₃N₄ nanosheets to form BIF-20@g-C₃N₄ nanocomposite for CO₂ reduction (Fig. 30a) [317]. CO and CH₄ were detected as the reduction products. In the hybrid catalyst, the B-H bonds in BIF-20 could trap photoelectrons from g-C₃N₄ to avoid charge carrier recombination and then supplied the long-lived electrons for CO₂ reduction. Otherwise, the B-H bonds could also activate the adsorbed CO₂, further enhancing the performance of the BIF-20@g-C₃N₄. With these advantages, the BIF-20@g-C₃N₄ nanosheet yields 9.7 times more CH₄ and 9.85 times more CO than g-C₃N₄ nanosheet.

Recently, Han and Wu et al. synthesized a ternary CdS/UiO-bpy/Co composite via a multi-step method (Fig. 30b) [318]. The CdS/UiO-bpy/Co composite yielded 10.2 times more CO than parent CdS. The excellent performance of CdS/UiO-bpy/Co composite was attributed to the promoted charge separation, the enhanced CO₂ adsorption capacity, and the abundant active sites.

In the systems based on MOF-composited catalysts, the photocatalytic performances toward CO₂RR are generally improved due to the strong CO₂ capture capability and the efficient charge separation ability. In addition, composite MOFs with inorganic semiconductors avoids the use of noble-metal based photosensitizers (e.g. Ru and Ir complexes). The homogeneous photosensitive noble-metal complexes usually suffer from photodegradation/pho-

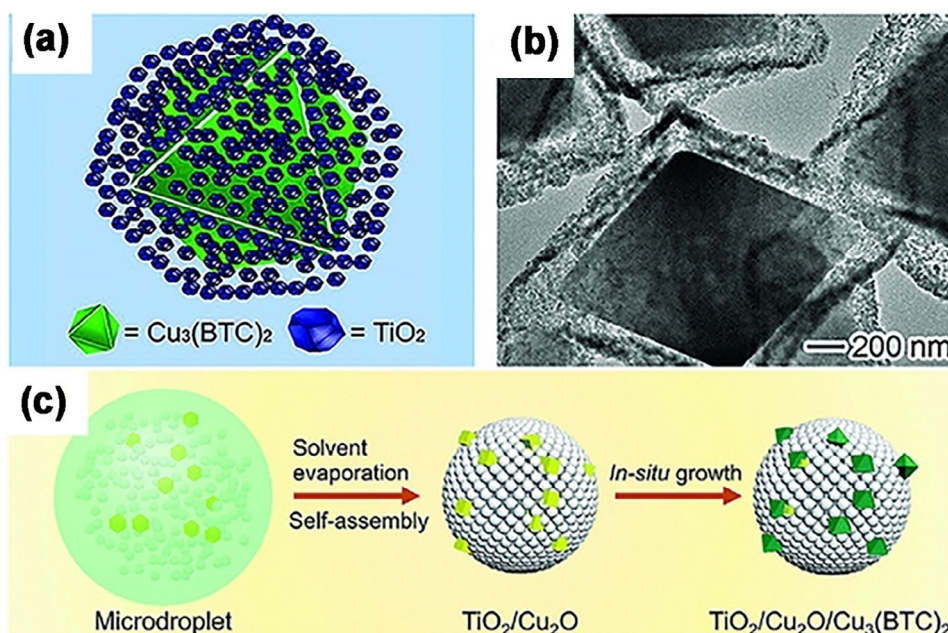


Fig. 29. (a) Structural illustration and (b) SEM image of Cu₃(BTC)₂@TiO₂ [311]. Copyright 2014 Wiley-VCH. (c) Construction of TiO₂/Cu₂O/Cu₃(BTC)₂ [312]. Copyright 2018 RSC.

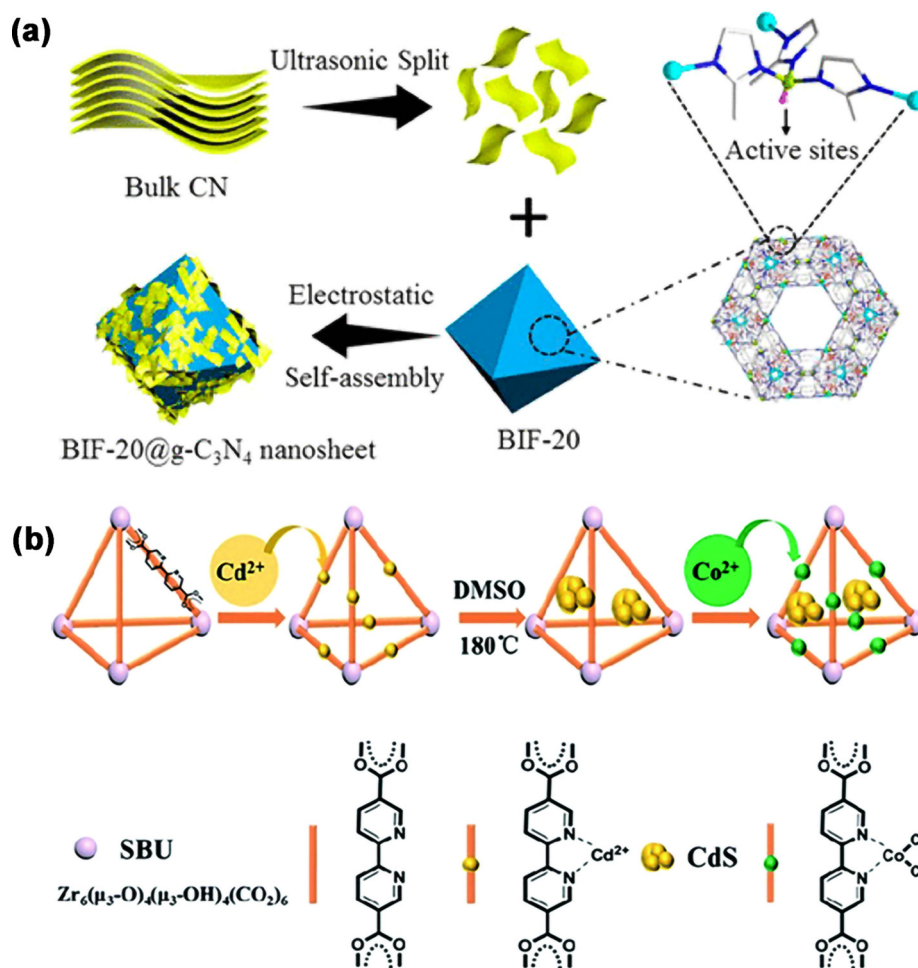


Fig. 30. (a) Construction of BIF-20@g-C₃N₄ nanosheet [317]. Copyright 2018 ACS®. (b) Construction of CdS/UiO-bpy/Co composite [318]. Copyright 2018 RSC®.

tobleaching effect, resulting in poor stability of the photocatalytic CO₂RR systems [163,258,319,320]. Meanwhile, noble-metals are expensive and rare on the earth. These aspects largely limit the development of the CO₂RR systems. Assembly of MOFs and photo-sensitive semiconductors provide a new opportunity for designing more sustainable photocatalytic system for CO₂RR. However, MOFs that can be used for constructing high stable heterojunction nanocomposites are still rare. Thus, in order to develop this strategy, the design and synthesis of new stable MOFs are still demanded.

4.2.2. MOFs-derived nanoparticles

In recent years, MOFs have been employed as precursors to construct variety of porous materials for catalytic applications [321–326]. Developing of the MOF-derived materials for photocatalytic CO₂RR has also been investigated. Strunk and Fischer et al. fabricated an Au/TiO₂ photocatalyst by pyrolysis of Au@NH₂-MIL-125 (Ti) (Fig. 31a) [327]. Including its nicely reproducible synthesis and high-water stability, NH₂-MIL-125(Ti) was chosen as precursors also because its highly ordered porous structure that could act as a support matrix for dispersing and stabilizing small gold nanoparticles (GNPs). The GNPs are mainly anchored at the outer surface of Au/TiO₂ composites for CO₂-to-CH₄ reduction.

Later on, Ye and coworkers prepared an iron nanoparticle overcoated with ultrathin (1–3 layers) carbon layers by using MIL-101 (Fe) as both self-sacrificing template and precursor [328]. A two-

step calcination method was utilized to control both the size of Fe nanoparticles and the thickness of graphite layers (Fig. 31b). Briefly, MIL-101(Fe) with a uniform size in μm scale was firstly heated at 500 °C to decompose the framework and simultaneously avoid the formation of large-sized Fe nanoparticles. Then, the presence of iron strongly enhanced the graphitization of carbon species on the surface of Fe nanoparticles at 700 °C. Attributed to their small particle sizes, the BET surface area of the Fe@C product was measured to be up to 146.26 m² g⁻¹. Photocatalytic experiments revealed that the core-shell Fe@C catalyst exhibited excellent photocatalytic activity towards CO₂-to-CO reduction. CO formation rate was calculated to be 26.12 mmol h⁻¹ g⁻¹ with 99.9% selectivity. Besides for its high BET surface area, the excellent performance of the core-shell Fe@C was attributed to the following reasons. Firstly, the Fe@C shows excellent light absorption ability over a very broad photo-irradiation range, including ultraviolet light, visible-light and infrared radiation. Secondly, due to the photothermal effect, the local temperature of the nanoparticles increased under light irradiation, which can help to initiate the CO₂ reduction process. Thirdly, UV-light-induced Fe local surface-plasmon resonances could furtherance the activation of the nonpolar molecules CO₂. In addition, thin carbon layers on the Fe particles could produce a confinement effect in realizing selectively CO₂-to-CO reduction.

Very recently, an ultrathin 2D ZIF-67 nanosheet was thermally decomposed into 2D porous Co₃O₄ nanosheets (Co₃O₄-NS) by air

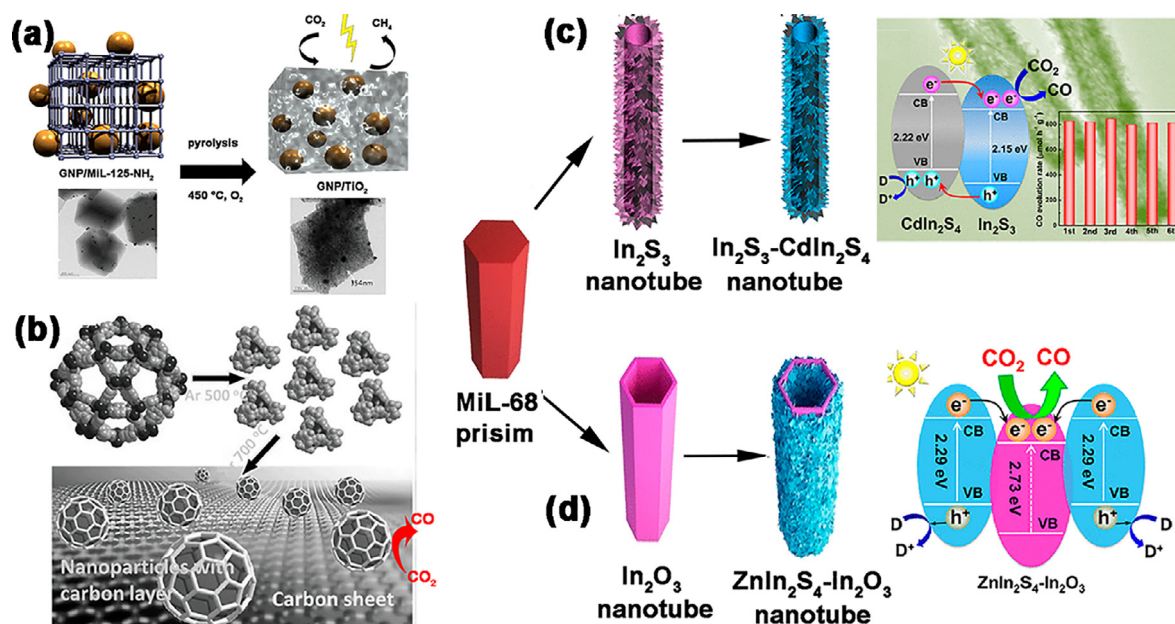


Fig. 31. (a) Construction of GNP/TiO₂ for CO₂-to-CH₄ reduction [327]. Copyright 2015 ACS. (b) Construction of the core-shell Fe@C for CO₂-to-CO reduction [328]. Copyright 2016 Wiley-VCH. (c) Synthetic process of the In₂S₃-CdIn₂S₄ nanotube and its catalytic mechanism for CO₂-to-CO reduction [330]. Copyright 2017 ACS. (d) Synthetic process of the ZnIn₂S₄-In₂O₃ nanotube and its catalytic mechanism for CO₂-to-CO reduction [332]. Copyright 2018 ACS.

calcining [329]. The calcined Co₃O₄-NS inherited the porosity structure with enhanced CO₂ adsorption capacity. In addition, the Co₃O₄ monolayer exhibited stronger CO₂ adsorption energy than that of the bulk Co₃O₄. As a result, CO evolution over the Co₃O₄-NS reached a rate of 4.52 μmol h⁻¹ (0.5 mg Co₃O₄-NS was added), which is much higher than that of bulk Co₃O₄.

Heterojunction of metal sulfides was delicately designed to improve their photocatalytic activity for CO₂ reduction [330]. Hierarchical In₂S₃-CdIn₂S₄ nanotubes were fabricated *via* two steps self-templated strategy (Fig. 31c). Firstly, the hierarchical In₂S₃ nanotube was obtained through a liquid phase sulfidation treatment of the hexagonal prism In-MIL-68 at 180 °C. Afterward, the

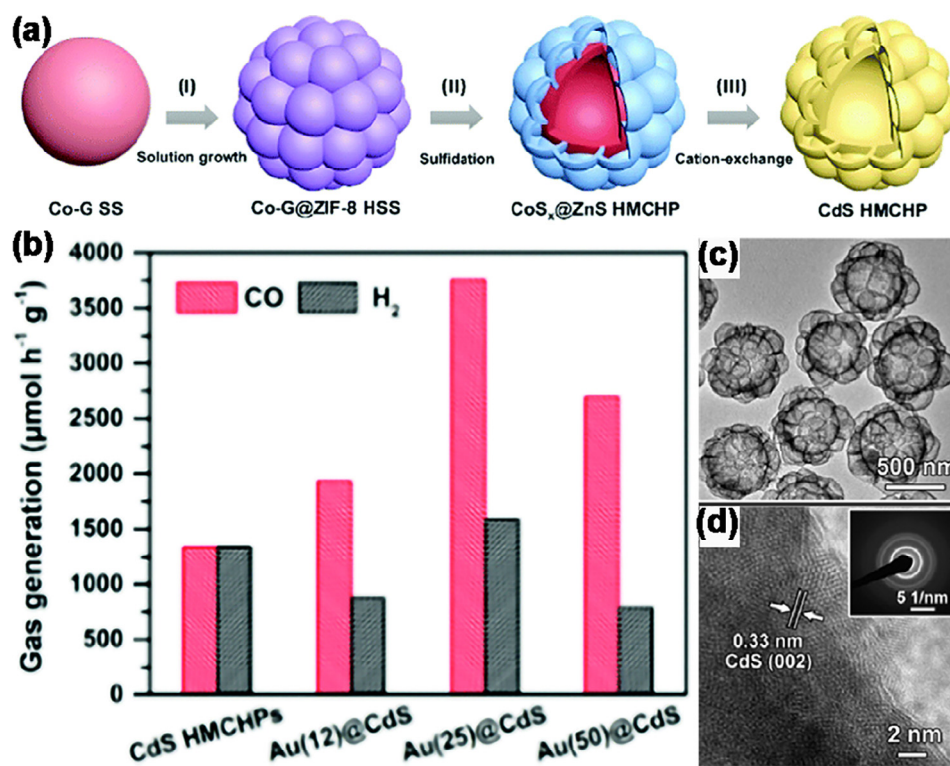


Fig. 32. (a) the formation process of CdS HMCHPs [333]. The four balls from left to right represent cobalt glycerate particles, ZIF-8 coated cobalt glycerate particles, CoS_x@ZnS HMCHPs and CdS HMCHPs, respectively. (b) CO and H₂ evolution rate over CdS HMCHPs with different Au loading. (c) and (d) shows TEM and HRTEM images of CdS HMCHPs. Copyright 2019 RSC.

as-prepared In_2S_3 nanotube was transformed into hierarchical In_2S_3 - CdIn_2S_4 hybrid nanotube through a cation exchange reaction. Attributed to its hollow structure, the hierarchical In_2S_3 - CdIn_2S_4 nanotubes showed a high BET surface area of $68 \text{ m}^2 \text{ g}^{-1}$. In addition, the In_2S_3 - CdIn_2S_4 -10 (molar ratio of Cd/In 1: 2.31) hybrid material exhibited enhanced ability to separate and migrate the photoinduced charge carriers. This is favorable for heterogeneous photocatalysis. With these structural advantages, the In_2S_3 - CdIn_2S_4 -10 sample manifested the highest CO production rate of $825 \mu\text{mol h}^{-1} \text{ g}^{-1}$. A hierarchical In_2S_3 - CuInS_2 nanotube with photocatalytic CO_2 -to- CO reduction activity was prepared through a similar approach [331]. The charge transfer in this heterojunction was also dramatically accelerated. Thus, CO evolution rate over In_2S_3 - CuInS_2 nanotube was up to five times than that on pure In_2S_3 . Later on, sandwich-like ZnIn_2S_4 - In_2O_3 hierarchical nanotubes were fabricated by assembling ZnIn_2S_4 nanosheets on the surfaces of In_2O_3 microtubes (Fig. 31d) [332]. Hollow ZnIn_2S_4 - In_2O_3 particles showed a higher CO_2 uptake ($\sim 20 \text{ cm}^3 \text{ g}^{-1}$ at 0°C) and a broader visible-light absorption ($< 500 \text{ nm}$) than that of In_2O_3 . ZnIn_2S_4 - In_2O_3 also showed higher photocatalytic activity towards CO_2 -to- CO reduction than both In_2O_3 and ZnIn_2S_4 . The CO evolution rate over ZnIn_2S_4 - In_2O_3 was calculated to be up to $3075 \mu\text{mol h}^{-1} \text{ g}^{-1}$.

Very recently, a CdS hierarchical multi-cavity hollow particle (HMCHP) was constructed by three steps strategy (Fig. 32) [333]. ZIF-8 was firstly grown on the surface of cobalt glycerate particles via *in situ* solution method. Then, the CoS_x @ ZnS HMCHPs were obtained through a liquid phase sulfidation treatment of the $\text{Co}@ZIF-8$ particles at 120°C . Finally, CdS HMCHPs were fabricated through a cation exchange reaction. Beyond its well-defined structure, CdS HMCHPs showed excellent photocatalytic active for CO_2 -to- CO reduction. After loading $0.25 \text{ wt}\%$ of Au, CdS HMCHPs showed a CO evolution rate of $3758 \mu\text{mol h}^{-1} \text{ g}^{-1}$.

5. Conclusions and outlooks

In conclusion, we classified the application of MMCs and MOFs for photocatalytic CO_2 reduction. Some strategies, including metal ions regulation, ligands modification, and composite with semiconductors, have been applied to enhance their catalytic performances and considerable progress has been achieved with MMCs and MOFs, promising their possibility of practical application in photo-induced CO_2 reduction. However, some drawbacks are still needed to be solved in this field. Firstly, many of the reported MMCs and MOFs are not stable enough under the photocatalytic condition. Up to now, the examples of CO_2 reduction based on MOF-based photocatalysts are still insufficient to elucidate the structure-activity relationship and reaction mechanism in the photocatalytic process. Secondly, the CO_2 reduction products are limited to C_1 compounds (including CO , CH_4 , HCOOH and MeOH) and C_2 compounds (including C_2H_4 , EtOH and CH_3COOH) with no report on the generation of C_3+ products (hydrocarbons with more than three carbons are very important fuel widely used). Thirdly, most of the photocatalytic CO_2 RR were carried out in organic solvents with photosensitizer (such as $\text{Ru}(\text{bpy})_3^{2+}$ and $\text{Ir}(\text{ppy})_3$) and sacrificial agents (such as TEOA and TEA). These processes are not economically viable and environmentally friendly. Fourthly, most of the reported MMCs and MOFs show narrow light harvesting range in the visible-light region. All in all, performances of MMCs and MOFs for photocatalytic CO_2 RR are still not efficient enough, and the above problems must be at least partially solved before they can be practically applied.

Some efforts should be made to address the above problems. Firstly, more alternative MMCs and MOFs should be investigated for photocatalytic CO_2 RR application, and it is best to combine rea-

sonable theoretical calculations. Extensive experimental and theoretical data are conducive to the summary of the reaction mechanism. Secondly, in-depth understanding to the structure-property relationships of catalysts based on MMCs and MOFs is desired. The active centers, such as open metal sites, are required to be chosen judiciously to achieve efficient activation of CO_2 molecules. For heterogeneous reaction, CO_2 molecules generally need to diffuse into the channels of catalysts to increase the utilization of the active sites within the solid. In these processes, the channel environment is key to achieve a higher CO_2 capture capacity and a faster reagent transfer. However, the CO_2 adsorption behavior of heterogeneous photocatalysts in CO_2 saturated solution is still not clear. Thus, it also needs to study the CO_2 adsorption-desorption properties of the photocatalysts in the solution. Thirdly, high optical efficiency is required for achieving high photocatalytic performance. It is preferred to develop new earth-abundant photosensitive materials (such as organic molecules and inorganic semiconductors) to enhance visible-light absorption of MMCs/MOFs. The use of noble-metal based photosensitizers should be gradually reduced. Fourthly, the photo-induced charge carriers need to be efficiently transferred to the active centers. Thus, the morphology effect should also be concerned to achieve an optimal activity. Fifthly, recycle experiments should be performed to study the stability of the photocatalytic system. Sixth, isotopic trace experiments should be performed by using tracer gas, such as $^{13}\text{CO}_2$, to verify the carbon source of the reduction product. During the CO_2 reduction process, other organic components in the photocatalytic system, such as photocatalysts, solvents and sacrificial agents, will also be decomposed. Thus, it is very important to ascertain the carbon source of the reduction products. In addition, it is grateful to couple the CO_2 RR with water oxidation or value-added organic oxidation process to avoid TEOA and TEA et al. as the electron donor. All in all, the development of photocatalysts based on MMCs/MOFs is a promising and sustainable way for CO_2 reduction.

Acknowledgements

We gratefully acknowledge financial support by the National Natural Science Foundation of China (No. 21622104, 21871141, 21871142 and 21701085), the China Postdoctoral Science Foundation (No. 2016M591875) and the Postdoctoral Science Foundation of Jiangsu Province (No. 1601239C), the Natural Science Foundation of Jiangsu Province (No. SBK2017040708), the University Science Research Project of Jiangsu Province (No. 16KJB150004, 17KJB150025), the Foundation of Jiangsu Key Laboratory of Function Control Technology for Advanced Materials, the Foundation of Jiangsu Collaborative Innovation Center of Biomedical Functional Materials, the Six Talents Peak Project of Jiangsu Province (XCL-009), Jiangsu Overseas Research & Training Program for University Prominent Yong & Middle-aged Teachers and Presidents and Priority Academic Program Development of Jiangsu Higher Education Institutions.

References

- [1] P.N. Pearson, M.R. Palmer, *Nature* 406 (2000) 695.
- [2] H. Fischer, M. Wahlen, J. Smith, D. Mastroianni, B. Deck, *Science* 283 (1999) 1712–1714.
- [3] C.A. Deutsch, J.J. Tewksbury, M. Tigheelaar, D.S. Battisti, S.C. Merrill, R.B. Huey, R.L. Naylor, *Science* 361 (2018) 916–919.
- [4] H. Arakawa, M. Aresta, J.N. Armor, M.A. Barbeau, E.J. Beckman, A.T. Bell, J.E. Bercaw, C. Creutz, E. Dinjus, D.A. Dixon, K. Domen, D.L. DuBois, J. Eckert, E. Fujita, D.H. Gibson, W.A. Goddard, D.W. Goodman, J. Keller, G.J. Kubas, H.H. Kung, J.E. Lyons, L.E. Manzer, T.J. Marks, K. Morokuma, K.M. Nicholas, R. Periana, L. Que, J. Rostrup-Nielson, W.M.H. Sachtler, L.D. Schmidt, A. Sen, G.A. Somorjai, P.C. Stair, B.R. Stults, W. Tumas, *Chem. Rev.* 101 (2001) 953–996.
- [5] W.H. Wang, Y. Himeda, J.T. Muckerman, G.F. Manbeck, E. Fujita, *Chem. Rev.* 115 (2015) 12936–12973.

- [6] C.A. Trickett, A. Helal, B.A. Al-Maythaly, Z.H. Yamani, K.E. Cordova, O.M. Yaghi, *Nat. Rev. Mat.* 2 (2017) 17045.
- [7] E.S. Sanz-Pérez, C.R. Murdock, S.A. Didas, C.W. Jones, *Chem. Rev.* 116 (2016) 11840–11841.
- [8] B. Yu, B. Zou, C.W. Hu, J. CO₂ Util. 26 (2018) 314–322.
- [9] T. Inoue, A. Fujishima, S. Konishi, K. Honda, *Nature* 277 (1979) 637–638.
- [10] N. Zhang, R. Long, C. Gao, Y. Xiong, *Sci. China Mater.* 61 (2018) 771–805.
- [11] P. Usubharatana, D. McMartin, A. Veawab, P. Tontiwachwuthikul, *Ind. Eng. Chem. Res.* 45 (2006) 2558–2568.
- [12] V.P. Indrakanti, J.D. Kubicki, H.H. Schobert, *Energy Environ. Sci.* 2 (2009) 745–758.
- [13] W. Tu, Y. Zhou, Z. Zou, *Adv. Mater.* 26 (2014) 4607–4626.
- [14] K. Li, B. Peng, T. Peng, *ACS Cat.* 6 (2016) 7485–7527.
- [15] S. Yu, A.J. Wilson, G. Kumari, X. Zhang, P.K. Jain, *ACS Energy Lett.* 2 (2017) 2058–2070.
- [16] E. Fujita, *Coord. Chem. Rev.* 185–186 (1999) 373–384.
- [17] Y.Y. Lee, H.S. Jung, J.M. Kim, Y.T. Kang, *Appl. Catal. B: Environ.* 224 (2018) 594–601.
- [18] J.L. White, M.F. Baruch, J.E. Pander, Y. Hu, I.C. Fortmeyer, J.E. Park, T. Zhang, K. Liao, J. Gu, Y. Yan, T.W. Shaw, E. Abelev, A.B. Bocarsly, *Chem. Rev.* 115 (2015) 12888–12935.
- [19] C. Dong, C. Lian, S. Hu, Z. Deng, J. Gong, M. Li, H. Liu, M. Xing, J. Zhang, *Nat. Commun.* 9 (2018) 1252.
- [20] Y.X. Pan, Y. You, S. Xin, Y. Li, G. Fu, Z. Cui, Y.L. Men, F.F. Cao, S.H. Yu, J.B. Goodenough, *J. Am. Chem. Soc.* 139 (2017) 4123–4129.
- [21] M. Zhou, S. Wang, P. Yang, C. Huang, X. Wang, *ACS Cat.* 8 (2018) 4928–4936.
- [22] L. Lu, B. Wang, S. Wang, Z. Shi, S. Yan, Z. Zou, *Adv. Funct. Mater.* 27 (2017) 1702447.
- [23] A. Bachmeier, V.C.C. Wang, T.W. Woolerton, S. Bell, J.C. Fontecilla-Camps, M. Can, S.W. Ragsdale, Y.S. Chaudhary, F.A. Armstrong, *J. Am. Chem. Soc.* 135 (2013) 15026–15032.
- [24] A. Dei, D. Gatteschi, C. Sangregorio, L. Sorace, *Accounts Chem. Res.* 37 (2004) 827–835.
- [25] D.E. De Vos, M. Dams, B.F. Sels, P.A. Jacobs, *Chem. Rev.* 102 (2002) 3615–3640.
- [26] M. Sittig, *Adv. Chem.* 23 (1959), <https://doi.org/10.1021/ba-1959-0023.pr001>.
- [27] D. Hayes, L. Kohler, R.G. Hadt, X. Zhang, C. Liu, Karen L. Mulfort, L.X. Chen, *Chem. Sci.* 9 (2018) 860–875.
- [28] X. Liu, C. Manzur, N. Novoa, S. Celedón, D. Carrillo, J.R. Hamon, *Coord. Chem. Rev.* 357 (2018) 144–172.
- [29] M.R. Momeni, D.R. Pahls, D. Yang, S.O. Odoh, J. Borycz, T.C. Wang, O.K. Farha, J. T. Hupp, C.J. Cramer, L. Gagliardi, B.C. Gates, *ACS Cat.* 8 (2018) 2364.
- [30] G. Maurin, C. Serre, A. Cooper, G. Férey, *Chem. Soc. Rev.* 46 (2017) 3104–3107.
- [31] Q. Xu, H. Kitagawa, *Adv. Mater.* 30 (2018) 1803613.
- [32] K. Hong, W. Bak, H. Chun, *Inorg. Chem.* 53 (2014) 7288–7293.
- [33] C.S. Diercks, Y. Liu, K.E. Cordova, O.M. Yaghi, *Nat. Mater.* 17 (2018) 301–307.
- [34] S. Fukuzumi, Y.M. Lee, H.S. Ahn, W. Nam, *Chem. Sci.* 9 (2018) 6017–6034.
- [35] S. Lian, M.S. Kodaimati, D.S. Dolzhenkov, R. Calzada, E.A. Weiss, *J. Am. Chem. Soc.* 139 (2017) 8931–8938.
- [36] J. Hawecker, J.M. Lehn, R. Ziessel, *Chem. Commun.* (1983) 536–538.
- [37] H. Takeda, C. Cometto, O. Ishitani, M. Robert, *ACS Cat.* 7 (2017) 70–88.
- [38] H. Furukawa, K.E. Cordova, M. O'Keefe, O.M. Yaghi, *Science* 341 (2013) 1230444.
- [39] J.Q. Shen, P.Q. Liao, D.D. Zhou, C.T. He, J.X. Wu, W.X. Zhang, J.P. Zhang, X.M. Chen, *J. Am. Chem. Soc.* 139 (2017) 1778–1781.
- [40] Y. Peng, M. Zhao, B. Chen, Z. Zhang, Y. Huang, F. Dai, Z. Lai, X. Cui, C. Tan, H. Zhang, *Adv. Mater.* 30 (2017) 1705454.
- [41] N.S. Bobbitt, M.L. Mendonca, A.J. Howarth, T. Islamoglu, J.T. Hupp, O.K. Farha, R.Q. Snurr, *Chem. Soc. Rev.* 46 (2017) 3357–3385.
- [42] G. Cai, H.L. Jiang, *Angew. Chem. Int. Edit.* 56 (2016) 563–567.
- [43] B. An, L. Zeng, M. Jia, Z. Li, Z. Lin, Y. Song, Y. Zhou, J. Cheng, C. Wang, W. Lin, *J. Am. Chem. Soc.* 139 (2017) 17747–17750.
- [44] S. Wang, X. Wang, *Small* 11 (2015) 3097–3112.
- [45] H. Zhang, J. Nai, L. Yu, X.W. Lou, *Joule* 1 (2017) 77–107.
- [46] B. Ghalei, K. Sakurai, Y. Kinoshita, K. Wakimoto, Ali P. Isfahani, Q. Song, K. Doitomi, S. Furukawa, H. Hirao, H. Kusuda, S. Kitagawa, E. Sivanah, *Nat. Energy* 2 (2017) 17086.
- [47] G. Zhang, G. Wei, Z. Liu, S.R.J. Oliver, H. Fei, *Chem. Mater.* 28 (2016) 6276–6281.
- [48] Q.G. Zhai, X. Bu, C. Mao, X. Zhao, L. Daemen, Y. Cheng, A.J. Ramirez-Cuesta, P. Feng, *Nat. Commun.* 7 (2016) 13645.
- [49] D.A. Yang, H.Y. Cho, J. Kim, S.T. Yang, W.S. Ahn, *Energy Environ. Sci.* 5 (2012) 6465–6473.
- [50] C. Wang, Z. Xie, K.E. deKrafft, W. Lin, *J. Am. Chem. Soc.* 133 (2011) 13445–13454.
- [51] J.W. Maina, C. Pozo-Gonzalo, L. Kong, J. Schütz, M. Hill, L.F. Dumée, *Mater. Horiz.* 4 (2017) 345–361.
- [52] A. Crake, *Mater. Sci. Tech.* 33 (2017) 1737–1749.
- [53] Y. Chen, D. Wang, X. Deng, Z. Li, *Cat. Sci. Tech.* 7 (2017) 4893–4904.
- [54] R. Li, W. Zhang, K. Zhou, *Adv. Mater.* 30 (2018) 1705512.
- [55] S. Wang, X. Wang, *Angew. Chem. Int. Edit.* 55 (2016) 2308–2320.
- [56] X. Liu, S. Inagaki, J. Gong, *Angew. Chem. Int. Edit.* 55 (2016) 14924–14950.
- [57] A. Dhakshinamoorthy, A.M. Asiri, H. García, *Angew. Chem. Int. Edit.* 55 (2016) 5414–5445.
- [58] T. Hirose, Y. Maeno, Y. Himeda, *J. Mol. Cat. A Chem.* 193 (2003) 27–32.
- [59] S. Sato, T. Morikawa, S. Saeki, T. Kajino, T. Motohiro, *Angew. Chem.* 122 (2010) 5227–5231.
- [60] A.J. Morris, G.J. Meyer, E. Fujita, *Accounts Chem. Res.* 42 (2009) 1983–1994.
- [61] Y. Yamazaki, H. Takeda, O. Ishitani, *J. Photochem. Photobiol. C* 25 (2015) 106–137.
- [62] G.F. Manbeck, E. Fujita, *J. Porphyr. Phthalocya.* 19 (2015) 45–64.
- [63] J. Bonin, A. Maurin, M. Robert, *Coord. Chem. Rev.* 334 (2017) 184–198.
- [64] J.W. Wang, W.J. Liu, D.C. Zhong, T.B. Lu, *Coord. Chem. Rev.* 378 (2019) 237–261.
- [65] Y. Kuramochi, O. Ishitani, H. Ishida, *Coord. Chem. Rev.* 373 (2018) 333–356.
- [66] Y. Tamaki, O. Ishitani, *ACS Cat.* 7 (2017) 3394–3409.
- [67] N. Elgrishi, M.B. Chambers, X. Wang, M. Fontecave, *Chem. Soc. Rev.* 46 (2017) 761–796.
- [68] Y. Zhao, Z. Liu, *Chinese J. Chem.* 36 (2018) 455–460.
- [69] A. Sinopoli, N.T. La Porte, J.F. Martinez, M.R. Wasielewski, M. Sohail, *Coord. Chem. Rev.* 365 (2018) 60–74.
- [70] D.C. Grills, M.Z. Ertem, M. McKinnon, K.T. Ngo, J. Rochford, *Coord. Chem. Rev.* 374 (2018) 173–217.
- [71] H. Joshi, S. Kharel, A. Ehnobom, K. Skopek, G.D. Hess, T. Fiedler, F. Hampel, N. Bhuvanesh, J.A. Gladysz, *J. Am. Chem. Soc.* 140 (2018) 8463–8478.
- [72] R. Francke, B. Schille, M. Roemelt, *Chem. Rev.* 118 (2018) 4631–4701.
- [73] J. Hawecker, J.M. Lehn, R. Ziessel, *Helv. Chim. Acta* 69 (1986) 1990–2012.
- [74] C. Kutal, M.A. Weber, G. Ferraudi, D. Geiger, *Organometallics* 4 (1985) 2161–2166.
- [75] C. Kutal, A.J. Corbin, G. Ferraudi, *Organometallics* 6 (1987) 553–557.
- [76] K. Kalyanasundaram, *J. Chem. Soc., Faraday T.* 2 82 (1986) 2401–2415.
- [77] H. Hori, F.P.A. Johnson, K. Koike, K. Takeuchi, T. Ibusuki, O. Ishitani, *Dalton T.* (1997) 1019–1024.
- [78] H. Hori, J. Ishihara, K. Koike, K. Takeuchi, T. Ibusuki, O. Ishitani, *J. Photochem. Photobiol. A* 120 (1999) 119–124.
- [79] K. Koike, N. Okoshi, H. Hori, K. Takeuchi, O. Ishitani, H. Tsubaki, I.P. Clark, M. W. George, F.P.A. Johnson, J.J. Turner, *J. Am. Chem. Soc.* 124 (2002) 11448–11455.
- [80] J. Agarwal, E. Fujita, H.F. Schaefer, J.T. Muckerman, *J. Am. Chem. Soc.* 134 (2012) 5180–5186.
- [81] J.R. Pugh, M.R.M. Bruce, B.P. Sullivan, T.J. Meyer, *Inorg. Chem.* 30 (1991) 86–91.
- [82] B.P. Sullivan, C.M. Bolinger, D. Conrad, W.J. Vining, T.J. Meyer, *Chem. Commun.* (1985) 1414–1416.
- [83] K. Koike, H. Hori, M. Ishizuka, J.R. Westwell, K. Takeuchi, T. Ibusuki, K. Enjouji, H. Konno, K. Sakamoto, O. Ishitani, *Organometallics* 16 (1997) 5724–5729.
- [84] F.P.A. Johnson, M.W. George, F. Hartl, J.J. Turner, *Organometallics* 15 (1996) 3374–3387.
- [85] T. Morimoto, T. Nakajima, S. Sawa, R. Nakanishi, D. Imori, O. Ishitani, *J. Am. Chem. Soc.* 135 (2013) 16825–16828.
- [86] T.W. Schneider, M.Z. Ertem, J.T. Muckerman, A.M. Angeles-Boza, *ACS Cat.* 6 (2016) 5473–5481.
- [87] P. Kurz, B. Probst, B. Spingler, R. Alberto, *Eur. J. Inorg. Chem.* 2006 (2006) 2966–2974.
- [88] G.J. Stor, F. Hartl, J.W.M. van Outersterp, D.J. Stufkens, *Organometallics* 14 (1995) 1115–1131.
- [89] H. Tsubaki, A. Sugawara, H. Takeda, B. Gholamkhash, K. Koike, O. Ishitani, *Res. Chem. Intermediat.* 33 (2007) 37–48.
- [90] H. Takeda, K. Koike, H. Inoue, O. Ishitani, *J. Am. Chem. Soc.* 130 (2008) 2023–2031.
- [91] A.J. Huckaba, E.A. Sharpe, J.H. Delcamp, *Inorg. Chem.* 55 (2016) 682–690.
- [92] T. Morimoto, C. Nishiura, M. Tanaka, J. Rohacova, Y. Nakagawa, Y. Funada, K. Koike, Y. Yamamoto, S. Shishido, T. Kojima, T. Saeki, T. Ozeki, O. Ishitani, *J. Am. Chem. Soc.* 135 (2013) 13266–13269.
- [93] J. Rohacova, O. Ishitani, *Chem. Sci.* 7 (2016) 6728–6739.
- [94] C.M. Boudreaux, N.P. Liyanage, H. Shirley, S. Siek, D.L. Gerlach, F. Qu, J.H. Delcamp, E.T. Papish, *Chem. Commun.* 53 (2017) 11217–11220.
- [95] Y. Kuramochi, M. Kamiya, H. Ishida, *Inorg. Chem.* 53 (2014) 3326–3332.
- [96] J. Hawecker, J.M. Lehn, R. Ziessel, *Chem. Commun.* (1985) 56–58.
- [97] J.M. Lehn, R. Ziessel, *J. Organomet. Chem.* 382 (1990) 157–173.
- [98] H. Ishida, T. Terada, K. Tanaka, T. Tanaka, *Inorg. Chem.* 29 (1990) 905–911.
- [99] Y. Tamaki, T. Morimoto, K. Koike, O. Ishitani, *P. Natl. Acad. Sci. USA* 109 (2012) 15673–15678.
- [100] M.N. Collomb-Dunand-Sauthier, A. Deronzier, R. Ziessel, *J. Phys. Chem.* 97 (1993) 5973–5979.
- [101] H. Ishida, K. Tanaka, T. Tanaka, *Organometallics* 6 (1987) 181–186.
- [102] P. Voyame, K.E. Toghill, M.A. Méndez, H.H. Girault, *Inorg. Chem.* 52 (2013) 10949–10957.
- [103] Y. Kuramochi, J. Itabashi, K. Fukaya, A. Enomoto, M. Yoshida, H. Ishida, *Chem. Sci.* 6 (2015) 3063–3074.
- [104] C.W. Machan, M.D. Sampson, C.P. Kubiak, *J. Am. Chem. Soc.* 137 (2015) 8564–8571.
- [105] Y. Kuramochi, K. Fukaya, M. Yoshida, H. Ishida, *Chem. Eur. J.* 21 (2015) 10049–10060.
- [106] Y. Kuramochi, J. Itabashi, M. Toyama, H. Ishida, *ChemPhotoChem* 2 (2018) 314–322.
- [107] J. Chauvin, F. Lafalet, S. Chardon-Noblat, A. Deronzier, M. Jakonen, M. Haukka, *Chem. Eur. J.* 17 (2011) 4313–4322.
- [108] C.E. Castillo, J. Armstrong, E. Laurila, L. Oresmaa, M. Haukka, J. Chauvin, S. Chardon-Noblat, A. Deronzier, *ChemCatChem* 8 (2016) 2667–2677.
- [109] S. Sato, T. Morikawa, T. Kajino, O. Ishitani, *Angew. Chem. Int. Edit.* 52 (2013) 988–992.
- [110] A. Genoni, D.N. Chirdon, M. Boniolo, A. Sartorel, S. Bernhard, M. Bonchio, *ACS Cat.* 7 (2017) 154–160.

- [111] K. Garg, Y. Matsubara, M.Z. Ertem, A. Lewandowska-Andralojc, S. Sato, D.J. Szalda, J.T. Muckerman, E. Fujita, *Angew. Chem. Int. Edit.* 54 (2015) 14128–14132.
- [112] S. Sato, T. Morikawa, *ChemPhotoChem* 2 (2017) 207–212.
- [113] H. Takeda, H. Koizumi, K. Okamoto, O. Ishitani, *Chem. Commun.* 50 (2014) 1491–1493.
- [114] G. Neri, J.J. Walsh, G. Teobaldi, P.M. Donaldson, A.J. Cowan, *Nat. Cat.* 1 (2018) 952–959.
- [115] M. Bourrez, F. Molton, S. Chardon-Noblat, A. Deronzier, *Angew. Chem. Int. Edit.* 50 (2011) 9903–9906.
- [116] J.M. Smieja, M.D. Sampson, K.A. Grice, E.E. Benson, J.D. Froehlich, C.P. Kubiak, *Inorg. Chem.* 52 (2013) 2484–2491.
- [117] P.L. Cheung, C.W. Machan, A.Y.S. Malkhasian, J. Agarwal, C.P. Kubiak, *Inorg. Chem.* 55 (2016) 3192–3198.
- [118] M. Stanbury, J.D. Compain, M. Trejo, P. Smith, E. Gouré, S. Chardon-Noblat, *Electrochim. Acta* 240 (2017) 288–299.
- [119] J.X. Zhang, C.Y. Hu, W. Wang, H. Wang, Z.Y. Bian, *Appl. Cat. A Gen.* 522 (2016) 145–151.
- [120] L. Chen, Z. Guo, X.G. Wei, C. Gallenkamp, J. Bonin, E. Anxolabéhère-Mallart, K. C. Lau, T.C. Lau, M. Robert, *J. Am. Chem. Soc.* 137 (2015) 10918–10921.
- [121] Z. Guo, S. Cheng, C. Cometto, E. Anxolabéhère-Mallart, S.M. Ng, C.C. Ko, G. Liu, L. Chen, M. Robert, T.C. Lau, *J. Am. Chem. Soc.* 138 (2016) 9413–9416.
- [122] H. Takeda, K. Ohashi, A. Sekine, O. Ishitani, *J. Am. Chem. Soc.* 138 (2016) 4354–4357.
- [123] H. Takeda, H. Kamiyama, K. Okamoto, M. Irimajiri, T. Mizutani, K. Koike, A. Sekine, O. Ishitani, *J. Am. Chem. Soc.* 140 (2018) 17241–17254.
- [124] P.G. Alsabeh, A. Rosas-Hernández, E. Barsch, H. Junge, R. Ludwig, M. Beller, *Cat. Sci. Technol.* 6 (2016) 3623–3630.
- [125] A. Rosas-Hernández, P.G. Alsabeh, E. Barsch, H. Junge, R. Ludwig, M. Beller, *Chem. Commun.* 52 (2016) 8393–8396.
- [126] A. Rosas-Hernández, C. Steinlechner, H. Junge, M. Beller, *Green Chem.* 19 (2017) 2356–2360.
- [127] J. Grodkowski, D. Behar, P. Neta, P. Hambricht, *J. Phys. Chem. A* 101 (1997) 248–254.
- [128] T. Dhanasekaran, J. Grodkowski, P. Neta, P. Hambricht, E. Fujita, *J. Phys. Chem. A* 103 (1999) 7742–7748.
- [129] D. Behar, T. Dhanasekaran, P. Neta, C.M. Hosten, D. Ejeh, P. Hambricht, E. Fujita, *J. Phys. Chem. A* 102 (1998) 2870–2877.
- [130] J. Bonin, M. Chaussemier, M. Robert, M. Routier, *ChemCatChem* 6 (2014) 3200–3207.
- [131] J. Bonin, M. Robert, M. Routier, *J. Am. Chem. Soc.* 136 (2014) 16768–16771.
- [132] H. Rao, J. Bonin, M. Robert, *Chem. Commun.* 53 (2017) 2830–2833.
- [133] H. Rao, J. Bonin, M. Robert, *ChemSusChem* 10 (2017) 4447–4450.
- [134] H. Rao, L.C. Schmidt, J. Bonin, M. Robert, *Nature* 548 (2017) 74.
- [135] H. Rao, J. Bonin, M. Robert, *J. Phys. Chem. C* 122 (2018) 13834–13839.
- [136] H. Rao, C.H. Lim, J. Bonin, G.M. Miyake, M. Robert, *J. Am. Chem. Soc.* 140 (2018) 17830–17834.
- [137] S. Lian, M.S. Kodaimati, E.A. Weiss, *ACS Nano* 12 (2018) 568–575.
- [138] J.M. Lehn, R. Ziessel, P. Natl, *Acad. Sci. USA* 79 (1982) 701–704.
- [139] R. Ziessel, J. Hawecker, J.M. Lehn, *Helv. Chim. Acta* 69 (1986) 1065–1084.
- [140] F. Wang, B. Cao, W.P. To, C.W. Tse, K. Li, X.Y. Chang, C. Zang, S.L.F. Chan, C.M. Che, *Cat. Sci. Technol.* 6 (2016) 7408–7420.
- [141] C.Y. Zhu, Y.C. Huang, J.C. Hu, Q.K. Li, H. Tan, M.X. Gui, S.F. Deng, F. Wang, *J. Photochem. Photobio. A* 355 (2018) 175–179.
- [142] T. Shimoda, T. Morishima, K. Kodama, T. Hirose, D.E. Polyansky, G.F. Manbeck, J.T. Muckerman, E. Fujita, *Inorg. Chem.* 57 (2018) 5486–5498.
- [143] C. Creutz, H.A. Schwarz, J.F. Wishart, E. Fujita, N. Sutin, *J. Am. Chem. Soc.* 113 (1991) 3361–3371.
- [144] E. Fujita, D.J. Szalda, C. Creutz, N. Sutin, *J. Am. Chem. Soc.* 110 (1988) 4870–4871.
- [145] T. Ogata, Y. Yamamoto, Y. Wada, K. Murakoshi, M. Kusaba, N. Nakashima, A. Ishida, S. Takamuku, S. Yanagida, *J. Phys. Chem.* 99 (1995) 11916–11921.
- [146] A.H.A. Tinnemans, T.P.M. Koster, D.H.M.W. Thewissen, A. Mackor, *Recl. Trav. Chim. Pays-Bas* 103 (1984) 288–295.
- [147] S. Matsuoka, K. Yamamoto, C. Pac, S. Yanagida, *Chem. Lett.* 20 (1991) 2099–2100.
- [148] S. Matsuoka, K. Yamamoto, T. Ogata, M. Kusaba, N. Nakashima, E. Fujita, S. Yanagida, *J. Am. Chem. Soc.* 115 (1993) 601–609.
- [149] M.H. Schmidt, G.M. Miskelly, N.S. Lewis, *J. Am. Chem. Soc.* 112 (1990) 3420–3426.
- [150] E. Fujita, C. Creutz, N. Sutin, D.J. Szalda, *J. Am. Chem. Soc.* 113 (1991) 343–353.
- [151] E. Fujita, L.R. Furenliid, M.W. Renner, *J. Am. Chem. Soc.* 119 (1997) 4549–4550.
- [152] E. Fujita, C. Creutz, N. Sutin, B.S. Brunshwig, *Inorg. Chem.* 32 (1993) 2657–2662.
- [153] T. Ogata, S. Yanagida, B.S. Brunshwig, E. Fujita, *Energy Convers. Manage.* 36 (1995) 669–672.
- [154] M. Zhang, M. El-Roz, H. Frei, J.L. Mendoza-Cortes, M. Head-Gordon, D.C. Lacy, J.C. Peters, *J. Phys. Chem. C* 119 (2015) 4645–4654.
- [155] H. Sheng, H. Frei, *J. Am. Chem. Soc.* 138 (2016) 9959–9967.
- [156] J. Grodkowski, T. Dhanasekaran, P. Neta, P. Hambricht, B.S. Brunshwig, K. Shinokaki, E. Fujita, *J. Phys. Chem. A* 104 (2000) 11332–11339.
- [157] J. Grodkowski, P. Neta, E. Fujita, A. Mohammed, L. Simkhovich, Z. Gross, *J. Phys. Chem. A* 106 (2002) 4772–4778.
- [158] J. Grodkowski, P. Neta, *J. Phys. Chem. A* 104 (2000) 1848–1853.
- [159] S.L.F. Chan, T.L. Lam, C. Yang, S.C. Yan, N.M. Cheng, *Chem. Commun.* 51 (2015) 7799–7801.
- [160] C. Yang, F. Mehmood, T.L. Lam, S.L.F. Chan, Y. Wu, C.S. Yeung, X. Guan, K. Li, C. Y.S. Chung, C.Y. Zhou, T. Zou, C.M. Che, *Chem. Sci.* 7 (2016) 3123–3136.
- [161] S.L.F. Chan, T.L. Lam, C. Yang, J. Lai, B. Cao, Z. Zhou, Q. Zhu, *Polyhedron* 125 (2017) 156–163.
- [162] J.W. Wang, H.H. Huang, J.K. Sun, T. Ouyang, D.C. Zhong, T.B. Lu, *ChemSusChem* 11 (2018) 1025–1031.
- [163] T. Ouyang, H.H. Huang, J.W. Wang, D.C. Zhong, T.B. Lu, *Angew. Chem. Int. Edit.* 56 (2017) 738–743.
- [164] Q.Q. Bi, J.W. Wang, J.X. Lv, J. Wang, W. Zhang, T.B. Lu, *ACS Cat.* 8 (2018) 1821–1821.
- [165] T. Ouyang, H.J. Wang, H.H. Huang, J.W. Wang, S. Guo, W.J. Liu, D.C. Zhong, T.B. Lu, *Angew. Chem. Int. Edit.* 57 (2018) 16480–16485.
- [166] T. Ouyang, C. Hou, J.W. Wang, W.J. Liu, D.C. Zhong, Z.F. Ke, T.B. Lu, *Inorg. Chem.* 56 (2017) 7307–7311.
- [167] D.C. Liu, H.J. Wang, T. Ouyang, J.W. Wang, L. Jiang, D.C. Zhong, T.B. Lu, *ACS Appl. Energy Mater.* 1 (2018) 2452–2459.
- [168] D.C. Liu, H.H. Huang, J.W. Wang, L. Jiang, D.C. Zhong, T.B. Lu, *ChemCatChem* 10 (2018) 3435–3440.
- [169] J.L. Grant, K. Goswami, L.O. Spreer, J.W. Otvos, M. Calvin, *Dalton T.* (1987) 2105–2109.
- [170] C.A. Craig, L.O. Spreer, J.W. Otvos, M. Calvin, *J. Phys. Chem.* 94 (1990) 7957–7960.
- [171] M.A. Méndez, P. Voyame, H.H. Girault, *Angew. Chem.* 123 (2011) 7529–7532.
- [172] K. Mochizuki, S. Manaka, I. Takeda, T. Kondo, *Inorg. Chem.* 35 (1996) 5132–5136.
- [173] V.S. Thoi, N. Kornienko, C.G. Margarit, P. Yang, C.J. Chang, *J. Am. Chem. Soc.* 135 (2013) 14413–14424.
- [174] D. Hong, Y. Tsukakoshi, H. Kotani, T. Ishizuka, T. Kojima, *J. Am. Chem. Soc.* 139 (2017) 6538–6541.
- [175] D.B. Burks, S. Davis, R.W. Lamb, X. Liu, R.R. Rodrigues, N.P. Liyanage, Y. Sun, C. E. Webster, J.H. Delcamp, E.T. Papish, *Chem. Commun.* 54 (2018) 3819–3822.
- [176] Z. Guo, F. Yu, Y. Yang, C.F. Leung, S.M. Ng, C.C. Ko, C. Cometto, T.C. Lau, M. Robert, *ChemSusChem* 10 (2017) 4009–4013.
- [177] W.J. Liu, H.H. Huang, T. Ouyang, L. Jiang, D.C. Zhong, W. Zhang, T.B. Lu, *Chem. Eur. J.* 24 (2018) 4503–4508.
- [178] N. Komatsuzaki, Y. Himeda, T. Hirose, H. Sugihara, K. Kasuga, B. Chem. Soc. JPN 72 (1999) 725–731.
- [179] E. Kimura, S. Wada, M. Shionoya, Y. Okazaki, *Inorg. Chem.* 33 (1994) 770–778.
- [180] C. Herrero, A. Quaranta, S. El Ghachtouli, B. Vauzeilles, W. Leibl, A. Aukauloo, *Phys. Chem. Chem. Phys.* 16 (2014) 12067–12072.
- [181] X. Wang, V. Goudy, G. Genesio, J. Maynadie, D. Meyer, M. Fontecave, *Chem. Commun.* 53 (2017) 5040–5043.
- [182] Z.Y. Bian, H. Wang, W.F. Fu, L. Li, A.Z. Ding, *Polyhedron* 32 (2012) 78–85.
- [183] B. Gholamkhass, H. Mametsuka, K. Koike, T. Tanabe, M. Furue, O. Ishitani, *Inorg. Chem.* 44 (2005) 2326–2336.
- [184] K. Koike, D.C. Grills, Y. Tamaki, E. Fujita, K. Okubo, Y. Yamazaki, M. Saigo, T. Mukuta, K. Onda, O. Ishitani, *Chem. Sci.* 9 (2018) 2961–2974.
- [185] S. Meister, R.O. Reithmeier, A. Ogrodnik, B. Rieger, *ChemCatChem* 7 (2015) 3562–3569.
- [186] Z.Y. Bian, K. Sumi, M. Furue, S. Sato, K. Koike, O. Ishitani, *Dalton T.* (2009) 983–993.
- [187] Y. Yamazaki, A. Umamoto, O. Ishitani, *Inorg. Chem.* 55 (2016) 11110–11124.
- [188] Z.Y. Bian, S.M. Chi, L. Li, W. Fu, *Dalton T.* 39 (2010) 7884–7887.
- [189] K. Koike, S. Naito, S. Sato, Y. Tamaki, O. Ishitani, *J. Photochem. Photobio. A* 207 (2009) 109–114.
- [190] Y. Tamaki, K. Koike, T. Morimoto, O. Ishitani, *J. Catal.* 304 (2013) 22–28.
- [191] T. Nakajima, Y. Tamaki, K. Ueno, E. Kato, T. Nishikawa, K. Ohkubo, Y. Yamazaki, T. Morimoto, O. Ishitani, *J. Am. Chem. Soc.* 138 (2016) 13818–13821.
- [192] Y. Tamaki, K. Watanabe, K. Koike, H. Inoue, T. Morimoto, O. Ishitani, *Faraday Discuss.* 155 (2012) 115–127.
- [193] S. Sato, K. Koike, H. Inoue, O. Ishitani, *Photochem. Photobio. Sci.* 6 (2007) 454–461.
- [194] E. Kato, H. Takeda, K. Koike, K. Ohkubo, O. Ishitani, *Chem. Sci.* 6 (2015) 3003–3012.
- [195] A. Nakada, K. Koike, T. Nakashima, T. Morimoto, O. Ishitani, *Inorg. Chem.* 54 (2015) 1800–1807.
- [196] A. Nakada, K. Koike, K. Maeda, O. Ishitani, *Green Chem.* 18 (2016) 139–143.
- [197] Y. Tamaki, K. Koike, O. Ishitani, *Chem. Sci.* 6 (2015) 7213–7221.
- [198] Y. Tamaki, O. Ishitani, *Faraday Discuss.* 198 (2017) 319–335.
- [199] D. Ghosh, H. Takeda, D.C. Fabry, Y. Tamaki, O. Ishitani, *ACS Sustainable Chem. Eng.* 7 (2019) 2648–2657.
- [200] Y. Tamaki, K. Koike, T. Morimoto, Y. Yamazaki, O. Ishitani, *Inorg. Chem.* 52 (2013) 11902–11911.
- [201] Y. Yamazaki, O. Ishitani, *Chem. Sci.* 9 (2018) 1031–1041.
- [202] Y. Kuramochi, O. Ishitani, *Inorg. Chem.* 55 (2016) 5702–5709.
- [203] K. Kiyosawa, N. Shiraishi, T. Shimada, D. Masui, H. Tachibana, S. Takagi, O. Ishitani, D.A. Tryk, H. Inoue, *J. Phys. Chem. C* 113 (2009) 11667–11673.
- [204] J. Schneider, K.Q. Vuong, J.A. Calladine, X.Z. Sun, A.C. Whitwood, M.W. George, R.N. Perutz, *Inorg. Chem.* 50 (2011) 11877–11881.
- [205] C.D. Windle, M.V. Câmpian, A.K. Duhme-Klair, E.A. Gibson, R.N. Perutz, *J. Schneider, Chem. Commun.* 48 (2012) 8189–8191.
- [206] C.D. Windle, M.W. George, R.N. Perutz, P.A. Summers, X.Z. Sun, A.C. Whitwood, *Chem. Sci.* 6 (2015) 6847–6864.

- [207] C. Matlachowski, M. Schwalbe, Dalton T. 44 (2015) 6480–6489.
- [208] C. Matlachowski, B. Braun, S. Tschierlei, M. Schwalbe, Inorg. Chem. 54 (2015) 10351–10360.
- [209] S.K. Lee, M. Kondo, M. Okamura, T. Enomoto, G. Nakamura, S. Masaoka, J. Am. Chem. Soc. 140 (2018) 16899–16903.
- [210] L. Zhu, X.Q. Liu, H.L. Jiang, L.B. Sun, Chem. Rev. 117 (2017) 8129–8176.
- [211] W.M. Liao, J.H. Zhang, Z. Wang, Y.L. Lu, S.Y. Yin, H.P. Wang, Y.N. Fan, M. Pan, C. Y. Su, Inorg. Chem. 57 (2018) 11436–11442.
- [212] W.M. Liao, J.H. Zhang, Z. Wang, S.Y. Yin, M. Pan, H.P. Wang, C.Y. Su, J. Mater. Chem. A 6 (2018) 11337–11345.
- [213] M. Liu, Y.F. Mu, S. Yao, S. Guo, X.W. Guo, Z.M. Zhang, T.B. Lu, Appl. Catal. B Environ. 245 (2019) 496–501.
- [214] J.D. Xiao, L. Han, J. Luo, S.H. Yu, H.L. Jiang, Angew. Chem. Int. Edit. 57 (2018) 1103–1107.
- [215] K.M. Choi, D. Kim, B. Rungtaweeworanit, C.A. Trickett, J.T.D. Barmann, A.S. Alshammari, P. Yang, O.M. Yaghi, J. Am. Chem. Soc. 139 (2017) 356–362.
- [216] M. Chen, L. Han, J. Zhou, C. Sun, C. Hu, X. Wang, Z. Su, Nanotechnology 29 (2018) 284003.
- [217] Y. Han, H. Xu, Y. Su, Z. Xu, K. Wang, W. Wang, J. Catal. 370 (2019) 70–78.
- [218] M.B. Chambers, X. Wang, N. Elgrishi, C.H. Hendon, A. Walsh, J. Bonnefoy, J. Canivet, E.A. Quadrelli, D. Farrusseng, C. Mellot-Draznieks, M. Fontecave, ChemSusChem 8 (2015) 603–608.
- [219] T. Kajiura, M. Fujii, M. Tsujimoto, K. Kobayashi, M. Higuchi, K. Tanaka, S. Kitagawa, Angew. Chem. Int. Edit. 55 (2016) 2697–2700.
- [220] Y. Lee, S. Kim, H. Fei, J.K. Kang, S.M. Cohen, Chem. Commun. 51 (2015) 16549–16552.
- [221] H. Fei, M.D. Sampson, Y. Lee, C.P. Kubiak, S.M. Cohen, Inorg. Chem. 54 (2015) 6821–6828.
- [222] L. Li, S. Zhang, L. Xu, J. Wang, L.X. Shi, Z.N. Chen, M. Hong, J. Luo, Chem. Sci. 5 (2014) 3808–3813.
- [223] S. Zhang, L. Li, S. Zhao, Z. Sun, J. Luo, Inorg. Chem. 54 (2015) 8375–8379.
- [224] Z.H. Yan, M.H. Du, J. Liu, S. Jin, C. Wang, G.L. Zhuang, X.J. Kong, L.S. Long, L.S. Zheng, Nat. Commun. 9 (2018) 3353.
- [225] D. Sun, Y. Gao, J. Fu, X. Zeng, Z. Chen, Z. Li, Chem. Commun. 51 (2015) 2645–2648.
- [226] X. Deng, J. Alberio, L. Xu, H. García, Z. Li, Inorg. Chem. 57 (2018) 8276–8286.
- [227] S. Zhang, L. Li, S. Zhao, Z. Sun, M. Hong, J. Luo, J. Mater. Chem. A 3 (2015) 15764–15768.
- [228] M. Zhao, Y. Huang, Y. Peng, Z. Huang, Q. Ma, H. Zhang, Chem. Soc. Rev. 47 (2018) 6267–6295.
- [229] L. Ye, Y. Gao, S. Cao, H. Chen, Y. Yao, J. Hou, L. Sun, Appl. Catal. B Environ. 227 (2018) 54–60.
- [230] G. Lan, Z. Li, S.S. Veroneau, Y.Y. Zhu, Z. Xu, C. Wang, W. Lin, J. Am. Chem. Soc. 140 (2018) 12369–12373.
- [231] B. Han, X. Ou, Z. Deng, Y. Song, C. Tian, H. Deng, Y.J. Xu, Z. Lin, Angew. Chem. 130 (2018) 17053–17057.
- [232] W. Zhu, C. Zhang, Q. Li, L. Xiong, R. Chen, X. Wan, Z. Wang, W. Chen, Z. Deng, Y. Peng, Appl. Catal. B Environ. 238 (2018) 339–345.
- [233] J.D. Xiao, H.L. Jiang, Acc. Chem. Res. 52 (2019) 356–366.
- [234] Y. Fu, D. Sun, Y. Chen, R. Huang, Z. Ding, X. Fu, Z. Li, Angew. Chem. Int. Edit. 51 (2012) 3364–3367.
- [235] M.W. Logan, S. Ayad, J.D. Adamson, T. Dilbeck, K. Hanson, F.J. Uribe-Romo, J. Mater. Chem. A 5 (2017) 11854–11861.
- [236] T. Luo, J. Zhang, W. Li, Z. He, X. Sun, J. Shi, D. Shao, B. Zhang, X. Tan, B. Han, ACS Appl. Mater. Inter. 9 (2017) 41594–41598.
- [237] D. Sun, Y. Fu, W. Liu, L. Ye, D. Wang, L. Yang, X. Fu, Z. Li, Chem. Eur. J. 19 (2013) 14279–14285.
- [238] M. Sun, S. Yan, Y. Sun, X. Yang, Z. Guo, J. Du, D. Chen, P. Chen, H. Xing, Dalton T. 47 (2018) 909–915.
- [239] M. Zhao, S. Ou, C.D. Wu, Accounts Chem. Res. 47 (2014) 1199–1207.
- [240] H.Q. Xu, J. Hu, D. Wang, Z. Li, Q. Zhang, Y. Luo, S.H. Yu, H.L. Jiang, J. Am. Chem. Soc. 137 (2015) 13440–13443.
- [241] Y. Liu, Y. Yang, Q. Sun, Z. Wang, B. Huang, Y. Dai, X. Qin, X. Zhang, ACS Appl. Mater. Inter. 5 (2013) 7654–7658.
- [242] H. Zhang, J. Wei, J. Dong, G. Liu, L. Shi, P. An, G. Zhao, J. Kong, X. Wang, X. Meng, J. Zhang, J. Ye, Angew. Chem. 128 (2016) 14522–14526.
- [243] E.X. Chen, M. Qiu, Y.F. Zhang, Y.S. Zhu, L.Y. Liu, Y.Y. Sun, X. Bu, J. Zhang, Q. Lin, Adv. Mater. 30 (2017) 1704388.
- [244] J. Liu, Y.Z. Fan, X. Li, Z. Wei, Y.W. Xu, L. Zhang, C.Y. Su, Appl. Catal. B Environ. 231 (2018) 173–181.
- [245] S. Wang, W. Yao, J. Lin, Z. Ding, X. Wang, Angew. Chem. 126 (2013) 1052–1056.
- [246] J. Qin, S. Wang, X. Wang, Appl. Catal. B Environ. 209 (2017) 476–482.
- [247] M. Wang, J. Liu, C. Guo, X. Gao, C. Gong, Y. Wang, B. Liu, X. Li, G.G. Gurzadyan, L. Sun, J. Mater. Chem. A 6 (2018) 4768–4775.
- [248] N. Li, J. Liu, J.J. Liu, L.Z. Dong, Z.F. Xin, Y.L. Teng, Y.Q. Lan, Angew. Chem. Int. Edit. 58 (2019), <https://doi.org/10.1002/anie.201814729>.
- [249] P. Wu, X. Guo, L. Cheng, C. He, J. Wang, C. Duan, Inorg. Chem. 55 (2016) 8153–8159.
- [250] J. Zhao, Q. Wang, C. Sun, T. Zheng, L. Yan, M. Li, K. Shao, X. Wang, Z. Su, J. Mater. Chem. A 5 (2017) 12498–12505.
- [251] X.K. Wang, J. Liu, L. Zhang, L.Z. Dong, S.L. Li, Y.H. Kan, D. Li, Y.Q. Lan, ACS Catal. 9 (2019) 1726–1732.
- [252] D. Chen, H. Xing, C. Wang, Z. Su, J. Mater. Chem. A 4 (2016) 2657–2662.
- [253] J. Qin, S. Yuan, L. Zhang, B. Li, D.Y. Du, N. Huang, W. Guan, H. Drake, J. Pang, Y. Q. Lan, A. Alsalmé, H.C. Zhou, J. Am. Chem. Soc. 140 (2019) 2054–2060.
- [254] S.L. Xie, J. Liu, L.Z. Dong, S.L. Li, Y.Q. Lan, Z.M. Su, Chem. Sci. 10 (2019) 185–190.
- [255] X. Kong, E. Scott, W. Ding, J.A. Mason, J.R. Long, J.A. Reimer, J. Am. Chem. Soc. 134 (2012) 14341–14344.
- [256] R.M. Marti, J.D. Howe, C.R. Morelock, M.S. Conradi, K.S. Walton, D.S. Sholl, S.E. Hayes, J. Phys. Chem. C 121 (2017) 25778–25787.
- [257] D. Wang, R. Huang, W. Liu, D. Sun, Z. Li, ACS Cat. 4 (2014) 4254–4260.
- [258] Y. Wang, N.Y. Huang, J.Q. Shen, P.Q. Liao, X.M. Chen, J.P. Zhang, J. Am. Chem. Soc. 140 (2018) 38–41.
- [259] D. Sun, W. Liu, M. Qiu, Y. Zhang, Z. Li, Chem. Commun. 51 (2015) 2056–2059.
- [260] Y. Lee, S. Kim, J.K. Kang, S.M. Cohen, Chem. Commun. 51 (2015) 5735–5738.
- [261] C.S. Diercks, M.J. Kalmutzki, N.J. Diercks, O.M. Yaghi, ACS Central Sci. 4 (2018) 1457–1464.
- [262] K. Niu, Y. Xu, H. Wang, R. Ye, H.L. Xin, F. Lin, C. Tian, Y. Lum, K.C. Bustillo, M.M. Doeff, M.T.M. Koper, J. Ager, R. Xu, H. Zheng, Sci. Adv. 3 (2017) e1700921.
- [263] T.M. Suzuki, H. Tanaka, T. Morikawa, M. Iwaki, S. Sato, S. Saeki, M. Inoue, T. Kajino, T. Motohiro, Chem. Commun. 47 (2011) 8673–8675.
- [264] K. Maeda, K. Sekizawa, O. Ishitani, Chem. Commun. 49 (2013) 10127–10129.
- [265] K. Maeda, R. Kuriki, M. Zhang, X. Wang, O. Ishitani, J. Mater. Chem. A 2 (2014) 15146–15151.
- [266] R. Kuriki, K. Sekizawa, O. Ishitani, K. Maeda, Angew. Chem. Int. Edit. 54 (2015) 2406–2409.
- [267] G. Zhao, H. Pang, G. Liu, P. Li, H. Liu, H. Zhang, L. Shi, J. Ye, Appl. Catal. B Environ. 200 (2017) 141–149.
- [268] L. Lin, C. Hou, X. Zhang, Y. Wang, Y. Chen, T. He, Appl. Catal. B Environ. 221 (2018) 312–319.
- [269] T. Wu, L. Zou, D. Han, F. Li, Q. Zhang, L. Niu, Green Chem. 16 (2014) 2142–2146.
- [270] C. Cometto, R. Kuriki, L. Chen, K. Maeda, T.C. Lau, O. Ishitani, M. Robert, J. Am. Chem. Soc. 140 (2018) 7437–7440.
- [271] M.F. Kuehn, K.L. Orchard, K.E. Dalle, E. Reisner, J. Am. Chem. Soc. 139 (2017) 7217–7223.
- [272] P. Li, X. Zhang, C. Hou, L. Lin, Y. Chen, T. He, Phys. Chem. Chem. Phys. 20 (2018) 16985–16991.
- [273] E.G. Ha, J.A. Chang, S.M. Byun, C. Pac, D.M. Jang, J. Park, S.O. Kang, Chem. Commun. 50 (2014) 4462–4464.
- [274] D.I. Won, J.S. Lee, J.M. Ji, W.J. Jung, H.J. Son, C. Pac, S.O. Kang, J. Am. Chem. Soc. 137 (2015) 13679–13690.
- [275] C.D. Windle, E. Pastor, A. Reynal, A.C. Whitwood, Y. Vaynzof, J.R. Durrant, R.N. Perutz, E. Reisner, Chem. Eur. J. 21 (2015) 3746–3754.
- [276] H.Y. Cheong, S.Y. Kim, Y.J. Cho, D.W. Cho, C.H. Kim, H.J. Son, C. Pac, S.O. Kang, Inorg. Chem. 56 (2017) 12042–12053.
- [277] D.I. Won, J.S. Lee, Q. Ba, Y.J. Cho, H.Y. Cheong, S. Choi, C.H. Kim, H.J. Son, C. Pac, S.O. Kang, ACS Cat. 8 (2018) 1018–1030.
- [278] S. Sato, T. Arai, T. Morikawa, Inorg. Chem. 54 (2015) 5105–5113.
- [279] S. Sato, T. Arai, T. Morikawa, T. Uemura, T.M. Suzuki, H. Tanaka, T. Kajino, J. Am. Chem. Soc. 133 (2011) 15240–15243.
- [280] T. Arai, S. Sato, T. Kajino, T. Morikawa, Energy Environ. Sci. 6 (2013) 1274–1282.
- [281] P. Li, X. Zhang, C. Hou, Y. Chen, T. He, Appl. Catal. B Environ. 238 (2018) 656–663.
- [282] K. Sekizawa, K. Maeda, K. Domen, K. Koike, O. Ishitani, J. Am. Chem. Soc. 135 (2013) 4596–4599.
- [283] A. Nakada, R. Kuriki, K. Sekizawa, S. Nishioka, J.J.M. Vequizo, T. Uchiyama, N. Kawakami, D. Lu, A. Yamakata, Y. Uchimoto, O. Ishitani, K. Maeda, ACS Cat. 8 (2018) 9744–9754.
- [284] F. Yoshitomi, K. Sekizawa, K. Maeda, O. Ishitani, ACS Appl. Mater. Inter. 7 (2015) 13092–13097.
- [285] R. Kuriki, M. Yamamoto, K. Higuchi, Y. Yamamoto, M. Akatsuka, D. Lu, S. Yagi, T. Yoshida, O. Ishitani, K. Maeda, Angew. Chem. 129 (2017) 4945–4949.
- [286] K. Maeda, D. An, C.S. Kumara Ranasinghe, T. Uchiyama, R. Kuriki, T. Kanazawa, D. Lu, S. Nozawa, A. Yamakata, Y. Uchimoto, O. Ishitani, J. Mater. Chem. A 6 (2018) 9708–9715.
- [287] R. Kuriki, O. Ishitani, K. Maeda, ACS Appl. Mater. Inter. 8 (2016) 6011–6018.
- [288] G. Zhao, W. Zhou, Y. Sun, X. Wang, H. Liu, X. Meng, K. Chang, J. Ye, Appl. Catal. B Environ. 226 (2018) 252–257.
- [289] K. Wada, C.S.K. Ranasinghe, R. Kuriki, A. Yamakata, O. Ishitani, K. Maeda, ACS Appl. Mater. Inter. 9 (2017) 23869–23877.
- [290] H. Takeda, M. Ohashi, T. Tani, O. Ishitani, S. Inagaki, Inorg. Chem. 49 (2010) 4554–4559.
- [291] Y. Ueda, H. Takeda, T. Yui, K. Koike, Y. Goto, S. Inagaki, O. Ishitani, ChemSusChem 8 (2014) 439–442.
- [292] Y. Kuramochi, M. Sekine, K. Kitamura, Y. Maegawa, Y. Goto, S. Shirai, S. Inagaki, H. Ishida, Chem. Eur. J. 23 (2017) 10301–10309.
- [293] M. Waki, K.I. Yamanaka, S. Shirai, Y. Maegawa, Y. Goto, Y. Yamada, S. Inagaki, Chem. Eur. J. 24 (2018) 3846–3853.
- [294] X. Wang, I. Thiel, A. Fedorov, C. Copéret, V. Mougél, M. Fontecave, Chem. Sci. 8 (2017) 8204–8213.
- [295] C. Liu, K.D. Dubois, M.E. Louis, A.S. Vorushilov, G. Li, ACS Cat. 3 (2013) 655–662.
- [296] H.M. Sung-Suh, D.S. Kim, C.W. Lee, S.E. Park, Appl. Organomet. Chem. 14 (2000) 826–830.
- [297] J.S. Hwang, D.S. Kim, C.W. Lee, S.E. Park, Korean J. Chem. Eng. 18 (2001) 919–923.
- [298] K.D. Dubois, A. Petushkov, E. Garcia Cardona, S.C. Larsen, G. Li, J. Phys. Chem. Lett. 3 (2012) 486–492.

- [299] K.D. Dubois, H. He, C. Liu, A.S. Vorushilov, G. Li, J. Mol. Catal. A-Chem. 363–364 (2012) 208–213.
- [300] T. Fenton, S. Gillingham, T. Jin, G. Li, Dalton T. 46 (2017) 10721–10726.
- [301] H. He, C. Liu, M.E. Louis, G. Li, J. Mol. Catal. A Chem. 395 (2014) 145–150.
- [302] Y. Kou, S. Nakatani, G. Sunagawa, Y. Tachikawa, D. Masui, T. Shimada, S. Takagi, D.A. Tryk, Y. Nabetani, H. Tachibana, H. Inoue, J. Catal. 310 (2014) 57–66.
- [303] G. Sahara, R. Abe, M. Higashi, T. Morikawa, K. Maeda, Y. Ueda, O. Ishitani, Chem. Commun. 51 (2015) 10722–10725.
- [304] M. Schreier, J. Luo, P. Gao, T. Moehl, M.T. Mayer, M. Grätzel, J. Am. Chem. Soc. 138 (2016) 1938–1946.
- [305] K. Sekizawa, S. Sato, T. Arai, T. Morikawa, Acs Cat. 8 (2018) 1405–1416.
- [306] Q. Liu, Z.X. Low, L. Li, A. Razmjou, K. Wang, J. Yao, H. Wang, J. Mater. Chem. A 1 (2013) 11563–11569.
- [307] J.W. Maina, J.A. Schütz, L. Grundy, E. Des Ligneris, Z. Yi, L. Kong, C. Pozo-Gonzalo, M. Ionescu, L.F. Dumée, ACS Appl. Mater. Inter. 9 (2017) 35010–35017.
- [308] S. Wang, J. Lin, X. Wang, Phys. Chem. Chem. Phys. 16 (2014) 14656–14660.
- [309] S. Wang, X. Wang, Appl. Catal. B Environ. 162 (2015) 494–500.
- [310] S. Yan, S. Ouyang, H. Xu, M. Zhao, X. Zhang, J. Ye, J. Mater. Chem. A 14 (2016) 15126–15133.
- [311] R. Li, J. Hu, M. Deng, H. Wang, X. Wang, Y. Hu, H.L. Jiang, J. Jiang, Q. Zhang, Y. Xie, Y. Xiong, Adv. Mater. 26 (2014) 4783–4788.
- [312] X. He, W.N. Wang, J. Mater. Chem. A 6 (2018) 932–940.
- [313] M. Wang, D. Wang, Z. Li, Appl. Catal. B Environ. 183 (2016) 47–52.
- [314] H. Zhao, X. Wang, J. Feng, Y. Chen, X. Yang, S. Gao, R. Cao, Cat. Sci. Technol. 8 (2018) 1288–1295.
- [315] S. Wan, M. Ou, Q. Zhong, X. Wang, Chem. Eng. J. 358 (2019) 1287–1295.
- [316] Z.C. Kong, J.F. Liao, Y.J. Dong, Y.F. Xu, H.Y. Chen, D.B. Kuang, C.Y. Su, A.C.S. Energ. Lett. (2018) 2656–2662.
- [317] G. Xu, H. Zhang, J. Wei, H.X. Zhang, X. Wu, Y. Li, C. Li, J. Zhang, J. Ye, ACS Nano 12 (2018) 5333–5340.
- [318] C. Chen, T. Wu, H. Wu, H. Liu, Q. Qian, Z. Liu, G. Yang, B. Han, Chem. Sci. 9 (2018) 8890–8894.
- [319] S. Wang, B.Y. Guan, X.W. Lou, Energy Environ. Sci. 11 (2018) 306–310.
- [320] X. Lin, Y. Gao, M. Jiang, Y. Zhang, Y. Hou, W. Dai, S. Wang, Z. Ding, Appl. Catal. B Environ. 224 (2018) 1009–1016.
- [321] B. Liu, H. Shioyama, T. Akita, Q. Xu, J. Am. Chem. Soc. 130 (2008) 5390–5391.
- [322] Y.Z. Chen, R. Zhang, L. Jiao, H.L. Jiang, Coord. Chem. Rev. 362 (2018) 1–23.
- [323] C.Y. Hu, J. Zhou, C.Y. Sun, M.M. Chen, X.L. Wang, Z.M. Su, Chem. Eur. J. 25 (2019) 379–385.
- [324] P. Zhang, B.Y. Guan, L. Yu, X.W. Lou, Chem 4 (2018) 162–173.
- [325] S. Wang, B.Y. Guan, X. Wang, X.W. Lou, J. Am. Chem. Soc. 140 (2018) 15145–15148.
- [326] L. Jiao, Y. Wang, H.L. Jiang, Q. Xu, Adv. mater. 30 (2018) 1703663.
- [327] K. Khaletskaya, A. Pougin, R. Medishetty, C. Rösler, C. Wiktor, J. Strunk, R.A. Fischer, Chem. Mater. 27 (2015) 7248–7257.
- [328] H. Zhang, T. Wang, J. Wang, H. Liu, T.D. Dao, M. Li, G. Liu, X. Meng, K. Chang, L. Shi, T. Nagao, J. Ye, Adv. Mater. 28 (2016) 3703–3710.
- [329] W. Chen, B. Han, C. Tian, X. Liu, S. Liang, H. Deng, Z. Lin, Appl. Catal. B Environ. 244 (2019) 996–1003.
- [330] S. Wang, B.Y. Guan, Y. Lu, X.W. Lou, J. Am. Chem. Soc. 139 (2017) 17305–17308.
- [331] J. Yang, X. Zhu, Z. Mo, J. Yi, J. Yan, J. Deng, Y. Xu, Y. She, J. Qian, H. Xu, H. Li, Inorg. Chem. Front. 5 (2018) 3163–3169.
- [332] S. Wang, B.Y. Guan, X.W. Lou, J. Am. Chem. Soc. 140 (2018) 5037–5040.
- [333] P. Zhang, S. Wang, B.Y. Guan, X.W. Lou, Energy Environ. Sci. 12 (2019) 164–168.